FATIGUE CRACKING OF LUMBER BANDSAW BLADES

By

Hongtao Lu

B. E. The Northern Jiao-Tong University, Beijing, P.R. China

A THESIS SUBMITTED IN PARTIAL FULFILLMENT OF

THE REQUIREMENTS FOR THE DEGREE OF

MASTER OF APPLIED SCIENCE

in

THE FACULTY OF GRADUATE STUDIES

MECHANICAL ENGINEERING

We accept this thesis as conforming

to the required standard

THE UNIVERSITY OF BRITISH COLUMBIA

April 1993

In presenting this thesis in partial fulfilment of the requirements for an advanced degree at the University of British Columbia, I agree that the Library shall make it freely available for reference and study. I further agree that permission for extensive copying of this thesis for scholarly purposes may be granted by the head of my department or by his or her representatives. It is understood that copying or publication of this thesis for financial gain shall not be allowed without my written permission.

(Signature)

Department of MECHANICAL ENGINEERING

The University of British Columbia
Vancouver, Canada

Date April 28, 1993

DE-6 (2/88)

Abstract

The focus of this research is on the fatigue cracking problem in the tooth gullet region of wide bandsaw blades used in the lumber industry. This thesis presents both the theory and the experiment aspects of this research in terms of the tasks defined as follows.

The current literature was reviewed to critically examine the current state-of-the-art in smooth and cracked body analysis techniques and their application in the failure analysis of a bandsaw blade. The advantage of the fracture mechanics approach in solving the problem was recognized and useful information was identified. Experimental testing was conducted to obtain the mechanical properties of the blade material and to establish the cracking resistance curve which defines the stability threshold of cracks in this material. Experimental testing was also conducted to determine crack propagation behaviour in bandsaw blade material subjected to representative loading conditions.

Based on the experiment data obtained, a failure analysis of a blade under assumed loading conditions was performed. Critical crack lengths which a blade can tolerate under the assumed loads were calculated. A fatigue crack propagation model has been proposed and used in the failure analysis of commonly used blades. The results offer explanations for cracking problem in the tooth gullet.

The failure analysis also shows that careful handling of the blade resharpening process can substantially prolong the fatigue life of a saw blade.

Table of Contents

List of Tables

List of Figures

Nomenclature

The symbols are listed in the order of their appearance.

σ = generic symbol for stress.

σ_T = nominal average stress produced in a blade by tensile load.

F = pre-strain force used in a bandsaw machine.

w = effective blade width.

t = the blade thickness.

σ_B = maximum stress induced by bending.

E = Young's modulus of elasticity.

R_w = bandsaw machine wheel radius.

σ_{cent} = stress produced by centrifugal force.

ρ = density of bandsaw steel.

v = velocity of bandsaw blade.

K_{IC} = plane strain fracture toughness.

ΔK = stress intensity factor range.

k_T = stress concentration factor for pure tensile load.

k_B = stress concentration factor for out-of-plane bending.

k_{T+B} = stress concentration factor for the combined load of tension and bending, reference stress is $(\sigma_T + \sigma_B)$.

e_1 = strain at location 1 on the Crack-Line-Wedge-Loaded specimen.

e_3 = strain at location 3 on the Crack-Line-Wedge-Loaded specimen.

a = generic symbol for crack length .

B = thickness of the Crack-Line-Wedge-Loaded specimen.

W = width of Crack-Line-Wedge-Loaded specimen.

P = symmetrical force acting at point A and B on the Crack-Line-Wedge-Loaded sepcimen.

C_1, C_2 = constants.

K = generic symbol for stress intensity factor (SIF) at the crack tip, or the so-called *crack driving force.*

K_C = critical stress intensity factor (plane stress condition).

R_r = the so-called *crack growth resistance*, material property with same dimension as K.

dK/da = the change rate of the driving force with respect to crack growth da.

dR_r/da = the change rate of the resistance with respect to crack growth da.

a_0, a_i = initial crack length.

Δa = physical crack growth at crack tip.

r_Y = plastic zone adjustment to Δa.

σ_Y = 2% offset yield strength.

N = number of fatigue load cycles.

da/dN = crack propagation (or growth) rate.

R = stress ratio ($\sigma_{min}/\sigma_{max}$).

$\dot{\epsilon}$ = strain rate.

T = ambient temperature.

C, b = material constants.

α_n = notch depth.

ρ_n = notch bottom curvature radius.

U = elastic energy contained in the body.

F_e = work performed by external force system.

E_p = energy consumed by crack propagation.

$G = d(F_e - U)/da$ = elastic energy release rate.

$R_r = dE_p/da$ = crack growth resistance force.

G_{IC} = critical energy release rate, a material property.

υ = Possion's ratio.

K_R = crack resistance force in terms of stress intensity factor.

Acknowledgement

I would like to thank everyone who helped during this research program. In particular, I would like to extend my appreciation to my supervisor, Dr.D.P. Romilly, for his valued advice, guidance and patience; Mr.Leonard Drakes, for his valued work in making the experiment equipment; and Mr.Robert Connop, for his valued assistance in making special specimens.

I would like to express my special thanks to Mr.John Crowden for spending a lot of time reading the manuscript of this thesis and making valued comments.

Finally, I would also like to thank my wife for her constant support and patience.

Chapter 1

Introduction

The bandsaw is a wood cutting machine which consists of two large wheels of 5-8 ft.(1.5-2.4m) in diameter and one closed-loop blade (Fig.1.1). The blade used on the bandsaw machine is a toothed closed-loop strip of high-strength alloy steel, which is driven by one of the two wheels. The so-called cutting region on the blade is a straight section of the blade supported between two guides (D-D'in Fig.1.1). The cutting process is carried out by feeding logs laterally into the downward moving cutting edge. Because of its long and straight cutting region and its high edge stability, bandsaws are especially suitable for deep cuts. Therefore bandsaws of various blade sizes and types are widely employed in the primary and secondary breakdown of logs. The high edge stability of bandsaw blades are a result of the high stiffness of the cutting edge, which is achieved directly by applying a tensile axial pre-load into the blade. This pre-load is imposed by a loading system (Fig.1.1) that lifts the top wheel of the machine to stretch the blade. As the pre-load increases, the stiffness of the cutting region of the blade increases. Therefore it is desirable to increase the pre-load as much as possible to obtain better cutting accuracy which strongly depends on the edge stability of the blade. The recently introduced 'high-strain system' is based on this idea. However, practical experience shows that increasing pre-load is limited by the increasing probability of the onset of cracks in the blade, as cracking problems occur much more often in high-strain systems. These cracks usually occur in the tooth gullet or in the mid-section of the blade.

However, the pre-load is not the only load acting on the blade. There are others, the

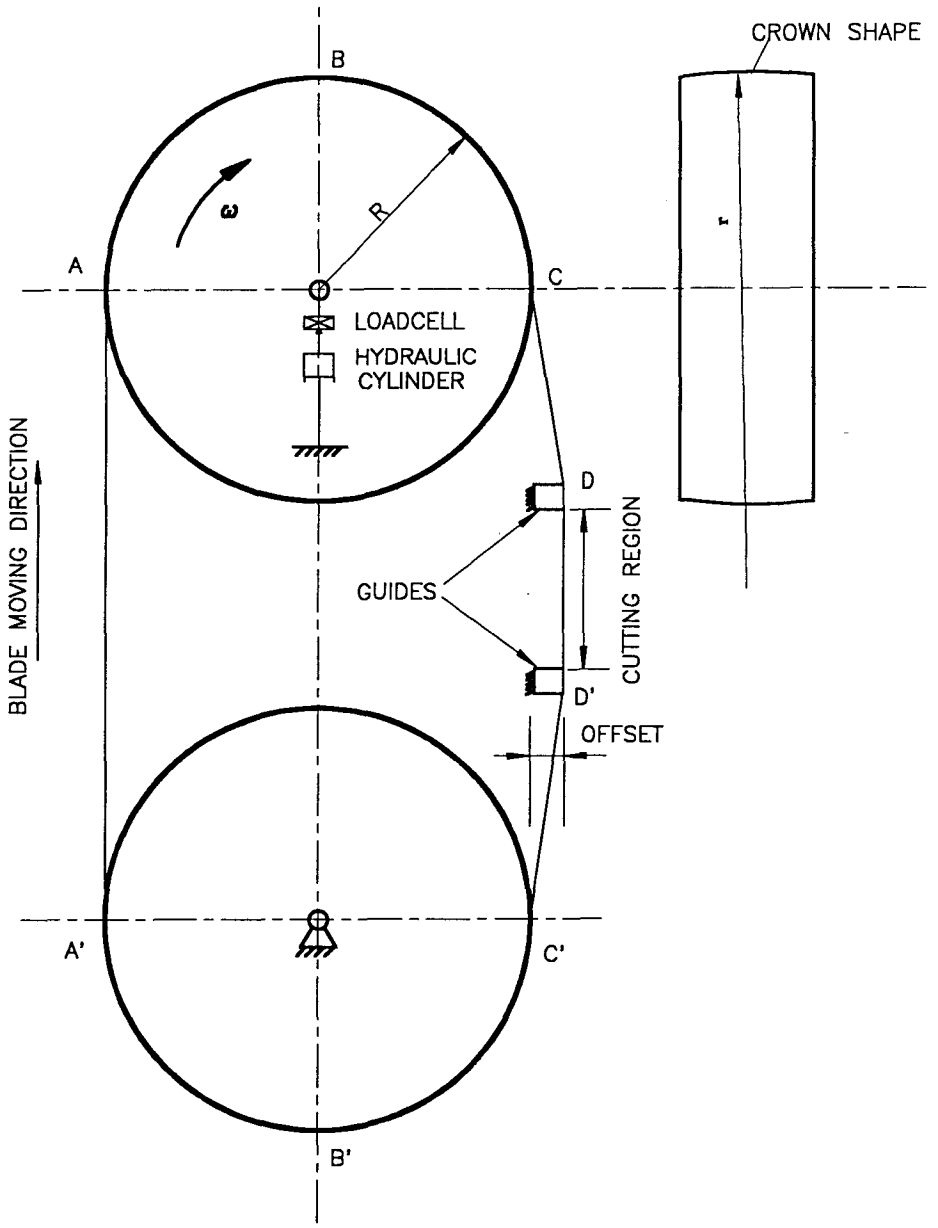

Figure 1.1: Bandsaw geometry

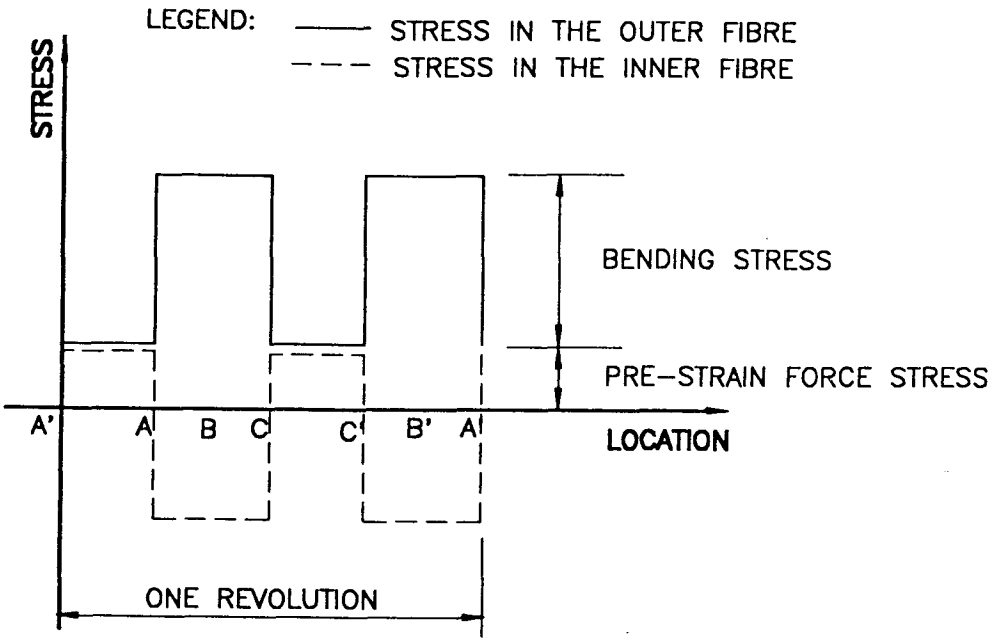

Figure 1.2: Change of load on the blade

most prominent one is the bending load. The bending load is suddenly induced on the fast moving blade when it comes into contact with the back of the wheel (at points A or C' in Fig.1.1). When the blade is in motion and travelling through the arcs, ABC, C'B'A', the blade is subjected to a combined load, i.e. a bending load in addition to the pre-load. The bending load disappears when the blade leaves the back of the wheel (at points C or A' in Fig.1.1). The Fig.1.2 shows the schematic change of the regular load on the blade.

In addition, there is also a cutting force, a centrifugal force and possibly some accidental loads. Therefore the blade actually experiences a dynamic fatigue loading. In terms of stress, the tensile axial stress caused by the pre-load is typically about one-third of the maximum stress, while magnitudes of the stress in the blade caused by cutting

and centrifugal loads are only about 6% of the total stress [2]. The accidental loads (e.g. those caused by improper tilting or by objects caught between the blade and the back of wheels) may induce a very high stress in the blade.

One important 'load' that should be mentioned is the residual (or built-in) stress induced by the blade during the manufacturing or reconditioning process, (such as rolling, tensioning, and levelling etc.). Stresses of this nature are hard to quantify and have not been generalized mathematically. Residual stresses can be either superimposed onto the stresses caused by the external loads or they may act to cancel or reduce externally induced stress. Thus residual stresses can greatly influence the cracking behaviour of the blade.

There are two types of cracks often observed in bandsaw blades after some period of time in service (Fig.1.3). One is the so-called *gullet crack*, which is the most common and therefore the focus of this research program. It is typically located at the bottom of the tooth gullet with a length varying from 1/16 in. (1.6mm), i.e. just visible, to 1.5 in.(40mm) maximum. Another type is the *center or quarter crack* which consists of two crack tips and is contained within the blade section. These are thought to be caused by local overloading induced by wood chips traped between the blade and the back of the wheel. The probability of the center/quarter cracks can be reduced by keeping the cutting area clean.

After a gullet crack starts, it is driven by the cyclic loads and will continue to grow slowly at first, then propagate quickly into the blade up to some critical length beyond which the crack will extend in a catastrophic manner, i.e. the blade will be separated completely in the final failure. For a center or quarter crack, extension occurs from both tips of the crack into the blade until the critical crack length is reached.

Unlike problems which occur in the operation of a bandsaw system, which generally result in poor quality products (e.g. vibration of the blades), cracking of a blade also

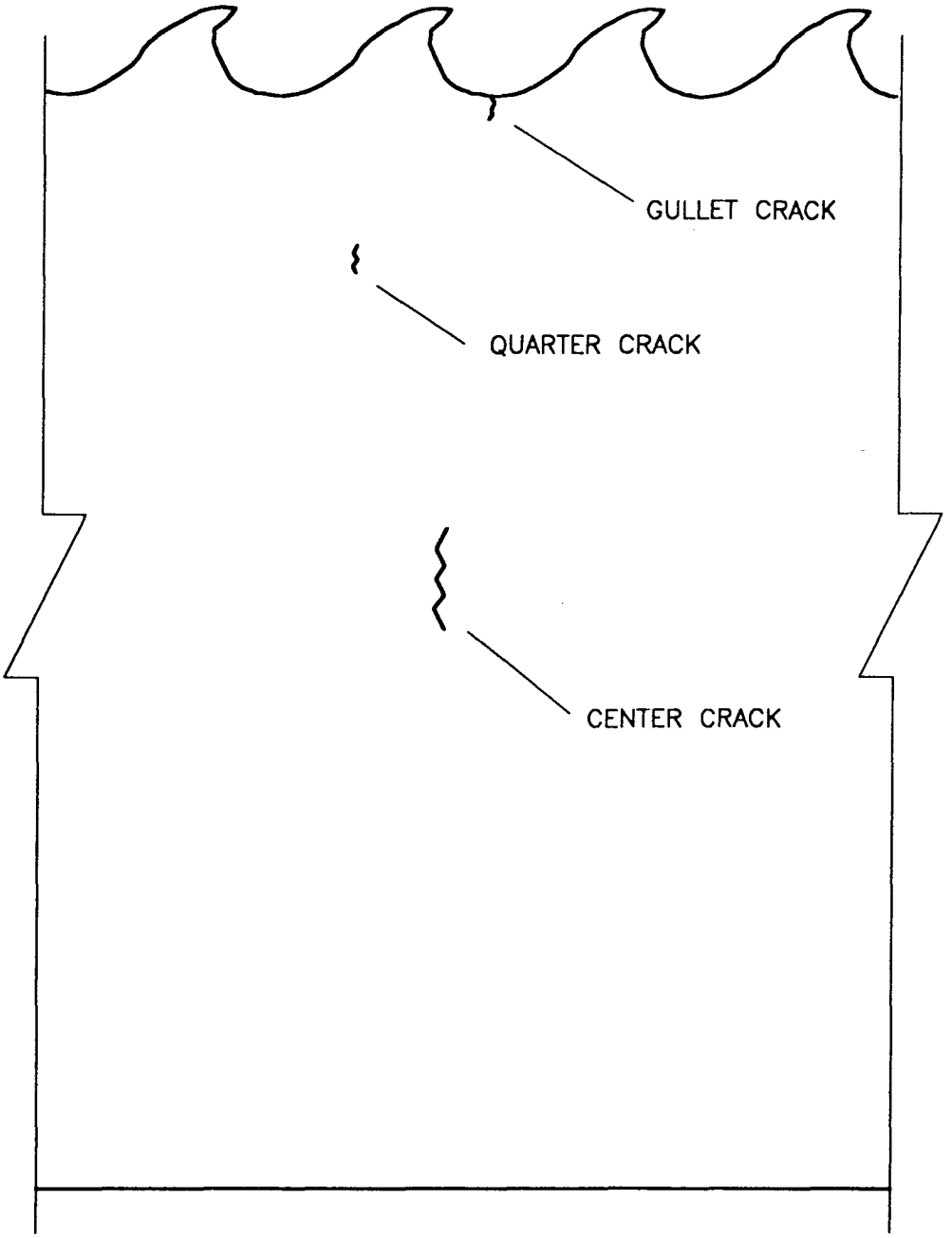

Figure 1.3: Cracks in the blade

produces damage to the blade itself. Furthermore, growth of a small crack can result in a catastrophic failure of the blade, which means not only a high operational costs (blade repair cost, and downtime etc.) but a concern for human safety. The use of bandsaw systems has increased, especially in recent years since the 'high-strain system' method was introduced to increase cutting accuracy. Cracking problems have thus become more evident. This has generated the need for a more specific qualitative and quantitative understanding of cracking behaviour in bandsaw blades.

The cracking problem is, to a large extent, beyond the traditional strength theory and failure analysis, both of which are based on a **smooth body** assumption, i.e. the conventional strength theory can not explain why a component (like a saw blade) can fail under a nominal stress far below the yield strength of the material (less than 1/3 of the yield strength). Conventional fatigue theory can not predict how a crack grows after initiation and the critical crack length for this growth. **Fracture mechanics**, a concept which has been developed since the early sixties, offers a consistent framework for understanding the cracking phenomena. Fracture mechanics theory is based on a **cracked body** assumption. A new parameter, the *stress intensity factor* (SIF for abbreviation or denoted as K), is employed to characterize the stress field around the crack tip. An associated material property, the *fracture toughness*, or its counterpart in the case of thin sheet material, the **crack growth resistance curve (R-curve)** is utilized in a fracture analysis. From a fracture mechanics point of view, final failure of a component is considered as the ultimate consequence of continuous growth of a crack which initially may be a micro crack. This growth process is first stable and then becomes unstable at a critical point, the stable part being represented by a **crack growth curve**. The fracture toughness (or R-curve) defines a critical point which is the boundary between stable and unstable crack growth. Therefore if the information concerning fracture properties for a material available, crack growth behaviour in a component made of that material can be

predicted.

The primary effort of this investigation is to employ fracture mechanics concepts in cooperation with experimentally obtained fracture properties of saw blade material to explain and predict the nature and behaviour of gullet cracks in the blade. Therefore the following are the objectives of this research program:

1. To review the current literature to critically examine the state-of-the-art in smooth and cracked body analysis techniques and information related to determining bandsaw blade integrity.

2. To identify the major loading components responsible for gullet cracking.

3. To perform experimental testing to establish the resistance curve and define the stability threshold of cracks in typically employed saw material.

4. To perform experimental testing to determine the crack propagation behaviour in bandsaw blade material subjected to representative loading conditions.

5. To provide recommendations for the development of improved prediction techniques related to blade integrity.

Chapter 2

Literature Review

2.1 Introduction

Bandsaw blade cracking problems came under examination in the wood production industry in the early 70's. Up to the present, investigators have suggested some possible causes for the problems, and some operational measures to prevent cracks from happening have been investigated. In the previous studies, the typical loads on the bandsaw blade were identified, some initial physical models were put forward, stress analysis was attempted using elasticity theory, and local stress distributions as well as stress concentration factors at the tooth gullet were investigated by both experimental and numerical modelling techniques. only limited basic mechanical properties of the material have been obtained by some researchers. Some researchers made life assessments for the blades, based on the smooth body design philosophy. However, the analysed or predicted bandsaw life were much longer than that found in practical service. Two factors could be responsible for the substantial difference between the theoretical prediction and real service life. First, there is a lack of specific information on saw blade material as manufacturers consider the material properties to be confidential. Second, and more fundamentally, there is the inherent shortcoming in the analysis based on the smooth body design philosophy. The new methods and techniques of analysis based on fracture mechanics can be considered as a more promising approach to understanding, both qualitatively and quantitatively, the nature of the cracking. To utilize these new techniques, it is essential that some basic

experimental work be carried out to obtain the important material properties related to the fracture characteristics of the material.

2.2 Component loads on the bandsaw blade

Some work has been done by previous investigators [1] [2] [6], to identify every type of load acting on the blade during its service. The following is a brief description of the results. The important point is that different loads are acting during different periods of time in each revolution. To indicate when (or at what position) each individual load acts, Fig.1.1 **Chapter 1** can be referred to, with the label **A, B,...** etc. indicating the corresponding positions.

Pre-strain Load

In order to transmit the power of the motor into cutting force, as well as to obtain high edge stability to ensure a high cutting accuracy, a pre-load, or the so-called 'pre-strain force' F is applied to the top wheel through its shaft so that a proper contact force between the circumference of the wheel and the bandsaw blade can be achieved. This tensile loading is one of the dominant loads on the blade and remains essentially constant throughout blade revolution. The tensile stress induced in the entire blade by the pre-strain loading is calculated as [11]

$$\sigma_T = \frac{F}{2tw} \tag{2.1}$$

Where

σ_T— the nominal average stress produced in the blade.

F— the pre-strain force.

w— the effective blade width.

t— the blade thickness.

Bending loads

Bending stresses found in the blade result from bending over the wheel and the support guides. These are defined below (refer to Fig.1.1 (**Chapter 1**) for specific positions):

1. Longitudinal bending caused by the wheel:

   When the blade comes into contact with the circumference of the wheel (at point **A or C'**, the stress induced in the outer and inner fiber of the band due to its bending over the wheel is

   $$\sigma_B = \pm \frac{Et}{2R_w} \tag{2.2}$$

   where

   σ_B— maximum stress induced in outer fiber (tensile) and inner fiber (compression).

   t— bandsaw thickness.

   E— Young's modulus of elasticity.

   R_w— bandsaw machine wheel radius.

   This stress remains until the blade arrives at point **C or A'** respectively.

2. Longitudinal bending caused by the guides:

   This component of loading is introduced by the offset of the guide from the unaltered path of the blade and strongly depends on the contour of the guide surface. Experience shows that the guide loading can be reduced by up to 50% if the guides are contoured properly. For example, a typical stress of 4-6 ksi (27-40 MPa) can result from guide displacement in a blade with a thickness of 0.065 in.(1.65mm) on a 5 ft. diameter (1524mm) sawmill [5]. This stress acts locally on the blade section in the blade guide region **D and D'**.

3. Transverse bending:

   This component of loading is caused by the crown-shape of the back of the wheel (given by r in Fig.1.1) as the pre-strain force is applied. It is difficult to quantify the stress level produced. However, as the curvature is relatively large, the bending stresses produced are considered to be small compared to other loading components. This loading only occurs in the blade section in contact with the wheel.

Cutting force

The parallel and normal in-plane cutting forces acting upon the teeth are, in general, proportional to kerf width (on the order of 50 lbs.(222 N) per tooth for kerf of 0.15 in.(4mm)[5]). These loads are only applied to the blade section within the cutting region (**D-D'** in Fig.1.1) and depend on the material which is being cut. Lee's study [3] shows that not only the stress produced by cutting is small but also that the stress field produced by cutting offsets from the tooth gullet. Therefore, the cutting force has a very small contribution to the gullet cracking problem when compared to the pre-strain force and bending.

Centrifugal loading

This blade stress results from the centrifugal force experienced by the moving blade around the wheel, i.e. a centrifugal force is produced when the mass of the blade is travelling on a circular path defined by the wheel circumference, a normal acceleration produces a centrifugal force which induces blade stress. This blade stress only occurs during blade-wheel contact, and generally is about 4-6% of the bending stress [2, 3] and therefore is not major factor in blade cracking. The stress caused by centrifugal force can be given by [1]:

$$\sigma_{cent} = \rho v^2 \tag{2.3}$$

where

σ_{cent}— stress produced by the centrifugal force.

ρ— density of the saw steel.

v— velocity of the blade.

Accidental loading

It should be mentioned that in actual service, bandsaw blades may experience accidental loads introduced either through improper use or adverse operating conditions. For example, a typical overload condition may result from an object becoming temporarily trapped between the wheel surface and the blade. This can greatly increases the blade stress level. It is clear that this type of loading happens in a random manner, and its probability can be reduced by proper maintenance and operation. No attempt has been made to consider this effect on blade integrity in this research.

2.3 Simplification of the loads

In recognition of the relative magnitudes of the various types of applied loads, the load condition experienced by a blade have been idealized by considering only the two most important loads in following experimental tests and calculations, these loads are:

- the pre-strain force obtained by equation (2.1)
- the longitudinal bending caused by the wheel, obtained by equation (2.2)

Loads other than the above two are ignored because of either their insignificance in magnitude or their random nature. The static measurements made by Eschler [6] (Fig.2.4) can be used to support the validity of this simplification.

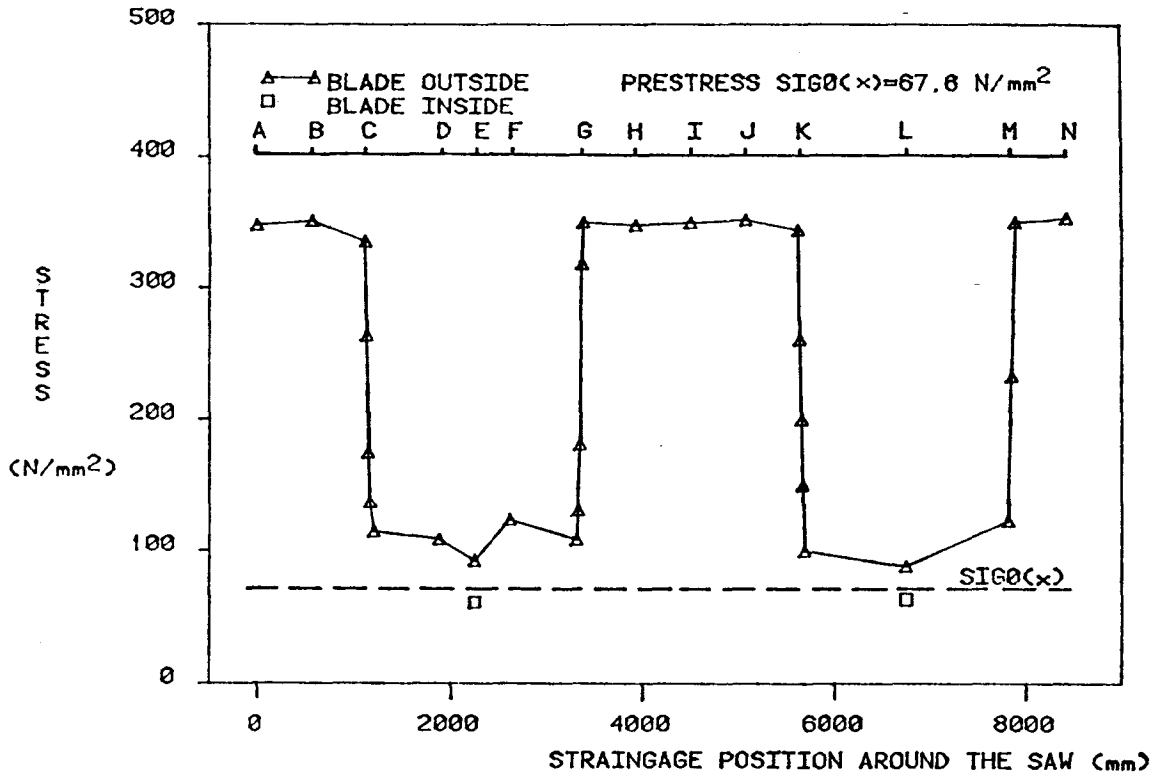

Figure 2.4: Stress in the blade: Eschler's work [6]

2.4 Stress concentration factor at the toothed edge of the blade

It is common knowledge in engineering practice that a local stress field will be severely distorted when a notch is introduced into an originally regular section having an uniform stress field. The magnitude of the stress at a certain part of the edge of the notch will rise sharply to multiples of the uniform stress level. This feature can be described by a ratio between maximum stress at the edge of the notch and nominal stress. The ratio is called the *stress concentration factor* (or SCF). In a bandsaw blade, hundreds of teeth are punched out on one or both sides of the strip of raw material, thus a stress concentration exists at every tooth gullet when the blade is loaded. The very high stress concentration at the gullet bottom is considered to be one of the many factors which are responsible for blade cracking.

In 1965, experimental tests on a blade were conducted by Jones [4]. His static photoelasticity results show that under a pure tensile load the SCF near the gullet region ranges from 1.5 to 2.5, and reaches its maximum at the bottom of the gullet. Different tooth profiles have an appreciable effect on the stress concentration (Fig.2.5).

In 1988, a finite element analysis was conducted by Lee et al [3] to quantify the local stress distribution near the gullet region. Their results show that under a pure tensile loading, the SCF is about 2.35 for the tooth profile studied. Lee et al also proposed two methods to modify the geometry of the gullet region—'shaving' and 'flattening' the gullet region— to reduce the SCF. Approximately 21% reduction was achieved.

As indicated in their report, the amount of material around the gullet region available for shaving and flattening is very limited and the overall performance of the blade must be taken into account since removal of material from the bottom of the gullet weakens the tooth and reduces its stiffness.

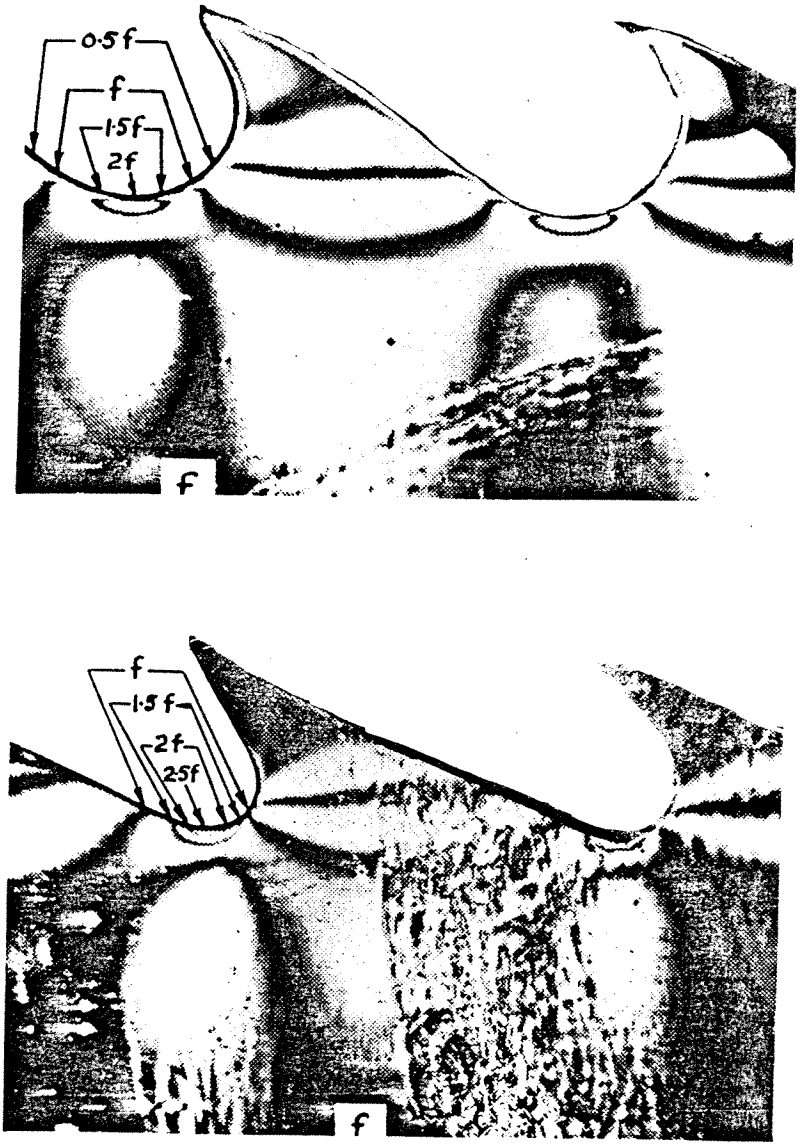

f= Nominal uniform stress at two boundaries.

Figure 2.5: Stress concentration at the gullet region: Jones' work [4]

2.5 An approximation of stress concentration factor for a blade

In the previous research work [1, 4, 2, 3], the difference between SCF's under pure tension and pure bending loads were not mentioned. In some investigations [1, 2], the SCF for a pure tension load was directly used for the assessment of fatigue life of saw blades. However, theoretical research [21] shows that SCF's are very different under pure tension and pure bending loads even if the geometry of the components are identical. In the case of the bandsaw blade, in one revolution a blade experiences two different load conditions, a pure tension and a combination of tension and bending. Therefore, a separate treatment of different SCF's is not only necessary but especially important for crack propagation studies.

The combined SCF at the blade tooth can be approximated by using the SCF's at the edge of an elliptical hole in a infinite plate subjected to tension and cylindrical bending respectively. The following outlines the details of this analysis. If it is assumed that the maximum stress produced by stress concentration is still within elastic region, the superposition of the loading can be applied. Therefore, at the gullet bottom of the tooth of a blade, the maximum stress should be identical if calculated in two different ways, i.e.,

$$k_T\sigma_T + k_B\sigma_B = k_{T+B}(\sigma_T + \sigma_B) \tag{2.4}$$

Rearrange the equation,

$$k_{T+B} = k_T(\frac{\sigma_T}{\sigma_T + \sigma_B}) + k_B(\frac{\sigma_B}{\sigma_T + \sigma_B}) \tag{2.5}$$

Where

k_T—SCF under pure tension load (reference stress σ_T).

k_B—SCF under pure bending load (reference stress σ_B).

k_{T+B}—SCF under combination of tension and bending load (reference stress (σ_T+σ_B).

σ_T—nominal tensile stress produced by pre-strain force.

σ_B—maximum bending stress produced by the wheel.

From the above equation, it can been seen that the SCF for the combined stress condition depends on both the tension and bending loads. Therefore a conclusion can be made that Lee and his co-workers' result [3] of combined SCF is only valid for the specific load magnitudes used. For the same wheel radius, the combined SCF should be different for the different pre-strain forces which range from 20,000 to 13,000 lb.. Therefore a separate treatment of the SCF's for tension and bending seems more convenient.

The SCF at the edge of an elliptical hole in an infinite plate

In order to approximate k_T and k_B at the gullet region of a saw blade, the standard formula for SCF at the edge of an elliptical hole in an infinite plate can be used [21] (see Fig.2.6). For a pure tension load, the saw tooth can be approximated by an elliptical notch at the edge of a half infinite plate, whose SCF can be obtained by multiplying the SCF for an infinite plate by factor of 1.12, this being the free edge geometry factor which is usde in stress-intensity-factor (SIF) calculation [9]. For the bending load, this factor is 1 [27].

SCF for a elliptical hole — tensile load

The stress concentration factor for an infinite plate with elliptical hole subjected to tensile load is following (see Fig.2.6),

$$\frac{\sigma_{Tmax}}{\sigma_T} = (1 + 2\frac{h}{l}) \tag{2.6}$$

Where

σ_T—far field stress level.

σ_{Tmax}—peak stress at edge of the elliptical hole.

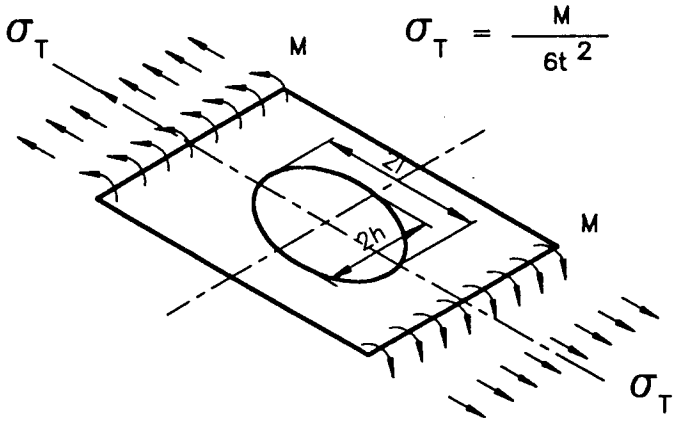

Figure 2.6: SCF at a elliptical notch

l—half major axis.

h—half minor axis.

SCF for a elliptical hole — bending load

$$\frac{\sigma_B}{\sigma_{Bn}} = 1 + \frac{2(1+\nu)(1-m)}{(3+\nu)(1+m)} \tag{2.7}$$

Where

σ_B— peak stress at edge of the elliptical hole.

σ_{Bn}— maximum nominal stress produced by bending moment.

m—$(l-h)/(l+h)$. l and h are defined as in Fig.2.6

Assessment of SCF for a bandsaw blade

In order to show the effectiveness of equation (2.5), Lee's results were used for comparison.

Consider the standard formula of SCF for and elliptical hole in an infinite plate subjected to far field tension (eqn.(2.6)), an equivalent l/h ratio for a blade tooth profile can be obtained. In Lee's analysis, $k_T = 2.35$. From equation (2.6), $k_T = (1+2h/l)1.12 = 2.35$, the equivalent ratio can be obtained as $h/l = 0.55$. By inserting this ratio into equation (2.7), We have $k_B = 1.43$. Finally, the equation (2.5) can be used for the combined SCF, i.e. $k_{T+B} = 1.68$. There is virtually no difference between the above result and Lee's. This example shows that as long as k_T for blade is known, which is relative easy to obtain, k_B and k_{T+B} can be easily assessed by equation (2.7) and (2.5) for specific load conditions.

2.6 Two approaches to the fatigue cracking problem

There are two basic approaches in both design and failure analysis to deal with cracking problems. One is the so-called *smooth body* approach—a conventional method very well

documented in reference [8]. The other is the *fracture mechanics* approach or *cracked body* approach.

Smooth body approach

This approach makes no assumptions about crack length in the specimen or component studied. A very important phase in crack behaviour, i.e. *crack propagation*, can not be quantified. The information for this approach is based on the data obtained by testing standard small polished specimens (e.g. Goodman Diagram and S–N curves). Further modifications counting for surface conditions and stress concentration etc. are made by applying modifying factors. In this approach the Goodman diagram is often used. A Goodman diagram is constructed by plotting stress amplitude versus mean stress for failure at 2×10^6 cycles (equivalent 97.5 hrs for 5.7 Hz. used in this research). Generally the data for the Goodman diagram is obtained by testing standard small, smooth specimens, and should be modified accounting actual surface conditions and the SCF of the component studied from which a reduced Goodman diagram can be obtained. The reduced Goodman diagram can be used to predict, with a desired safety factor, maximum stress amplitude the that material can sustain at a certain mean stress without fatigue failure.

Ingema's work [1] is a typical treatment of this kind. He modified the Goodman diagram by considering a) surface condition; b) stress concentration factor; and c) residual stress. Ingemar's approach is based on achieving an infinite life of two million cycles, which is unlikely to be achieved in practice. It is difficulty to use the safety factor he obtained to explain an actual failure in more specific details.

Lehmann [5] made use of the Allene's modified Goodman diagram [10] and S–N diagram to do a life prediction. He predicted 18.7 hours of blade life in the case considered, which was an improvement on Ingemer's and Allene's work, but is still far longer than the actual blade life, which is sometimes less than four hours. Although smooth body theory predictions can be made close to the actual life of the blade by including every

factor which is likely to be involved, there are some fundamental questions which can not be answered using smooth body theory, for example, why in practice, a blade actually still can carry on for a period of time after a crack occurs, which means that the blade can tolerate a certain length of crack. Actual existence of cracks in a working blade raises another question, i.e. what is the critical crack size which a working saw blade can tolerate and how long it takes for a crack to reach this critical size. All these questions are beyond smooth body theory. On the other hand, the fracture mechanics based fatigue theory can give quantitative answers to these questions and can offer a consistent framework to understand and quantify the blade cracking process.

Fracture mechanics approach

Fracture mechanics is based on the assumption of cracked body. The focus is on the behaviour of a crack in the body or component being examined. The assumption is that once a crack is initiated, it will extend due to cyclic fatigue in a stable manner until some critical crack length is reached beyond which the cracked body will fail catastrophically. Failure is ultimately a consequence of a continuous propagation of an initial smaller crack. In fracture mechanics the cracking process is divided into three phases : a) crack initiation, i.e. a very short crack occurs ; b) crack propagation. the initial crack will grow due to some external cyclic loading. (stable growth); c) failure. when the critical length is reached, the crack will extend in an unstable manner until the component is separated.

The key concept in fracture mechanics is the *stress intensity factor* (SIF) [9] which is defined by a combination of characteristic stress, crack length and geometric parameters (for example, an infinite plate with a transverse crack of length a is subjected to a uniform stress σ at far boundary parallel to the crack, the stress intensity factors at both its crack tips are $K = \sigma\sqrt{\pi a}$). The stress intensity factor is a parameter which characterizes the stress field at the tip of the crack and is a measure of intensity of the

stress field at the crack tip. Based on the concept of a SIF, a material property, **fracture toughness** (denoted as K_{IC}), has been proposed for a material to measure its ability to resist cracking. From the fracture toughness the critical crack length or critical load can be predicted for a specific case.

In the case of fatigue propagation of cracks, the *stress intensity factor range* (denoted as ΔK) is the proposed parameter, which characterizes the stress field at the crack tip under cyclic loading and controls the crack growth rate during the propagation stage of the cracking process.

In 1988, Lehmann [5] tried to apply fracture mechanics to explain cracking in the blade. He predicted the critical crack length and life-time of the blade under assumed conditions. The predicted critical crack length is 0.11 in.(2.8mm) and blade life-time ranges from 2.2 to 23.7 hours depending on the surface roughness. The predictions are encouraging. It is worth mentioning that in his analysis he assumed that the surface roughness measurement, center-line-average (CLA), is the average dimension of micro-cracks produced by the re-sharpening process, therefore CLA can be treated as the initial crack length. The surface condition, therefore, could be well defined and introduced as a quantity into the cracking analysis.

The weak point of his analysis, as he himself noted, was the lack of experimental information, especially that related to the cracking process. For example, he employed a plane strain K_{IC} of AISI 4340 steel for the bandsaw blade material and had to use the general material crack growth rate for crack propagation calculations. In fracture mechanics theory, if a crack length is on the order of the surface roughness, the propagation behaviour is much more complicated, and crack propagation behaviour may take a very different form from that assumed by Lehmann [9]. These factors prevented his analysis from being used to develop more detailed and useful predictions.

Crack resistance curve (R-curve): plane stress condition

Previous research [9] has shown that within the so-called *Linear Elastic Fracture Mechanics* (LEFM) framework, a crack behaves differently under a *plane stress* condition from that under *plane strain*. Under a plane strain condition the crack growth resistance (in terms of SIF) is essentially constant, independent of crack length, and can be conservatively estimated by a single parameter, K_{IC}. In contrast while under a plane stress condition the crack growth resistance increases as crack length increases. This difference shows its influence more clearly in the dynamical aspect of critical crack length and crack propagation. In the case of thin sheet materials, e.g. saw blades (sometimes as thin as 0.065 in. (1.65mm) in thickness), a plane stress condition exists. Therefore, the fracture resistance can be described fully only by a *crack resistance curve* (**R-curve**) which can be applied to predict the instability condition of crack growth.

In 1961, Krafft et al [13] postulated as a working hypothesis that *for a given material and thickness, there is a unique relationship between the amount of stable crack growth and the stress intensity factor applied to the structure, this relationship being the crack growth resistance curve or R-curve.* A significant amount of work conducted since then has been devoted to the development of experimental methods intended to verify this hypothesis. ASTM E561 standard [14], in which the above hypothesis has been adopted, has been established for determination of a material R-curve.

In this research program, in order to understand and quantify the behaviour of gullet cracks in bandsaw blades, fracture mechanics theory is employed to guide experimental tests to obtain various properties regarding cracking behaviour, such as the crack growth resistance curve ,or *R-curve*, for bandsaw steel, its crack initiation and crack propagation rates, which are not currently available. Once all the above information is available, failure analysis and bandsaw life predictions are made. It is also expected that this investigation can offer more useful information for further studies into the cracking problem

in bandsaw blades.

Chapter 3

Material Property Determination—Strength and Fracture Resistance

3.1 Introduction

Currently, little information is available on the causes and quantitative treatment of cracking in bandsaw blades. Certain data, such as the chemical composition and mechanical properties of blade steel are considered to be confidential by manufacturers. material properties, such as the critical stress intensity factor or crack growth resistance curve, according to this author's survey, are not available at all. There have been some independent investigators who have experimentally obtained some chemical compositions [5] and basic mechanical strength properties [1]. However, in order to collect first-hand information about the material used in this research, its chemical composition was obtained via an independent analysis [7]. A series of tests were also performed to obtain the yield strength and ultimate strength of the bandsaw material.

As discussed in **Chapter 2**, in the case of thin material, fracture resistance can be fully described only by the crack growth resistance curve. For bandsaw blade thicknesses of about 0.1 in.(2.5mm), an entire R-curve is necessary to obtain complete information related to its fracture behavior.

There are several different methods recommended in ASTM E561 [14] to determine the R-curve for the material. The displacement control and CLWL (Crack-Line-Wedge-Loaded) specimen method were chosen because of the relative ease of control. In this testing, a series of three specimens were employed to minimize uncertainty in the results.

The chemical composition of the bandsaw blade steel
(In Percentage)

Elements	C	Cu	Cr	Ni	Si	Mo
Contents	0.38	0.15	0.16	2	0.23	0.01
Elements	Mn	V	Al	Ti	P	S
Contents	0.35	<0.01	<0.01	<0.01	0.05	0.05

Table 3.1: The chemical composition of saw steel

This chapter is devoted to the experimental work used to determine the saw steel strength and crack growth resistance properties.

3.2 Bandsaw material composition

The chemical composition of the saw blade steel used in this research have been analyzed by an independent institute [7] and are reported in Table 3.1. The composition is, as Lehmann noted [5], close to that of AISI 4340 steel.

3.3 Strength properties determination

It has been noted by some researcher that saw steels from different manufacturers are similar both in composition and mechanical properties [5]. In order to have first-hand

information regarding the mechanical properties of the blade material used in this research, tests on the saw steel were conducted. The following is the brief description of this testing.

Specimen

Ten rectangular specimens were cut from a used blade in such a way that the long side of each specimen is parallel to the rolling direction (Fig.3.7). The dimensions of the specimens are shown in Fig.3.8. Therefore the properties obtained relate to the rolling orientation of this material.

Equipment, test and results

The tension tests were performed on a Tinius Olsen testing machine. The load-strain curves were automatically recorded by the built-in Model 51 electrically driven recorder. The strain was monitored by a S-1000-2A series clamp type extensometer, and the electrical signal was sent to the recorder. The yield strength was determined by the 0.2% strain offset method. The test results are shown in Fig.3.9

The average yield strength was found to be 184 ksi.(1270 MPa), with a standard deviation of 9.49 ksi.(65.5 MPa) The average ultimate strength was found to be 206 ksi. (1420 MPa)), with a standard deviation of 2.21 ksi. (15.2 MPa). The Young's modulus was found to be 26650 ksi.(184000 MPa). The above results agree closely with the results by Porter, i.e. a yield point of 179 ksi.(1230 MPa), 207 ksi.(1430 MPa) of the ultimate strength [2].

3.4 R-curve experimental tests

R-curve establishment is based on an energy balance concept. According to the energy balance concept [9], there is a continuous balance between released and consumed energy during slow stable crack growth. In other words, a stable-cracking event occurs only when

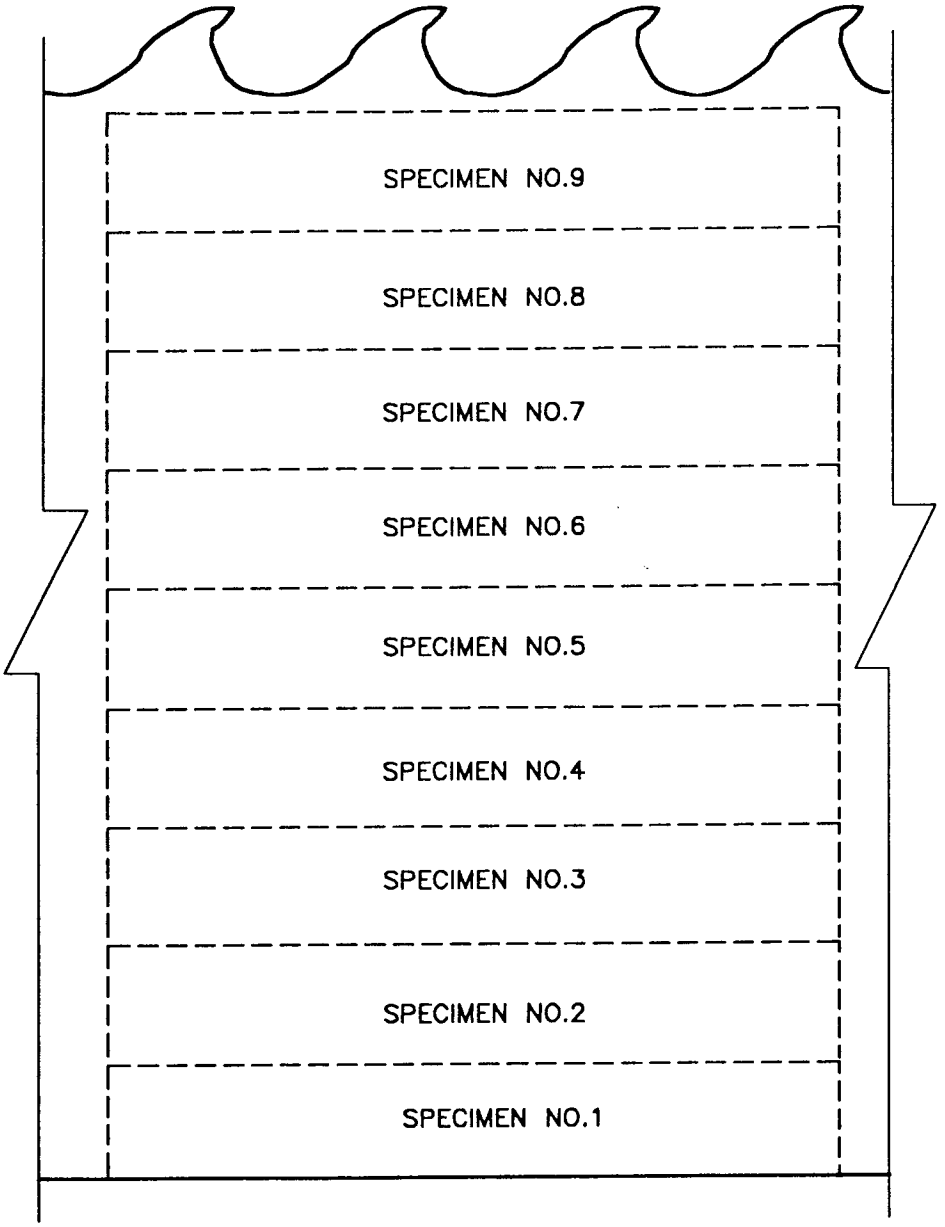

Figure 3.7: Orientation of the specimens in the blade

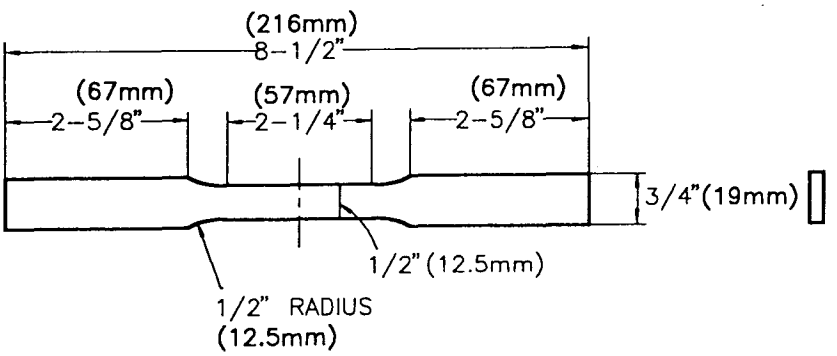

Figure 3.8: The geometry of a specimen for a strength test

the energy supply rate from the stress field around the crack tip is just enough for the energy demand rate for material cracking. Therefore the energy consumed rate represents a material ability (or its toughness) to resist cracking. If there were no balance, then either crack growth would arrest or become unstable. Consequently, during slow stable crack extension, the energy release rate equals the energy consumption rate at the crack tip. The instantaneous values of the energy release rate will indicate how the energy consumed rate depends upon crack size and applied stress. An R-curve is a continuous record of the toughness development in terms of R_r plotted against crack extension in the material as a crack is driven in a stable manner with a continuously increasing stress intensity factor, K.

In principle, there are two methods to deliver crack extension force to the material. One is the *load control* method, the other is the *displacement control* method.

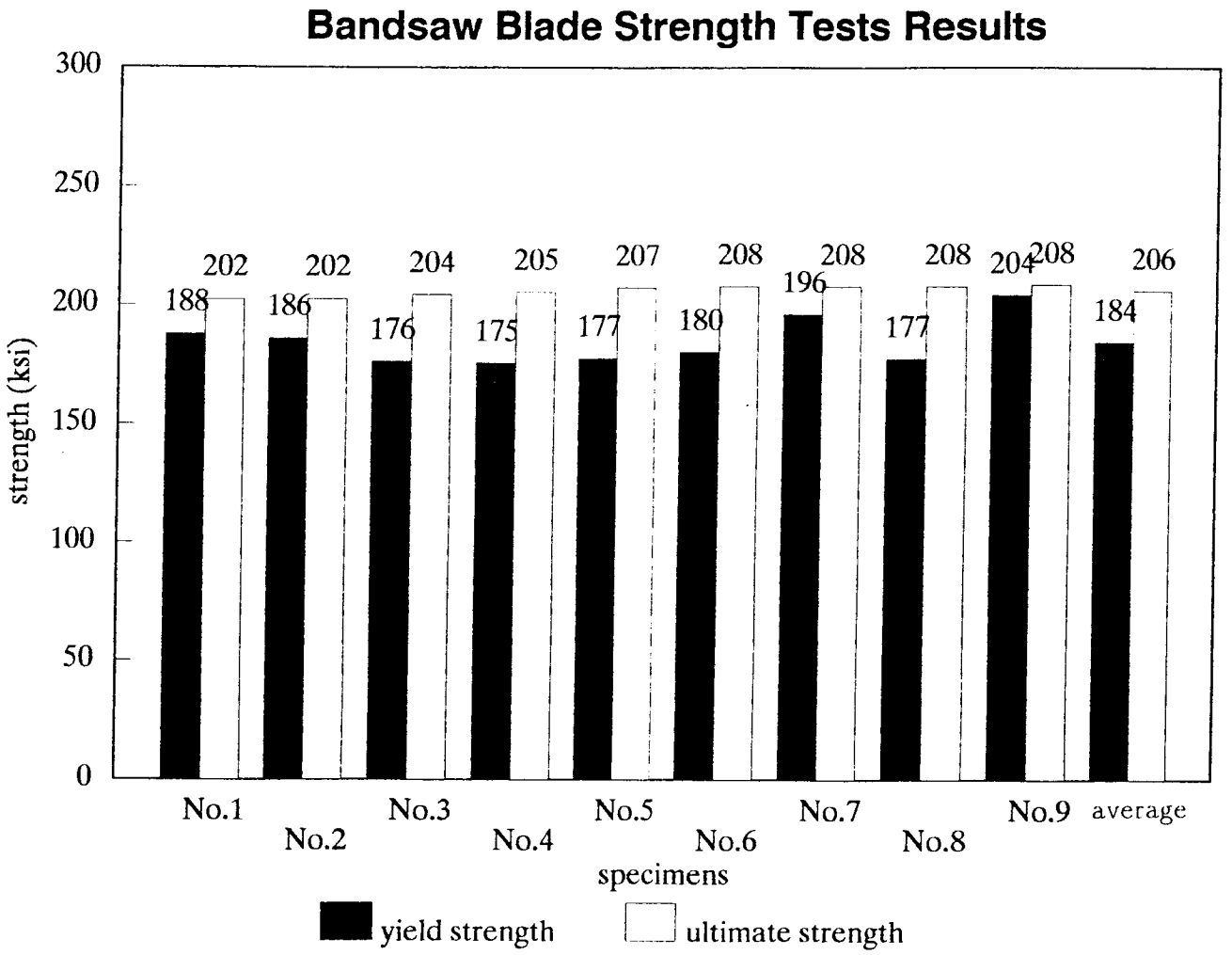

Figure 3.9: Test results of strength for 9 specimens

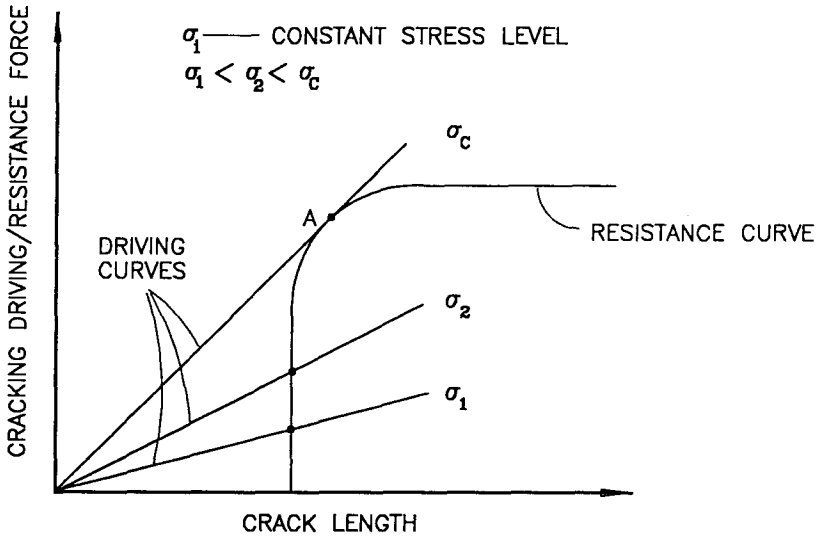

Figure 3.10: Critical condition in load control case

Load control method

In this method, the load is controlled and the corresponding crack length at various points are obtained. This method usually uses a machine with a closed-loop feedback control. A constant load, however, is still very difficult to maintain. Also, the data points beyond a certain point A can not be obtained. (Fig.3.10).

Displacement control method

In this method, the specimen crack opening displacement is controlled and the corresponding load and crack length are monitored over the range of interest.. The advantage of this method is that the displacement control is achieved easily and every point is stable. Therefore, the entire R-curve can be obtained (Fig.3.11). The experimental test method employed in this research is of the displacement control type.

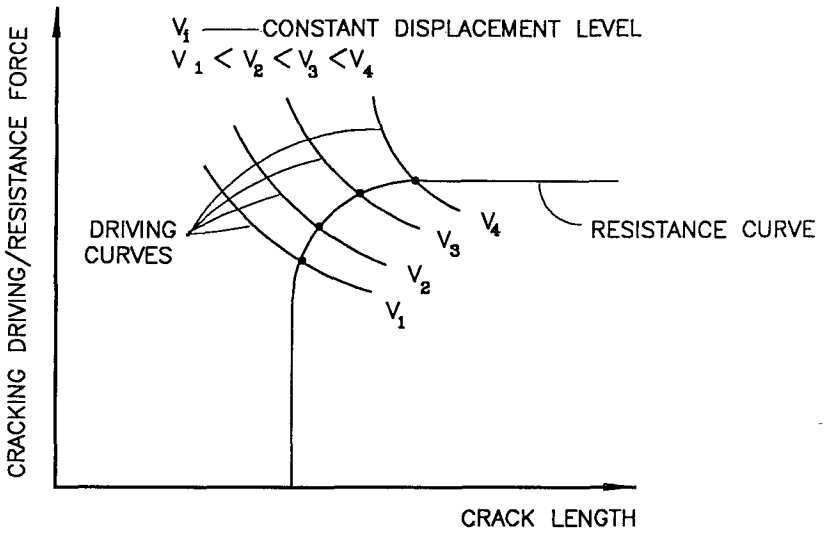

Figure 3.11: Critical condition in displacement control case

3.4.1 Specimens and material

To perform the R-curve tests, an ASTM E561 [14] standard CLWL specimen was used. CLWL is the abbreviation for Crack Line Wedge Loaded which is shown in Fig.3.12. The specimen is designed such that it can be loaded at point A and B on a horizontal base with a vertical wedge. This loading mechanism has several advantages 1) it is easy to achieve displacement control; 2) it eliminates machine stiffness involvement; and 3) it is easy to prevent the specimen from buckling when the load is high. A starting notch, 1/16in.(1.6mm) wide, was made by saw cutting. The specimens were the pre-cracked up to 0.35 to 0.45 times the specimen width by cyclic tension loading on a Sonntag fatigue testing machine.

The specimens were made from a strip of new bandsaw blade (not toothed) with a thickness of 0.073 in (1.85mm) in the as-received condition, having the chemical composition and mechanical properties as shown in the previous section of this Chapter.

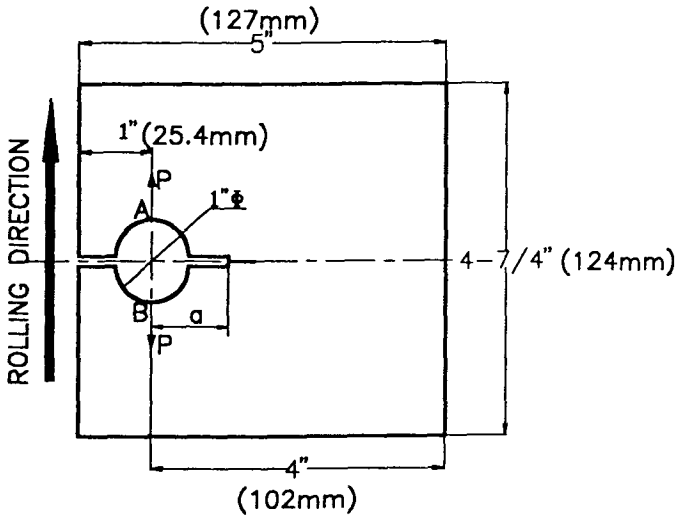

Figure 3.12: Geometry of CLWL specimen

3.4.2 Cracking opening devices and fixture

Corresponding to the CLWL specimen configuration, a special set of loading fixtures are needed. The basic idea is 1) to obtain displacement control; 2) to prevent the thin specimen from buckling. To this end, a loading system was designed and constructed, which consists of several parts as follows.

Die and cover plates

To hold the specimen in a horizontal position, a massive mild carbon steel die was designed to serve as a base (Fig.3.13). Its stiffness minimizes its deformation when the specimen is loaded, and its weight ensures stability of the system when the test is in progress. A group of parallel groves were cut in its top surface to hold the lubricant and to reduce the direct contact area between the specimen and die surface so as to minimize the friction which may induce some uncontrolled loading onto the specimen.

To keep the specimen from buckling under high loading, a pair of cover plates were

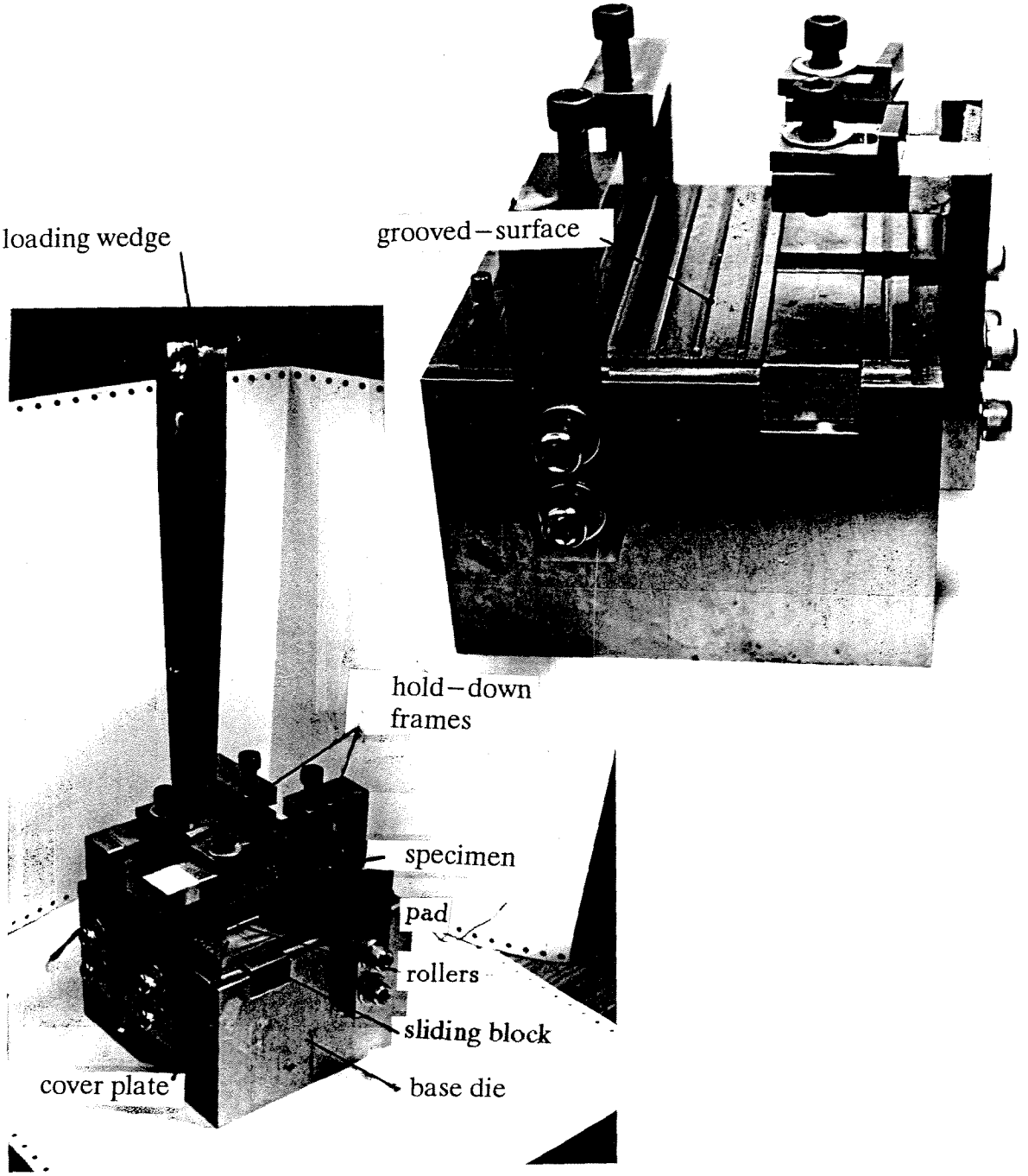

Figure 3.13: The loading system for CLWL specimen

employed (Fig.3.14). The cover plates were held down onto the loaded specimen through rollers and pads by five holding frames so that the necessary pressure was maintained to prevent the specimen from buckling while leaving the covers free to move laterally with the specimen to reduce friction between the contact surfaces.

Loading system

In this system, the crack loading is accomplished by using the loading wedge and two sets of small dies (Fig.3.14). The wedge was hardened and lubricated, with a total taper angle of 3 degrees on its working sides. To maintain an accurate load line as an angle between the crack surfaces becomes larger when the specimen crack extends, two sets of intermediate dies were designed and constructed. One pair consists of circular segments which make contact with the specimen, while the other pair has one of its surfaces relieved, which contacts with the working sides of the wedge. The vertical load on the wedge is transmitted through the contacts between dies providing a horizontal force acting at the loading points A and B on the specimen via the circular segments.

3.4.3 Double-calibration method

The information required to establish an R-curve from experimental data includes a) the current crack length ; b) the corresponding loads. For the CLWL specimen and the wedge loading system discussed above, the current load value must be obtained via an indirect method, i.e. calibration. The current crack length can be obtained by either direct monitoring or calibration. In this research, both monitoring and calibration were employed to obtain the crack length so that the results could be checked against or compared with each other, while the current loads were obtained by calibration.

The calibration relationship between the relevant quantities must be obtained by one of three methods:

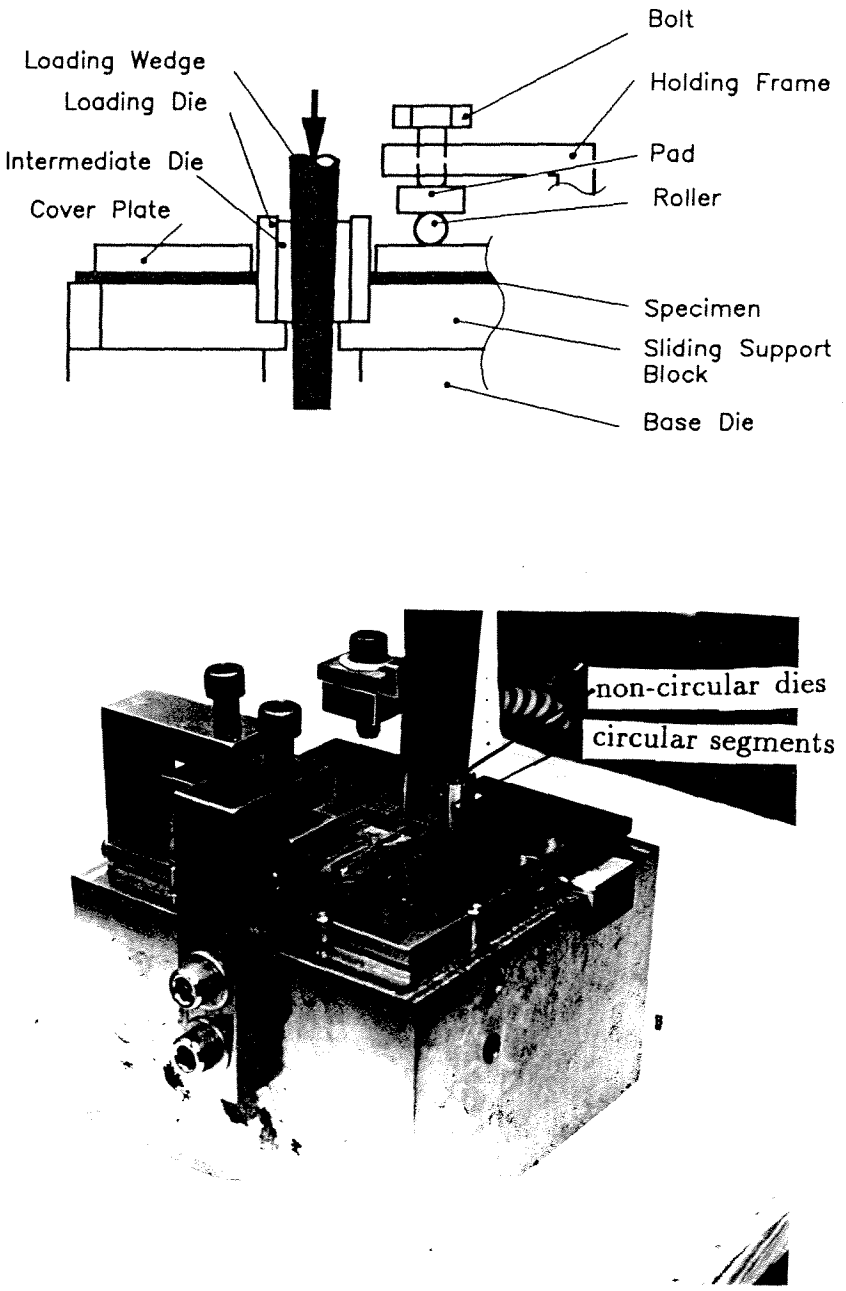

Figure 3.14: Loading wedge and dies

- analytical method (if mathematically possible)
- numerical method
- experimental method

Because of its complex geometry (especially its discontinuity at the boundaries), a closed-form solution is not available, therefore a finite element approach was employed to numerically obtain the physical quantities necessary for the calibration relations. An experiment was also conducted to confirm the finite element results.

3.4.4 Establishment of the calibration relations

The physical quantities for calibration relations

The calibration relationship is the relationship among relevant quantities in the form of dimensionless groups. How to choose the quantities largely depends on the particular case. For the CLWL specimen configuration, the quantities which are ultimately required are load P and crack length a. The experimental quantities used to determined these quantities can be the crack open displacement (COD), strains at particular locations on the specimen or some other relatable quantities. The COD related calibration relations are available in ASTM E561 [14]. However, when the specimen is large, acquisition of the COD information requires large clip-gauges which are more sensitive and more easily disturbed. Also, the large clip-gauges will present more difficulties for installation in a very limited space. In contrast to the COD, strains at chosen locations are much easier to obtain and handle. Also, common strain gauges are accurate enough to make the information more reliable. Therefore, in this research the strains at particular locations and orientations were used as calibration quantities, i.e. the calibration relations are accordingly strain related. Fig.3.15 shows the locations and orientations where the strains were measured.

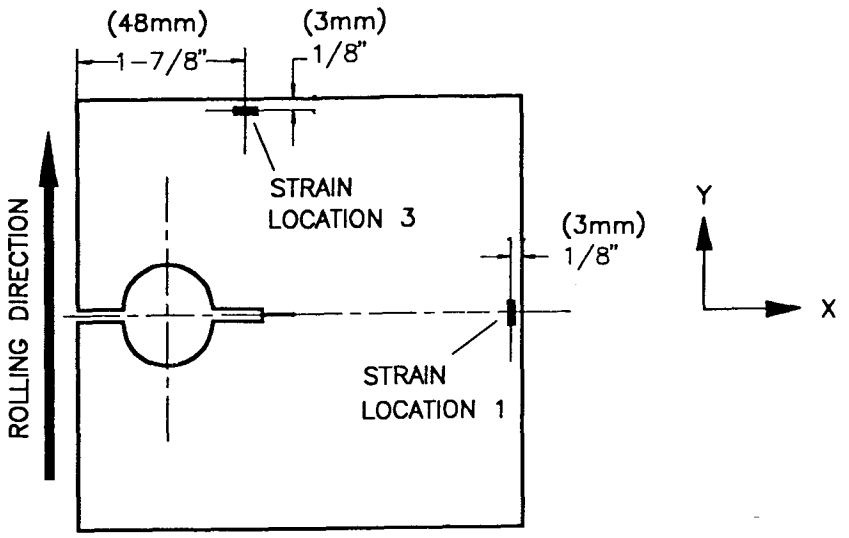

Figure 3.15: locations and orientations of strains

Mathematically, in order to determine the two unknowns, P and a, at least two equations are required, while to establish the two relations, two strains e_1 and e_3 are required. Based on the assumption that the specimen under load remains elastic, the following relationships are valid:

$$f(\frac{EBWe_1}{P}, \frac{a}{W}) = C_1$$

$$f(\frac{EBWe_3}{P}, \frac{a}{W}) = C_2$$

where

e_1— strain in Y direction at location 1.

e_3— strain in X direction at location 3.

B— thickness of the specimen.

P— symmetrical force acting at point A and B.

E— Young's elastic modulus.

C_1, C_2— constants, their values depends on the particular specimen.

The above equations can be expressed in more convenient way as follows:

$$\frac{EBWe_1}{P} = f_1(\frac{a}{W})$$

$$\frac{EBWe_3}{P} = f_2(\frac{a}{W})$$

Obtaining a ratio between the two strains e_1 and e_3 provides a further relationship:

$$\frac{e_1}{e_3} = \frac{f_1(\frac{a}{W})}{f_2(\frac{a}{W})} = f(\frac{a}{W})$$

Among these three equations, only two are independent. In R-curve determination, any two can be used as calibrating relationships to determine the crack length a and load P.

To evaluate the above equations for the specific CLWL specimen, data is required. This data includes:

1. The geometry and properties of the specimen i.e. W, B, elastic modulus E and load P. These are all given for the CLWL specimen.

2. The crack lengths corresponding to strains e_1 and e_3 over the range of crack growth. These are to be found either numerically or experimentally.

Numerical results—finite element method

In order to define the calibration relations, a finite element model was used to solve the problem numerically. The finite element method [20] (FEM) is a numerical procedure for discretizing continuum problems in order that they may be solved on digital computers. This method models a structure as an assemblage of small parts (elements). Each

element has a simple geometry and is therefore much easier to analyze than the structure. In essence, a complicated solution consists of a series of piecewise-continuous simple solutions. Elements are called "finite" to distinguish them from differential elements used in calculus. This model was implemented using the software program **ANSYS**[26] and was used in establishing the calibrations required in the R-curve test.

In the FEM modelling, the following assumptions were made:

1. The specimen is in plane stress.

2. No plastic deformation occurs.

In order to achieve the desired accuracy within a reasonable computing time, only the area where the strains e_1 and e_3 are located were densely meshed. In this model a load P=10,000 lb.(44.5 kN) was applied at point A and B. Young's modulus is 26000 ksi. (184000 MPa) as experimentally obtained. The strains e_1 and e_3 were calculated for 12 different a/W values covering a range from 0 to 0.60 so that it was easy to establish the entire curves. The final results were then least square fitted as follows:

$$\begin{aligned}\frac{e_1}{e_3} &= 114.08 - 2125.79(\frac{a}{W}) + 4439.79(\frac{a}{W})^{1.5} - \\ &\quad -5365.63(\frac{a}{W})^{2.5} + 4530.35(\frac{a}{W})^{3.5} - \\ &\quad -1591.79(\frac{a}{W})^{4.5} \end{aligned} \tag{3.8}$$

$$\begin{aligned}\frac{EBWe_3}{P} &= 10.30 + 163.24(\frac{a}{W}) - 63.70(\frac{a}{W})^{0.5} - 137.48(\frac{a}{W})^{1.5} + \\ &\quad +33.85(\frac{a}{W})^{2.5} \end{aligned} \tag{3.9}$$

Calibration relations—experimental results

Experimental measurements were conducted as confirmation of the FEM results. These experiments were performed using three identical specimens cut from the same band strip as the CLWL specimens for the R-curve testing. The Sonntag fatigue test machine was utilized to provide the load since it could be controlled manually. A special loading fixture (Fig.3.16) was designed and constructed to accommodate the specimen to the Sonntag. Two 300 ohm foil-type resistance strain gauges, a multi-channel switch box and a strain indicator were used to measure the strains at the required points.

The load levels were set manually through the scaled loading bolt in the machine, while the different crack lengths were provided via saw cutting. The whole process was controlled manually, i.e. load setting, crack cutting and strains recording. The procedure was the same for each crack length, i.e.

1. saw cut the crack to a desired length.

2. load the specimen to the desired level.

3. take the strain readings.

4. remove the specimen, and cut the new crack length...

Three different load levels were chosen for each crack length and three specimens were used to minimize the uncertainty of the data. Nine different crack lengths were measured for each specimen. The mean of the values for each crack length was used for the least-square fitting. The final fitted formulas are as follows:

$$\frac{e_1}{e_3} = 1.018 - 4.999(\frac{a}{W}) + 17.380(\frac{a}{W})^2 \tag{3.10}$$

$$\frac{EBWe_3}{P} = 2.686 + 2.172(\frac{a}{W}) \tag{3.11}$$

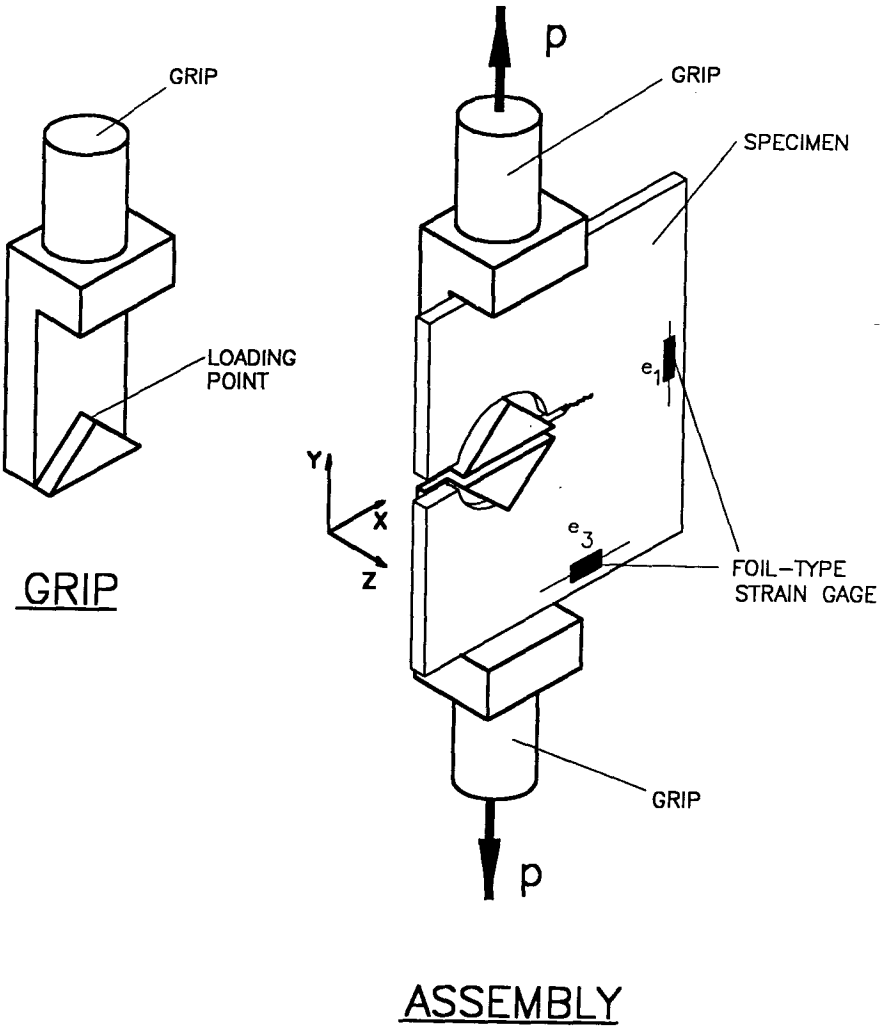

Figure 3.16: Fixture, specimen and sensor devices for experimental calibration

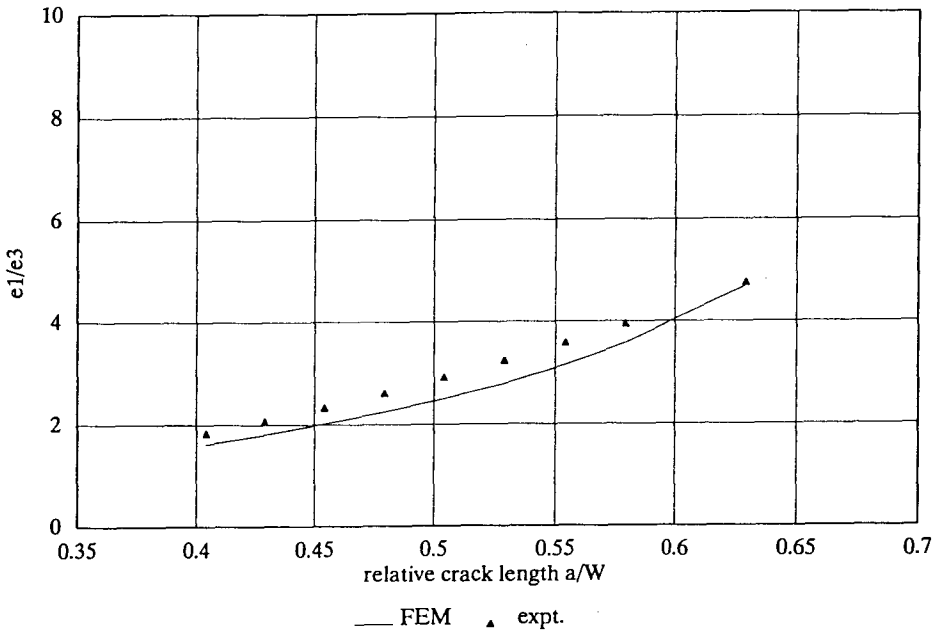

Figure 3.17: FEM vs experiment—e_1/e_3 calibration

The graphical representations are shown in Fig.3.17 and Fig.3.18. The equations (3.10) and (3.11) are valid for a/W range from 0.42 to 0.62.

Calibration results—FEM vs experiment

Fig.3.17 and Fig.3.18 show the comparison between the calibration curves from the FEM prediction and via the experiments. It is clear that e_1/e_3 curve for the experimental measurement is slightly higher, while the $EBWe_3/P$ curve the experimental calibration is slightly lower. These offsets may have been caused by some kind of system error on the data of the strain at location 3 (e3). If the data of strain at location 3 (e3) are corrected by a factor of 0.88, the difference between two sets of curves will disappear. The crack lengths obtained from the FEM calibration relation show agreement with the direct measurement results (Fig.3.21) and were, therefore used in the subsequent computations to establish the R-curve of the bandsaw material.

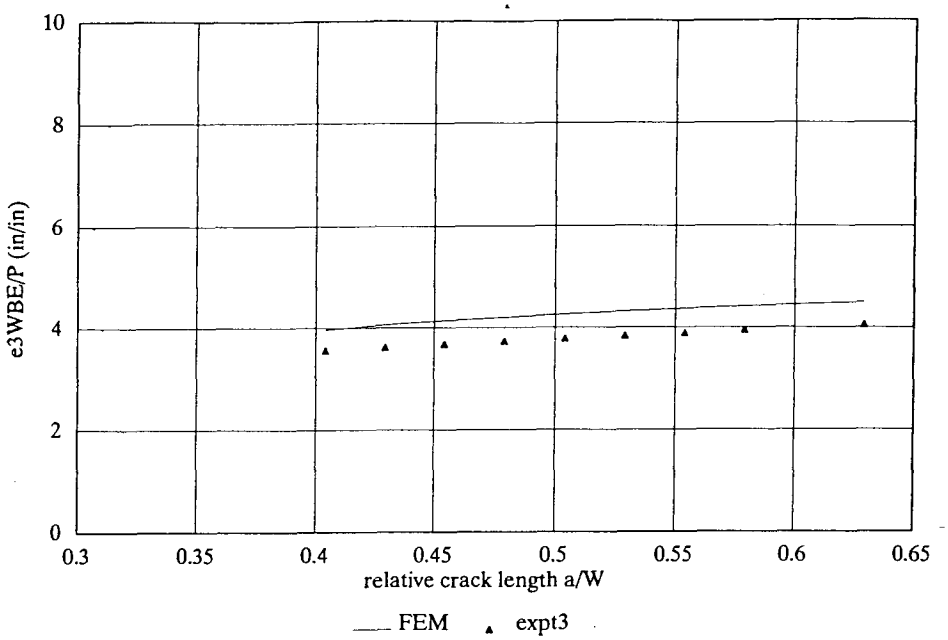

Figure 3.18: FEM vs experiment—$EBWe_3/P$ calibration

3.4.5 R-curve Tests

As discussed in the previous section, the R-curve test utilizes crack lengths and corresponding loads to compute the crack resistance (in the same unit as the stress intensity factor).

In addition to the strain measurement, a crack monitoring system, i.e. Fractomat and Krak-gage (Fig.3.19), was used so that a comparison with the result obtained via the calibration relations could be made. The Fractomat uses a potential drop technique. The crack length sensor, i.e. Krak-gage, is a special foil-type gauge. It is mounted on the specimen to cover the location where the crack will propagate so that it cracks the same amount as the specimen. When the crack grows, the electrical potential between the points A and B (Fig.3.19) will change proportionally. The monitoring device, i.e. Fractomat, measures the change in electric potential and directly relates it to crack length

so that the current crack length can be read directly from the panel of the Fractomat.

The wedge loading system and its support devices were specially designed and constructed. Its working mechanism is described in detail in the previous section. Loading of the wedge was provided using the Tinus Olsen testing machine, with a cross-head speed of 0.025in/min. (0.64mm/min.), i.e. the minimum speed the machine can achieve). A strain indicator with a multi-channel switch-box was used to monitor the strain changes e_1 and e_3 at the two different locations on each specimen. Fig.3.20 shows the test set-up for the R-curve test.

In order to gain more statistical confidence in the data a total of three identical specimens were tested. A minimum of 25 load steps were used to obtain a sufficient number of points to develop the entire continuous R-curve. For the first ten steps, an interval of five minutes between steps was allowed for the crack tip to reach a stable state, while for the later 15 steps, a 10-20 minute interval was required to stabilize the crack tip. These intervals were necessary as the crack extended in a 'pop-in' fashion, despite the fact that a slow quasi-static loading speed was used.

3.4.6 Experimental results

Based on the calibration curves, the experimental records were correlated into a crack resistance force, which according to the concept of energy balance [17], is quantitatively equal to the current stress intensity factor K available at the crack tip as quantified by the following expression [14]:

$$\begin{aligned}\frac{KBW^{\frac{1}{2}}}{P} &= 29.6(\frac{a}{W})^{0.5} - 185.5(\frac{a}{W})^{1.5} + \\ &+655.7(\frac{a}{W})^{2.5} - 1017.0(\frac{a}{W})^{3.5} + \\ &+638.9(\frac{a}{W})^{4.5} \end{aligned} \tag{3.12}$$

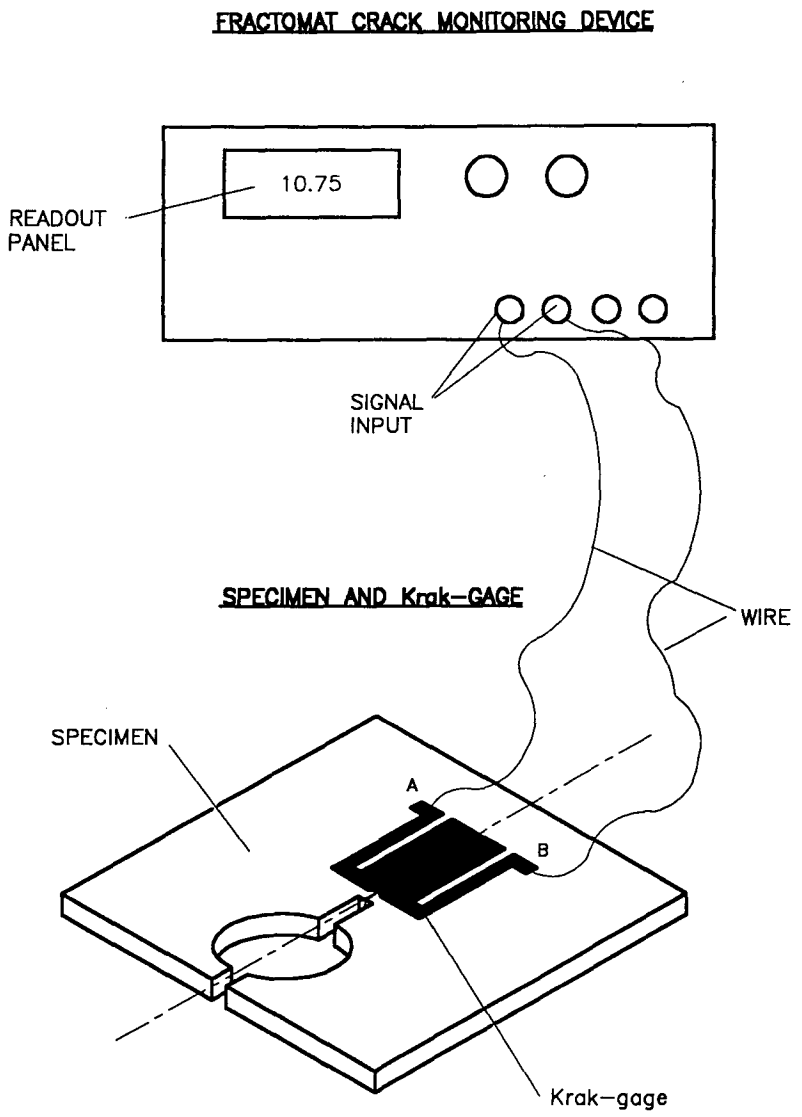

Figure 3.19: Fractomat crack monitoring device and Krak-gage

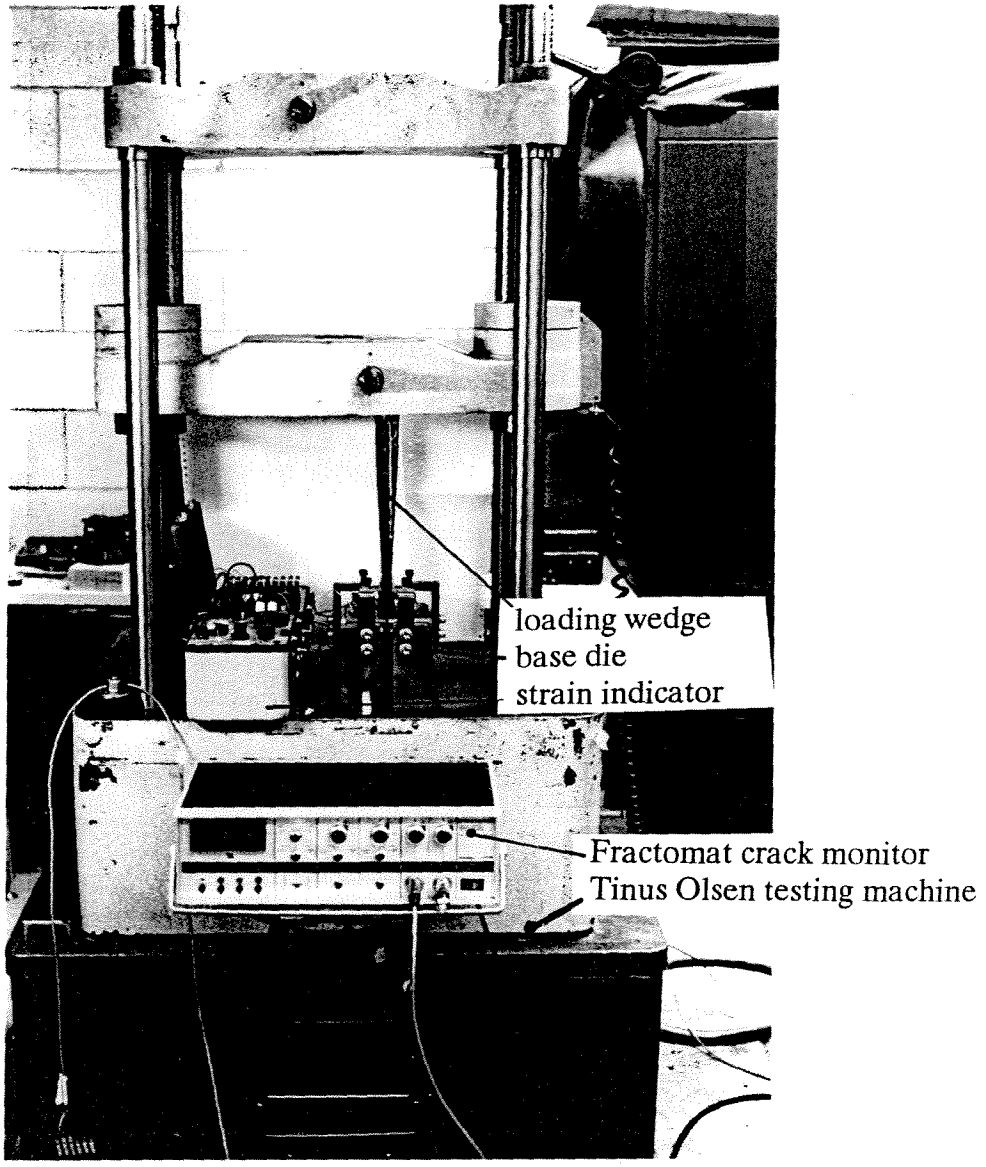

Figure 3.20: The test set-up for R-curve test

The least squares fitted expressions for the R-curve from calibrations were obtained as follows (Fig.3.22):

$$\begin{aligned}\frac{RBW^{\frac{1}{2}}}{P} &= 10.484 + 90.168(\frac{a}{W}) + 61.678(\frac{a}{W})^{0.5}) - \\ &\quad -1545.500(\frac{a}{W})^{2.5} + 3784.330(\frac{a}{W})^{3.5} \end{aligned} \tag{3.13}$$

As expected, the R-curve for the bandsaw steel tested shows a behavior similar to those of ultra-high strength sheet steels, i.e. the resistance increases, first steeply, then gradually.

Fig.3.21 shows a comparison between the crack lengths from Krak-gage and those obtained from the FEM calibrations. From Fig.3.21 it can be seen that fairly good agreement is obtained between the data using the two different methods (with the exception of the first few points), which in turn verifies these validity of the relationships. Considering that the FEM non-plasticity model was used for the calibration relations, the agreement means that the plastic region at the crack tip has little or no effect on the calibration results. The deviation shown by of the first few points (maximum 2.6%) may be a result of initial loose contact between the loading pieces which occurred at relatively low load values.

3.4.7 Critical stress intensity factor assessment

One of the significant features of an R-curve is that it can be used to assess the fracture toughness K_{IC} in the case of plane strain or K_C for the plane stress condition [9]. This assessment is based on an energy balance concept (if K refers to the cracking driving force, while R refers to the cracking resistance force, then the state of the crack is a result of balance between K and R)—where the critical stress intensity factor is defined as the critical point when a crack starts to grow in a unstable manner. At this point

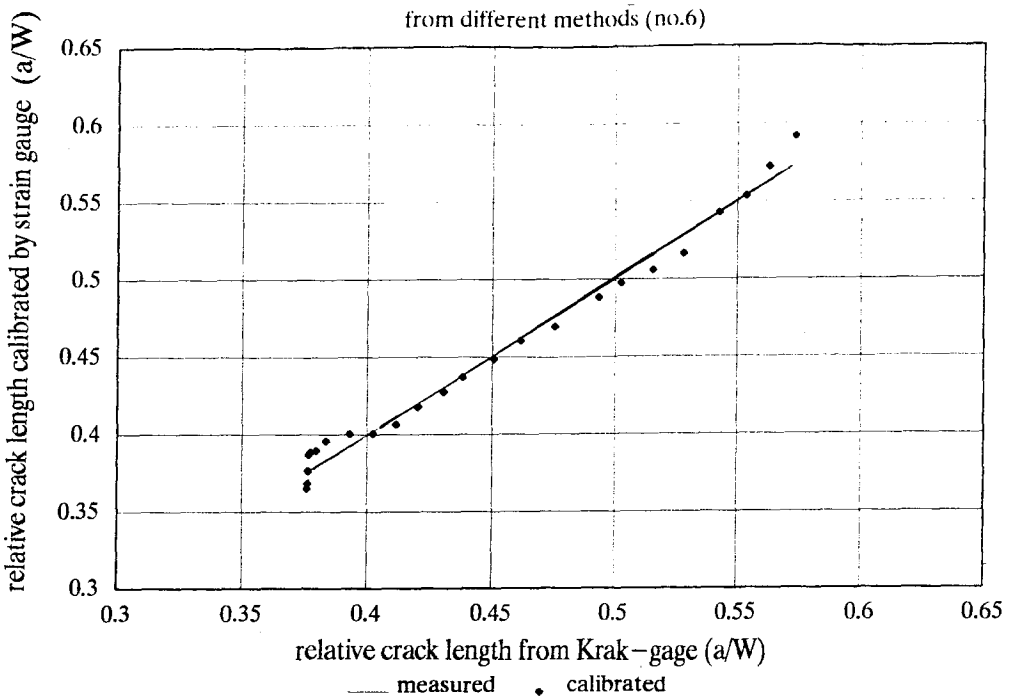

Figure 3.21: Comparison between the crack lengths from different methods

the energy available at the crack tip supplied by the external force is not only equal to the energy required for extension of a crack but that the energy rate provided exceeds the energy rate that the material can consume through stable growth, i.e. at this critical point, two conditions must be satisfied:

$$K = R_r \tag{3.14}$$

$$\frac{dK}{da} \geq \frac{dR_r}{da} \tag{3.15}$$

where

K—so-called *crack driving force*, i.e. the energy available for a crack extension.

R_r—so-called *crack growth resistance*, the energy required for a crack extension.

dK/da—the rate of change of the driving force with respect to crack growth da.

dR_r/da—the rate of change of the resistance with respect to crack growth da.

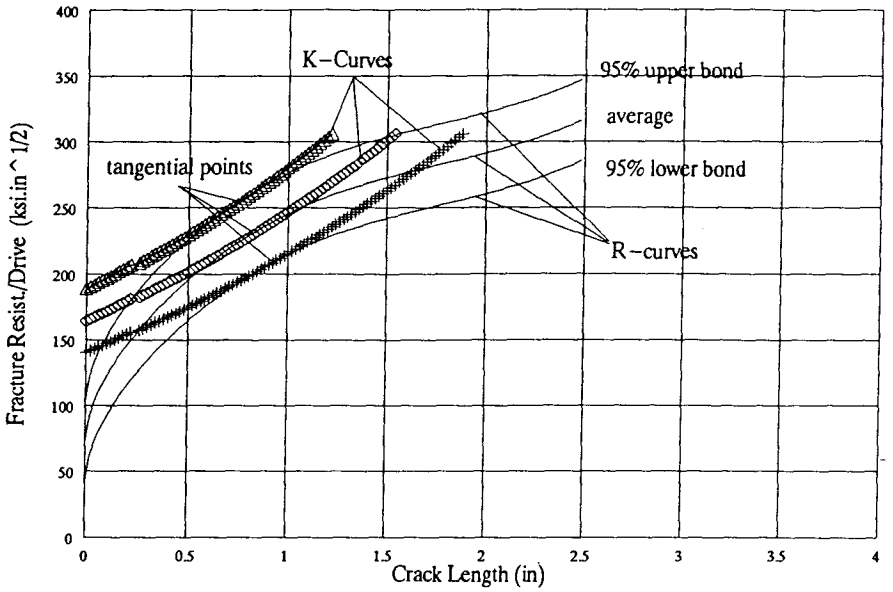

Figure 3.22: Graphical assessment of critical stress intensity factor

Fig.3.22 shows the geometric representation of the above relations. It is clear that the critical point is the point where the driving force curve and resistance curve are tangent to each other. Both numerical and graphical methods can be used to assess the critical stress intensity factor. Here a graphical method was employed for the determination of the critical stress intensity factor of the bandsaw steel.

In order to account for the range of scatter, all of the data from the three specimens were used to develop a single curve for the saw blade steel with the 95% confidence level. The upper and lower bounds were also determined. The K-curves were plotted using the equation (3.12). The fracture toughness assessed is 220 $ksi.in^{1/2}(242MPa.m^{1/2})$ with the upper bound $246ksi.in^{1/2}(270MPa.m^{1/2})$ and the lower bound $210ksi.in^{1/2}(231MPa.m^{1/2})$ (Fig.3.22).

The plastic zone correction

Within the frame of Linear-Elastic-Fracture Mechanics (LEFM), a cracked body under study is assumed to deform in a purely elastic manner, even at the crack tip. However, a portion of the material within the tip region always behaves plastically. The extent of this deviation from fully linear elastic behavior varies as a function of material and constraint conditions. For materials where a large plastic zone develops (relative to the crack length) an Elastic-Plastic Fracture Mechanics (EPFM) approach should be employed. For materials with a very high yield strength ($> 150ksi(1035MPa)$) the plastic zone at the tip of a crack can be considered as being very small such that a plastic correction to elasticity based theory is enough to make the theory work. The corrections available are mostly in the form of crack length, i.e. converting the plastic zone into an equivalent crack increment to the original crack length (or physical crack length) by means of an energy balance [9].

The following relationship is widely used to account for limited plasticity at the crack tip:

Irwin's Correction

The effective crack length:

$$a_e = a_0 + \Delta a + r_Y$$

where

a_0— starting crack length.

Δa— physical crack growth at crack tip.

r_Y— plastic zone adjustment.

$$r_Y = (\frac{1}{2\pi})(\frac{K^2}{\sigma_Y^2})$$

(for plane stress)

K— current stress intensity factor.

σ_Y—2% offset yield strength.

It should be mentioned that in many cases, Irwin's correction may over-estimated the true plastic zone effect [22].

Plastic effect

The necessity of the correction can be seen clearly from the R-curve, namely the plastic correction changes the shape of the R-curve, ultimately changing the assessment of critical stress intensity factor (Fig.3.22). For the saw blade steel tested, the difference of the assessed critical stress intensity factor is 10 $ksi.in^{1/2}(230ksi.in^{1/2})$. The correction r_P ranges from $2-11\%$ of the current crack length.

Chapter 4

Crack Initiation Tests

4.1 Introduction

Crack initiation in the gullet region of a bandsaw blade can be the result of contributions from many factors such as the stress (or strain) level (i.e. function of the diameter of the wheel) or stress ratio (i.e. pre-strain force level), the micro-structure of the steel, the surface condition of the gullet region (introduced by the sharpening process) and the environment (i.e. coolant, wood sap and temperature). Amongst these factors, the stress level, stress ratio and surface roughness in the gullet region are dominant. As in many components in engineering practice, the surface roughness of a blade plays a significant role in affecting its fatigue-life. The orientation and depth of scratches on a steel surface can severely affect the fatigue life. In routine sawmill practice, the saw blade is typically removed from the machine for resharpening after one shift of four hours of continuous running and cutting service. This process removes a very thin surface layer of the gullet region, grinding off most micro-cracks developed during the previous service period. However, at the same time, this process (Fig.4.23) can cause scratches in the most unfavorable orientation, some of which are very deep (Fig.4.24) and will serve as perfect crack starters in future service. High temperatures (i.e. red-hot) can be reached during the sharpening process, and the following rapid air-cooling can transform a thin layer of the blade adjacent to the surface of the gullet region into a very brittle structure which makes the region more susceptible to cracking [1]. The combination of these two

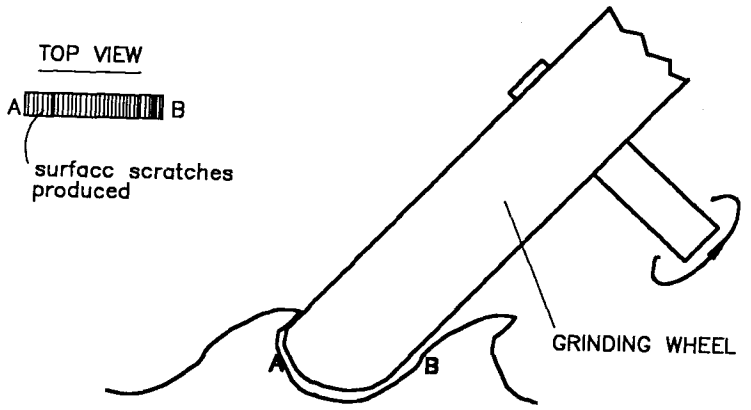

Figure 4.23: Resharpening process—stone wheel and tooth

unfavorable factors plus the severe stress concentration at the bottom of the gullet (1.5-2.5) [4] can greatly enhance the possibility of crack initiation.

One phase of this study was to investigate the effect of surface roughness of a blade and stress levels on its fatigue life. To gain some statistical information on the problem, two groups of small specimens with different surface roughnesses were tested. In order to simulate the actual loading condition experienced by a saw blade in service, the stress levels and stress ratio were set equal or close to the service levels used in sawmills (recognizing the presence of stress concentration).

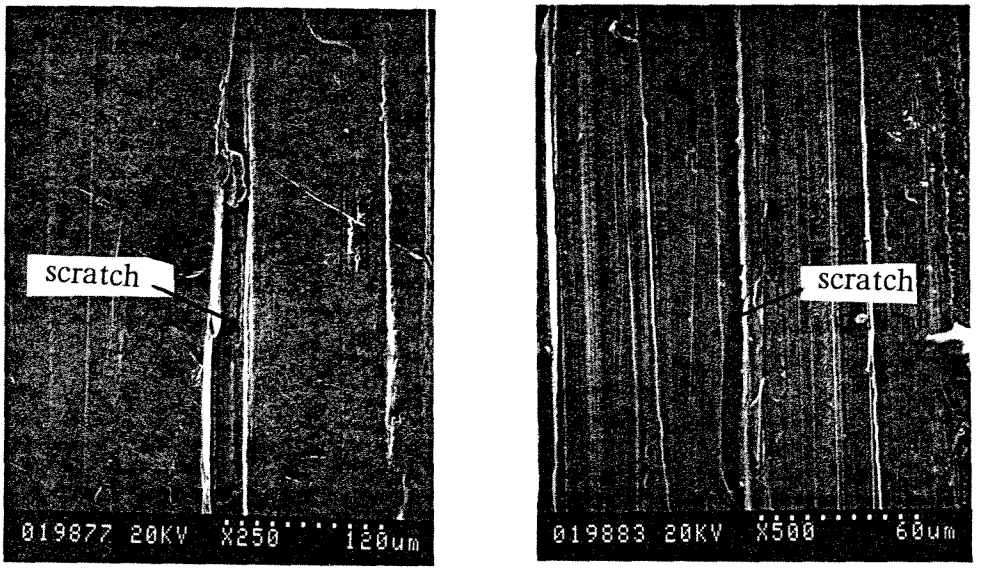

Figure 4.24: Close-up of a typical scratch produced by grinding process

4.2 Experiments

4.2.1 Specimen, load and equipment

Specimen and materials

A series of small, flat, rectangular-sectioned specimens with two different qualities of surface roughness were produced from a new blade steel band as in the as-received condition. The surface finish was prepared by an experienced sawfiler on a real bandsaw grinding machine using different feed speeds (Fig.4.26). The first group was ground to a surface roughness ranging from 115 to 194 micro-inch (central line average). The second group was ground to a surface roughness ranging from 300 to 400 micro-inch (central line average). The roughness in the second group was believed, by the sawfiler, to be close to the condition of a blade as used in a sawmill. The crack initiation was defined in this research as a crack length of 1/25.4 in.(1mm).

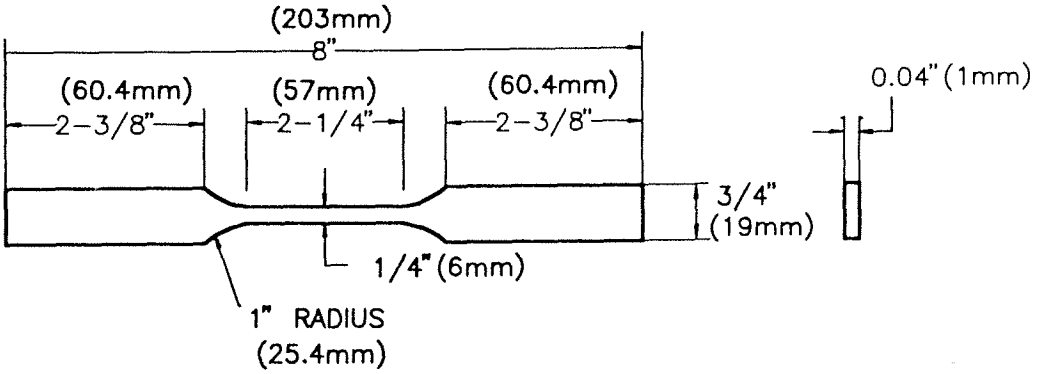

Figure 4.25: Crack initiation life specimen

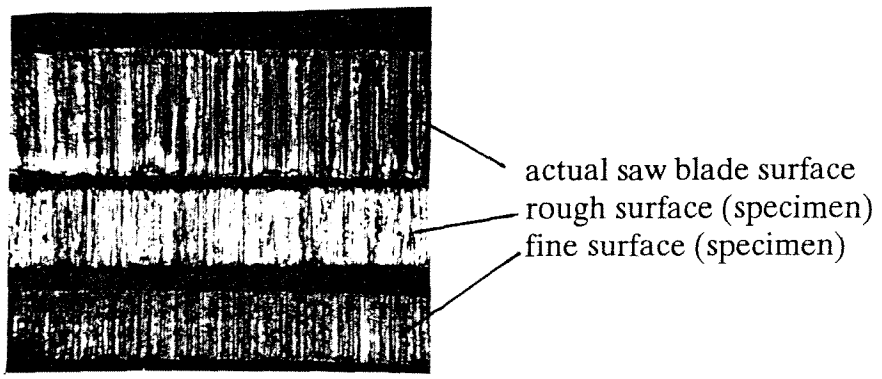

Figure 4.26: Photo of the surface roughness of the specimen

Loads chosen

In order to simulate the actual loading conditions which a real blade experiences in service, four tensile stress levels were chosen to simulate the stress fields produced by four different levels of pre-strain forces generally used in sawmills. The specific stresses were calculated by assuming that the blade has dimensions of 9.5 in.(241mm) in width and 0.073 in (1.85mm) in thickness, on a 5 ft.(1524mm) diameter bandsaw machine. The four pre-strain force levels chosen were:

1. 20,000 lb.(90,000 N)—used on the so-called 'high-strain' systems.
2. 18,000 lb.(81,000 N)—generally used in sawmills.
3. 15,000 lb.(67,500 N)—generally used in sawmills.
4. 13,000 lb.(58,500 N)—generally used in sawmills.

As for the stress concentration at the bottom of the tooth gullet, a factor of 2.2, obtained by Lee [3] was used to modified the stresses so as to obtain some degree of simulation to the real load conditions in the gullet region of a blade (Table.4.2). The theory used to calculate the stresses were those summarized in **Chapter 2**.

Equipment and devices

The machine employed for this testing was the Sonntag universal fatigue testing machine. Fig.4.27 shows schematically the working mechanism. The pre-load (static load) is controlled by a loading spring, the deflection of which can be adjusted manually. The alternating load (dynamic load) is produced by rotation of a centrifugal mass. The magnitude of the cyclic load is set by the adjustable distance from the mass center to the motor shaft to which the mass is attached. The fixed speed of the machine is 1800 rpm. The machine has a built-in mechanical counter which stops counting at the same moment as the machine is automatically shut off if the specimen fails (separated). In

Load Parameters Chosen

group	first group		second group	
surface *	100−200 (microin)		300−400 (microin)	
load	mean (ksi)	cyclic (ksi)	mean (ksi)	cyclic (ksi)
20,000 lb	67.45	35.33	67.45	35.33
18,000 lb	64.23	35.33	64.23	35.33
15,000 lb	59.43	35.33	59.43	35.33
13,000 lb	56.7	35.33	56.7	35.33

note: * inducates center line average

Table 4.2: Load parameters chosen

order to get a more reliable load setting, the static and dynamic loads were set by a strain indicator with a foil-type 300 ohm strain gage mounted on the specimen.

4.2.2 Test, results and analysis

The specimen was held using a stiff-bolted clamp/joint friction grips and cyclically loaded using the Sonntag fatigue testing machine. The cycles elapsed were counted automatically by the built-in mechanical counter. To gain some statistical certainty, a minimum of three specimens were tested for each load case. The cyclic life presented in the Table.4.3 is a statistical mean. The cyclic life was converted into service hours assuming a bend frequency of 5.7 Hz, a reasonable estimate based on sawmill operation.

Observations

From Table.4.3 and Fig.4.28, the following observations can be made:

1. The result at 20,000 lb.(90,000 N) and 18,000 lb.(81,000 N) pre-strain levels show a little variation in crack initiation time for the group with fine surface roughness. The 15,000 lb.(67,500 N) level has a life span of more than **4 times** as that of the 18,000 lb.(81,000 N) level.

2. For the group with a coarse surface, the 20,000 lb (90,000 N) and 18000 lb. (81,000 N) pre-strain force levels were found to have no difference in initiation time. The 15,000 lb. (67,500 N) level initiation time results is slightly longer than those for 20,000 lb and 18,000 lb levels. However, the 13,000 lb level has 50% longer life.

3. The initiation life of the group with fine surface roughness is about, at least, more than **10 times** that of the group with rough surface roughness.

4. In the coarse surface group, whose surfaces are believed to be closer to the real service condition of a blade, the longest initiation life was just over **one hour**, i.e.

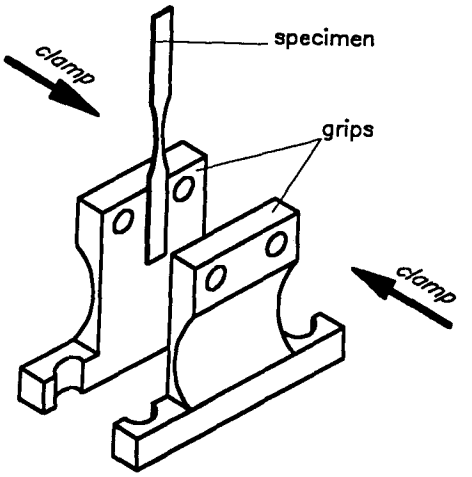

SPECIMEN AND GRIPS

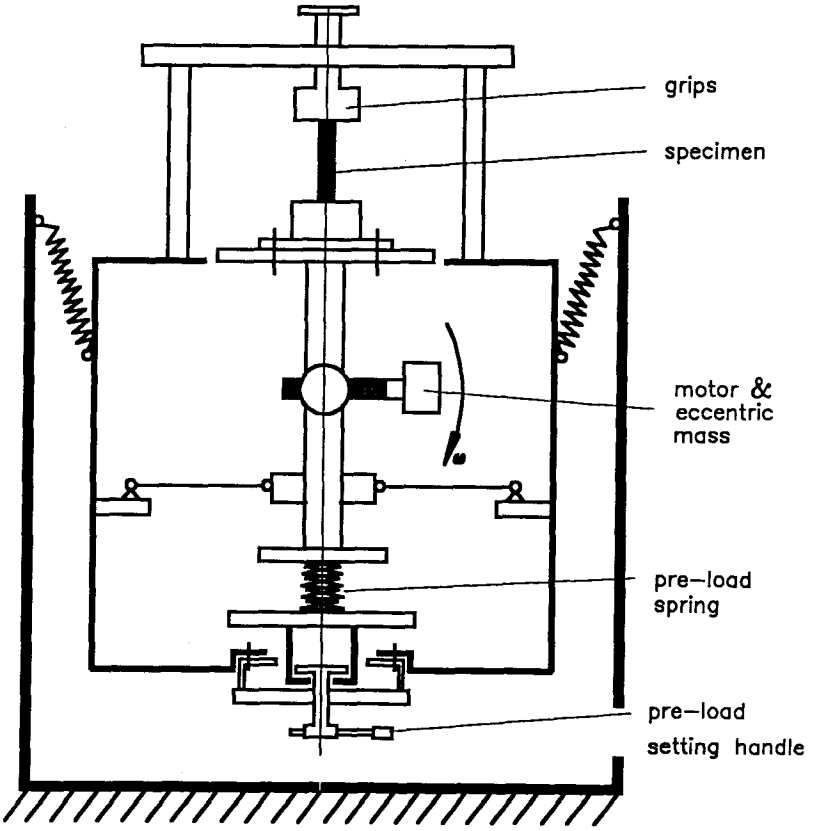

Figure 4.27: Fatigue testing machine working mechanism

pre-strain force level			20,000 lb	18,000 lb	15,000 lb	13,000 lb
maximum stress			102.78 ksi	99.56 ksi	94.76 ksi	92.03 ksi
fine surface	crack initial life	1000 cycles	146.3	156	not failed after 686	not failed after 700
		hours	7.12	7.59	>33	>38.4
rough surface		1000 cycles	15.3	15.3	16.3	22
		hours	0.74	0.74	0.78	1.07

Table 4.3: The crack initiation test results

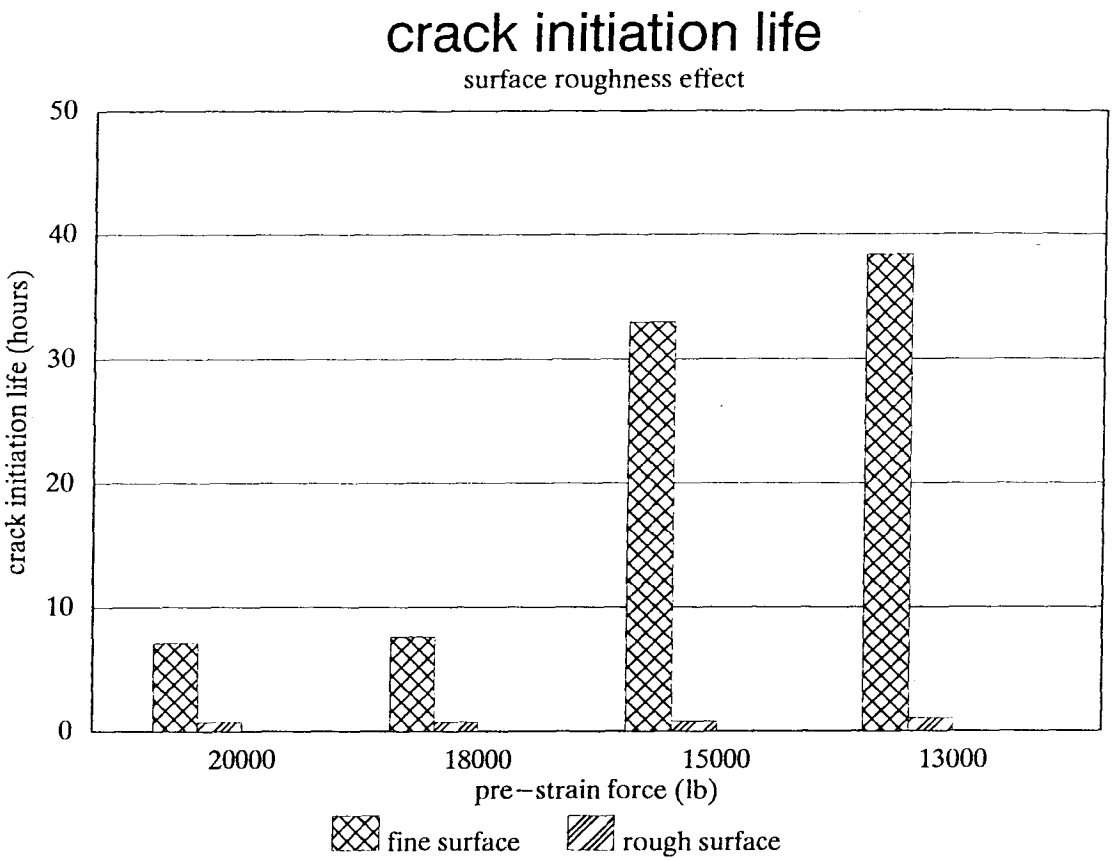

Figure 4.28: The crack initiation test results

25% of one shift. While in the fine surface group, whose surfaces were produced with greater care, even the shortest life lasted well beyond one shift of 4 hours in all load cases.

Possible explanations

According to Porter [2], the fatigue limit for bandsaw steel is estimated to be less than 120 ksi. (828 MPa). The specimens in this crack initiation test were working under a maximum stress 92.03–102.78 ksi (635-703 MPa) (Table.4.2), which is within a narrow margin of the fatigue limit. Previous investigations [8] have shown that surface roughness becomes a major degrading factor in component fatigue life when the maximum stress is near the fatigue limit. A SEM (Scanning Electronic Microscope) examination of the two groups shows that a poor surface finish often means more and deeper scratches which work as more severe stress raisers. Micro-cracks may also be formed, so that there are more chances for stress-favourable scratches to grow into micro-cracks at faster rate.

What is alarming is that SEM examination of a sample cut from a failed blade shows more and deeper scratches than on the specimen tested. Recognizing that there are several hundred teeth punched in one closed loop blade, thus providing a higher probability for deep scratches to be present, it is not unreasonable to expect that cracks can be nurtured in as short as 45 minutes, consequently, a dangerous stage II, i.e. crack propagation, begins. If this kind of situation happens to a blade in actual service, it means that a **cracked** blade will be working for the rest (82%) of one shift of four hours!

Chapter 5

Mode I Crack Growth Rate Test

5.1 Introduction

In contrast to smooth body fatigue analysis in which the crack growth stage is not separated, fracture mechanics based fatigue theory divides the fatigue process into three stages: (1) crack initiation; (2) stable (or subcritical) crack growth; (3) unstable (or critical) crack growth. It is in the second stage that fracture mechanics based fatigue analysis concentrates. Linear elastic fracture mechanics essentially assumes that a defect exists originally. Based on the concept of a *stress intensity factor*, fracture mechanics based fatigue theory focuses on the crack growth behaviour (actually the crack growth process occupies the major part of life-time for some large components in engineering practice) so as to quantify the process from initiation to final failure of a component.

In fracture mechanics a crack can be classified into one or a combination of three basic crack modes, i.e. *Mode I* (opening), *Mode II* (sliding) and *Mode III* (tearing) (see Fig.5.29). Although basic forms of stress intensity factors and crack growth rate laws are similar for the three different modes, their crack tip stress field and crack growth behavior are generally different. Therefore, a crack growth rate is always associated with the crack mode. It can be seen that a tooth gullet crack should be classified as Mode I (opening mode) crack, therefore its growth rate should be obtained using Mode I specimens.

Paris (1964) proposed the well-known Paris' law [15]. Based on the concept of stress intensity factor as proposed by Irwin in 1961 [17], Paris introduced a new parameter, the

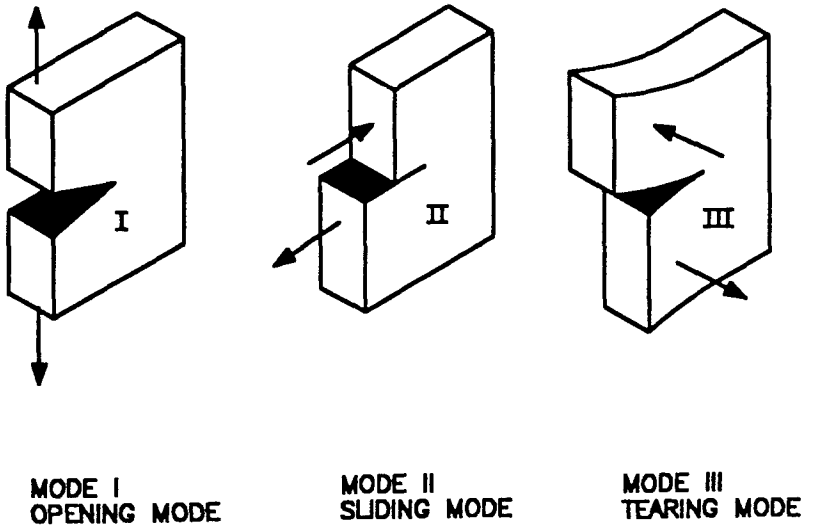

Figure 5.29: Three Modes of cracks

stress intensity range (Fig.5.30), to characterize the crack-tip field under fatigue loading and assumed a general relation:

$$\frac{da}{dN} = f(\Delta K, R, \dot{\epsilon}, T) \tag{5.16}$$

where

da/dN—Crack extension per cycle.

ΔK—Stress intensity range, defined as shown in Fig.5.30.

R—Stress ratio $\sigma_{min}/\sigma_{max}$.

$\dot{\epsilon}$—Strain rate.

T—Current temperature when a material is tested.

In the simplest case (no R effect), experimental results show that for most metallic materials the relation can be formulated as,

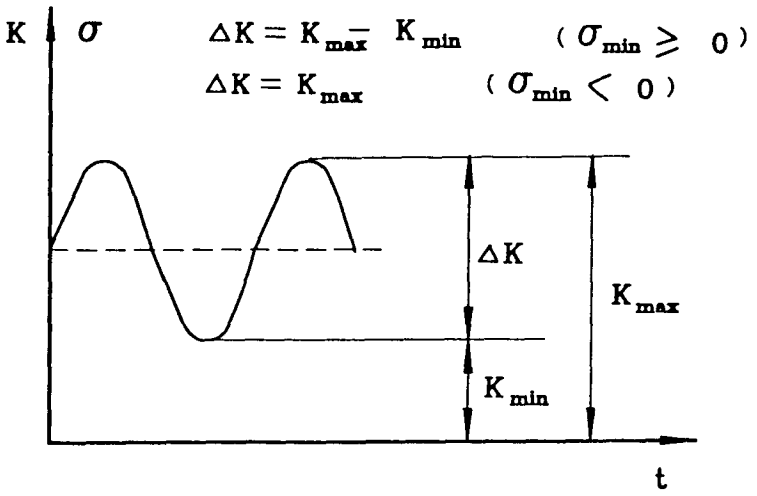

Figure 5.30: Definition of stress intensity range

$$\frac{da}{dN} = C(\Delta K)^b \tag{5.17}$$

Here C and b can be seen as material constants which depend on strain rate and environment.

There are many other formulas suggested to account for varying stress ratio and fatigue threshold effect to allow for prediction of component life. Forman's formula [9] is typical of this kind.

Through extensive experiments on a vast variety of engineering materials, a general range for C and b are suggested in fatigue design handbooks. However, in engineering practice, especially in the field where cracking problems are of most concern, experimental tests have to be carried out on specific materials with specific conditions. ASTM has issued a standard, E647 [19], for testing specifications and procedures related to fatigue tests.

As a first attempt to understand the growth behaviour of an gullet crack in a bandsaw blade material, and to obtain more complete information for further comparison study, a series of Mode I crack growth rate tests were designed and carried out on specimens cut from a strip of new bandsaw material. The following section discusses the testing procedure and the results.

5.2 Mode I crack growth rate experiment

5.2.1 Specimen and equipment

A compact-tension specimen (CT) was chosen with the configuration and dimensions of the specimen being obtained from the guidelines in ASTM E647 [19]. The crack orientation was perpendicular to the rolling direction (blade length) so as to simulate a gullet crack in a bandsaw blade. The crack was measured using Krak-gages connected to a Fractomat crack monitoring device (see Fig.3.20). The loading was monitored via a strain gage mounted at a location on the specimen as shown in Fig.5.31. To ensure accuracy in cycle counting, a separate digital electronic counter was employed.

The Sonntag universal fatigue testing machine (Fig.4.27), whose loading system is displacement controlled, was used. To maintain a nearly constant load during one cracking step, load adjustments were needed from time to time during each test. To ensure that the specimen was loaded accurately, a calibration relation based on load, crack length and strain at a defined location on the specimen (Fig.5.31) was established by using both a finite element analysis model and experimental tests. The relationship is shown graphically in Fig.5.32.

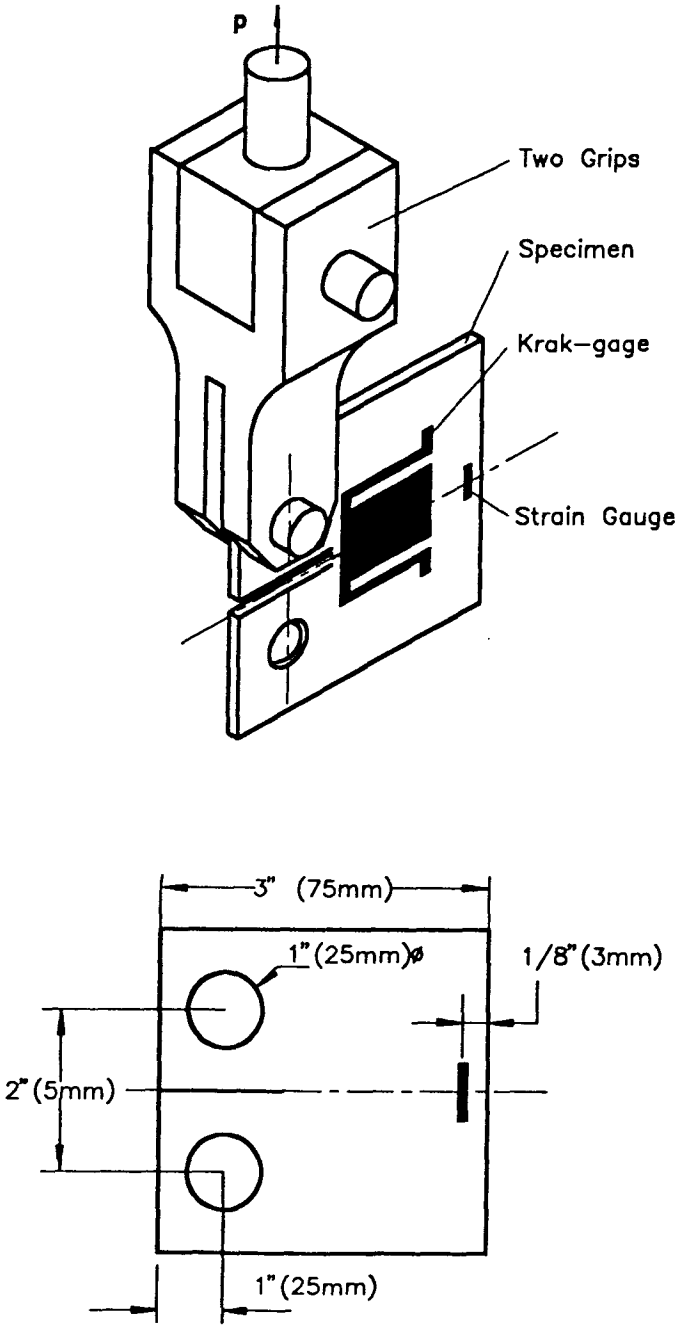

Figure 5.31: The specimen and fixtures for crack growth rate test

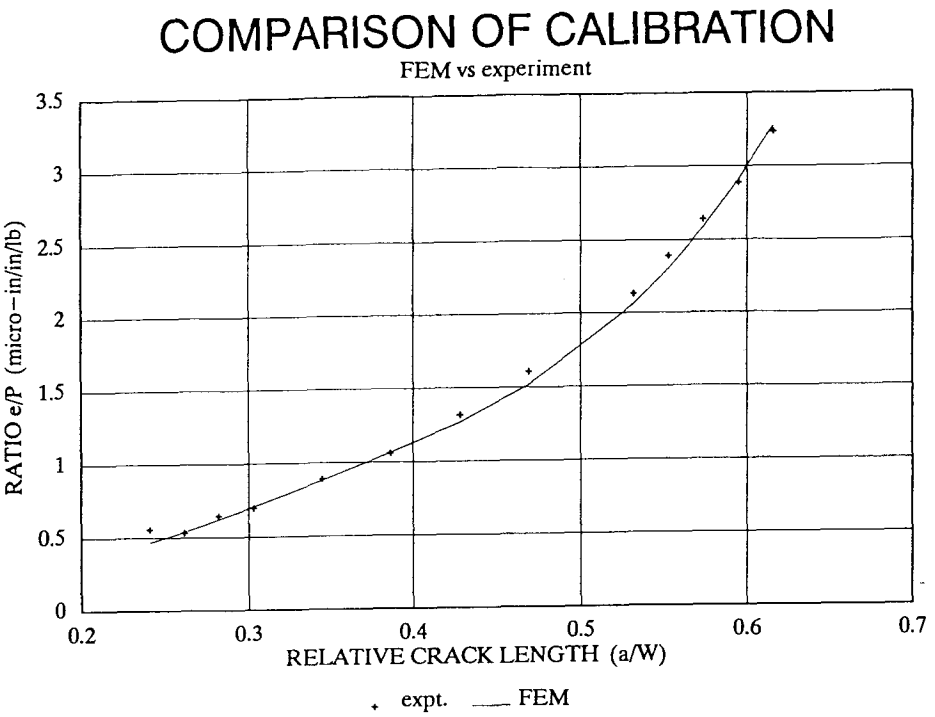

Figure 5.32: The calibration relation for CT specimen

5.2.2 Tests and data analysis

Experimental testing

In order to investigate stress ratio effects, the tests were divided into three groups having different stress ratios (R) corresponding to the range of commonly employed pre-strain force levels used in actual saw blade operations. Each group of three specimens was tested to obtain the data needed for establishment of a da/dN curve.

In order to cover a wide stress intensity range ΔK, as well as provide a reasonable density of points, three specimens from each group were tested, while each specimen was tested using a different method. One of them was tested with the so-called *load shedding* method, one with the *constant load* and one with the *load increasing* method.

- *load shedding*—the load is reduced stepwise (R ratio constant) so that ΔK decreases. When a desired low ΔK is reached, the load is increased stepwise. In this

method low as well as high values of ΔK can be covered. The data from the load increase and decrease process overlap each other so as to gain statistical certainty for each case.

- *constant load*—the load is kept constant so that a reasonable density of points as well as the medium and high range of ΔK can be covered.

- *load increasing*—the load is increased stepwise(R constant) so that ΔK increases quickly to reach a high level of ΔK before the crack grows beyond the Krak-gage limit length.

To minimize crack retardation effects [19] which may be introduced by a large load drop, 8% shedding and an increasing rate was used. An interval of 0.02-0.03 in.(0.5-0.8 mm) was used for each step [19]. The tests were conducted on the Sonntag universal fatigue testing machine. The tests were manually controlled with each load step.

Data and analysis

Using the discussed approach, a total of twelve specimens were tested to cover the four different stress ratios. The parameters measured included load, crack length and cycles elapsed (Fig.5.33). The data was correlated into typical da/dN vs ΔK form by means of the *secant method* [19] and were formulated by using the least-squares approach. Fig.5.33 is a typical record of $a-N$ curve. The $log-log$ plots of the $da/dN-\Delta K$ curves are shown in Fig.5.34—Fig.5.38.

The least-squares fitted expression for the range of $10ksi.in^{1/2} < \Delta K < 50ksi.in^{1/2}$ follows as (see Fig.5.38) (note: in eqn.(5.18), (5.19) and (5.20), the unit for ΔK is $ksi.in^{1/2}$ instead of $MPa.m^{1/2}$),

$$\frac{da}{dN} = 1.68(\Delta K)^{2.86} \qquad (10^{-8}mm/cycle) \tag{5.18}$$

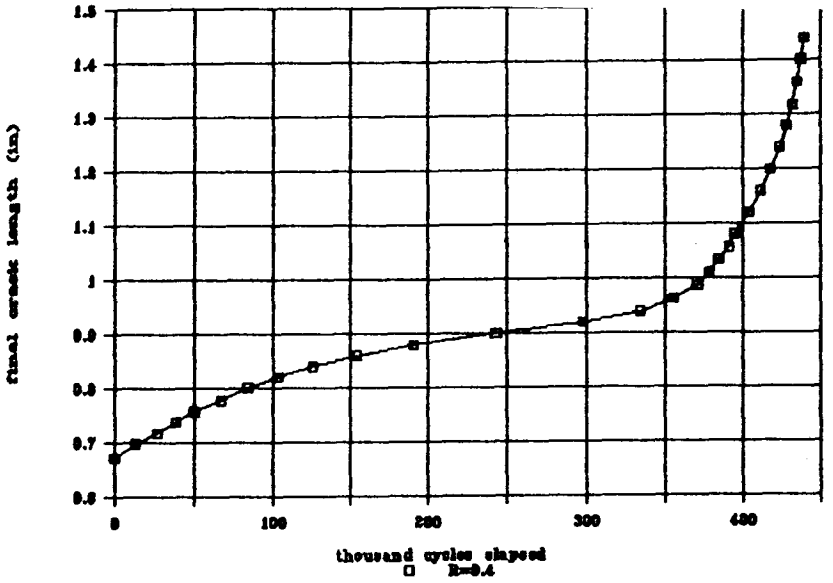

Figure 5.33: A typical crack length versus cycle record

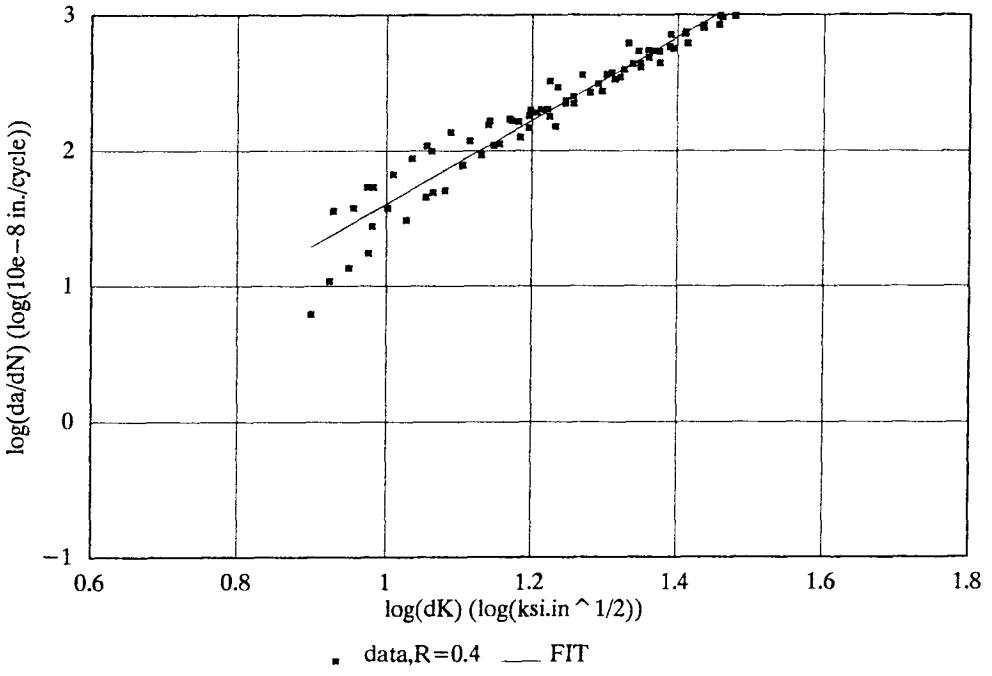

Figure 5.34: The crack growth rate: $R = 0.4$

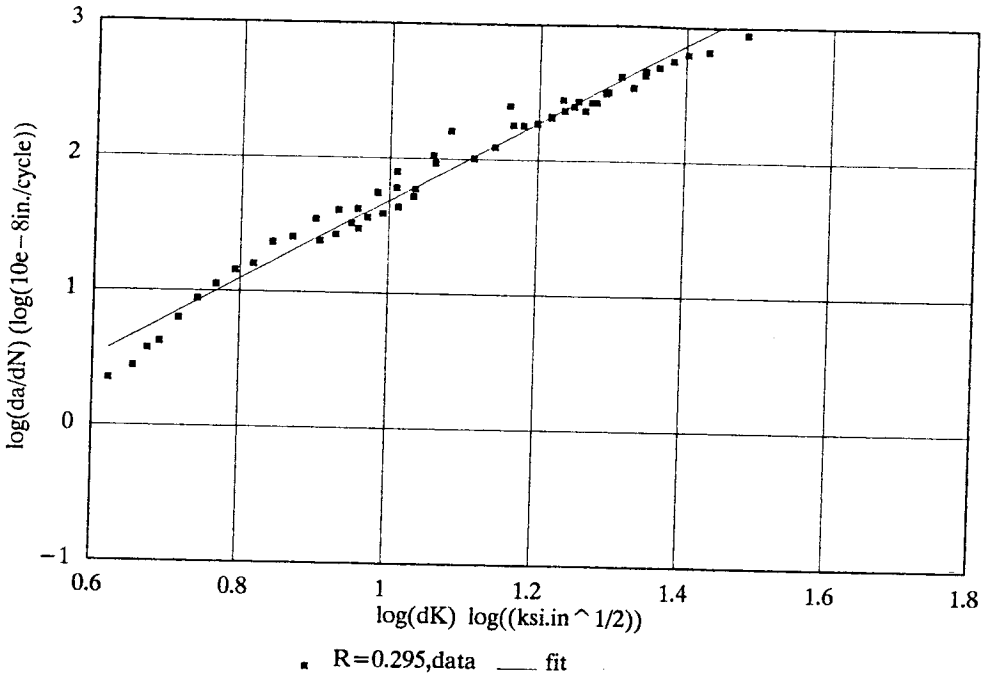

Figure 5.35: The crack growth rate: $R = 0.295$

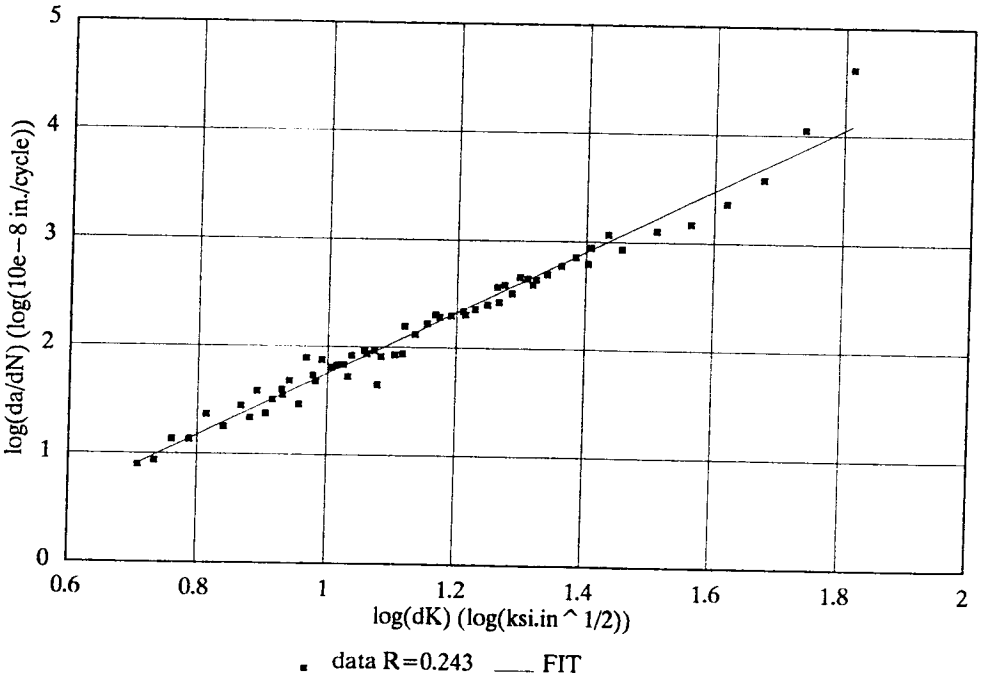

Figure 5.36: The crack growth rate: $R = 0.243$

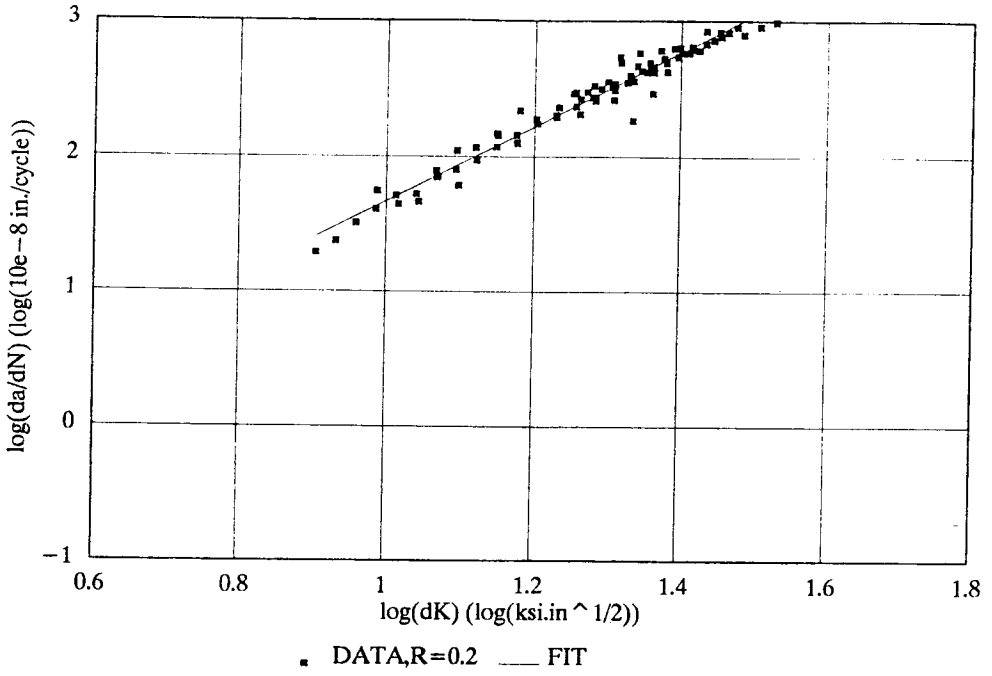

Figure 5.37: The crack growth rate: $R = 0.2$

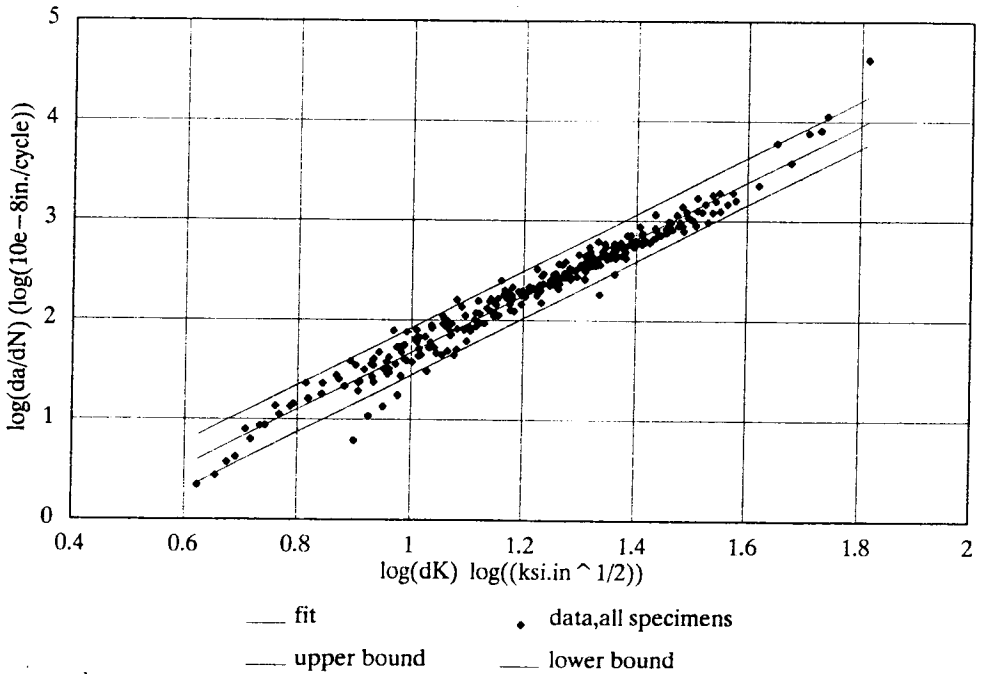

Figure 5.38: Comparison of crack growth rates

with an upper bound:

$$\frac{da}{dN} = 2.22(\Delta K)^{2.86} \qquad (10^{-8} mm/cycle) \tag{5.19}$$

a lower bound:

$$\frac{da}{dN} = 1.28(\Delta K)^{2.86} \qquad (10^{-8} mm/cycle) \tag{5.20}$$

The upper and lower bounds are produced by three standard deviations of da/dN data which, according to statistics theory, can cover the statistical behaviour with a 95% confidence level.

Based on the experimental results the following observations can be made:

Observations

1. There is little stress ratio effect on the propagation rate within $\Delta K = 10 - 50 ksi.in^{1/2} (11 - 55 MPa.m^{1/2})$. To see the stress ratio (R) effect, all of the data was plotted on the same graph (Fig.5.38). It can be clearly seen that in the range of stress intensity range $\Delta K = 10 - 50 ksi.in^{1/2} (11 - 55 MPa.m^{1/2})$ all data clusters closely to the fitted line. This means that within this range of ΔK, stress ratio has no significant influence on the propagation of a mode I crack in this material. Based on this data, it is reasonable to quantify the propagation rate by a single curve when operating within this ΔK range.

2. Stress ratio effects show up in the region of low ΔK ,i.e., $\Delta K < 10 ksi.in^{1/2}$ $(11 MPa.m^{1/2})$. A clear deviation begins when ΔK falls below 10 $ksi.in^{1/2}$ (11 $MPa.m^{1/2}$). The two deviating curves belong to the higher R ratio tested, i.e. $R = 0.295$ and $R = 0.4$ groups respectively. The different extent of crack closure, which is closely related to stress ratio, is believed to be responsible for this deviation.

While closure itself is caused by the permanent plastic deformation of the material in the wake of the crack [16]. The ultimate result of this kind of deviation from each other produces quite different values of the so-called *threshold stress intensity range*, denoted as ΔK_{th}, which is defined as a value of ΔK below which da/dN is so low that a crack does not practically grows. The ΔK_{th} can be defined according to engineering circumstances. For instance, ASTM E647 recommends that $\Delta K = \Delta K_{th}$ when $da/dN = 10^{-10}$m/cycle [19].

3. The maximum threshold value of the bandsaw steel under investigation is about $7.9ksi.in^{1/2}(8.69MPa.m^{1/2})$ in the case where R= 0.4. The minimum ΔK is below $3.16ksi.in^{1/2}(3.48MPa.m^{1/2})$ in the case where R= 0.2). The threshold values are obtained by the extrapolation method recommended in ASTM E647.

Chapter 6

Crack Propagation Test for Out-of-Plane Bending

6.1 Introduction

In the previous tests, crack propagation can be considered as one dimensional, i.e. the stress intensity factor is the same along the whole crack front. Therefore the whole stress field along crack front can be characterized by one single stress intensity factor. However, in actual service a bandsaw blade experiences both tensile and out-of-plane bending during one revolution. According to the simple beam theory [11], the out-of-plane bending produces a triangle stress distribution across the blade thickness, therefore the stress intensity factor varies along the crack front, which results in different crack extension rates along the crack front. Furthermore, out-of-plane bending may also make two crack surfaces contact each other (Fig.6.39). The contact force between the two crack surfaces introduces another stress field onto the existing field, which also may changes the crack extension rates. It can be expected that the pre-strain force has a strong effect on the stress intensity and crack growth rate. In order to find more evidence regarding the crack growth pattern under a out-of-plane bending load, a series of crack growth tests using on out-of-plane bending load were conducted. These tests were also used to investigate the effect of stress ratio. Description and discussion of these tests is presented in following sections.

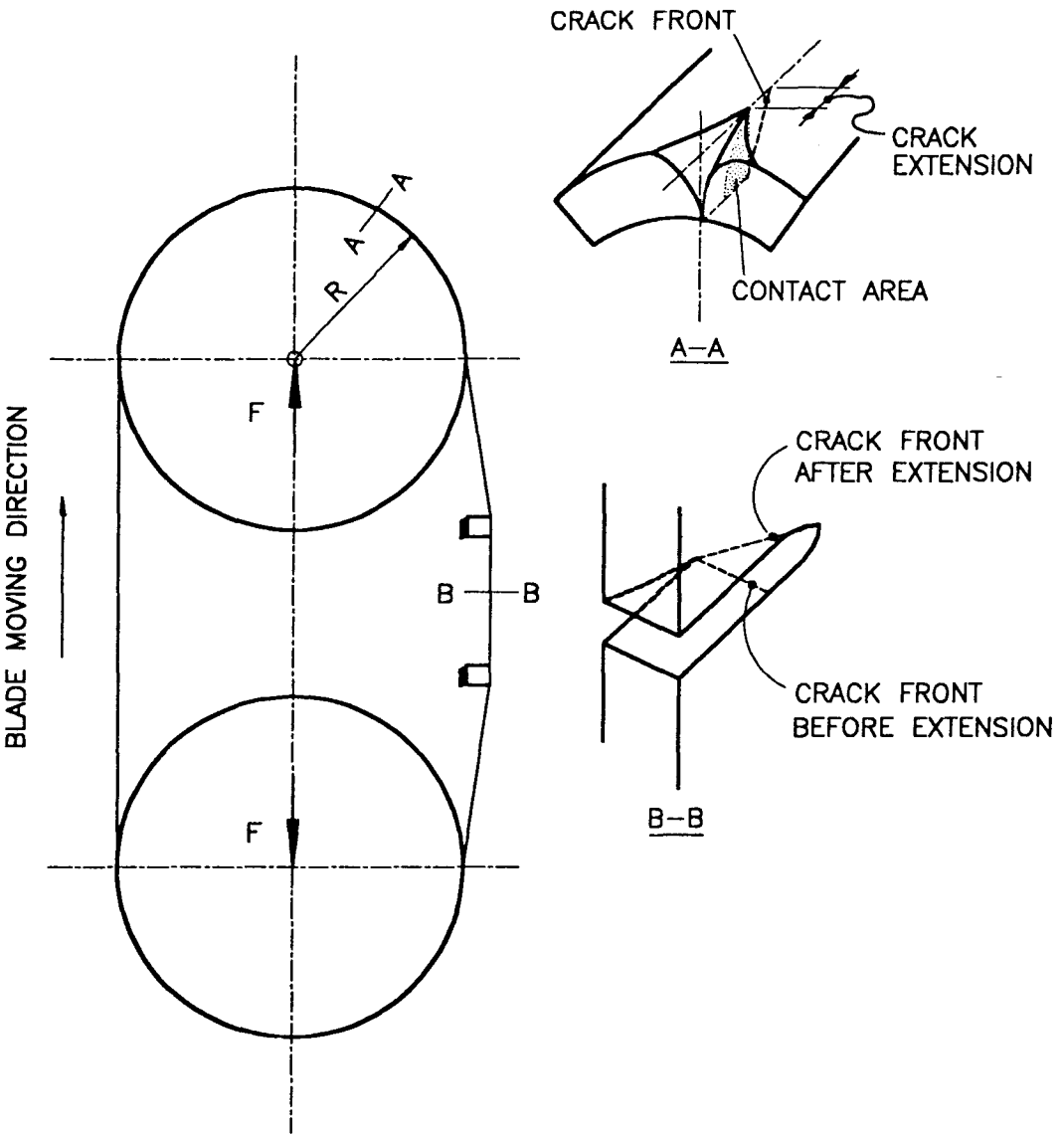

Figure 6.39: Schematic relation of crack surfaces interacting: saw blade and cracked gullet position

6.2 Experiment

6.2.1 Basic considerations

In order to assess the effect of the stress ratio, the tests were conducted at six different values of stress ratio. stress ratios. The stress ratios were selected such that the load conditions in both the inner and outer edges could be simulated to some extent, i.e. both the maximum and minimum stress in the outer and inner edges of the test specimen approximated those of a working blade, while at the same time maintaining the nominal stress intensity range ΔK at the tip of the crack in the outer edge.

6.2.2 Specimens, equipment and devices

Specimen

The test specimens were cut from new blade material in its 'as received' condition and were machined to the geometry shown in Fig.6.40. The specimens were pre-cracked under a cyclic tensile loading on the Sonntag fatigue testing machine (see Fig.4.28 in **Chapter 4**). The crack was oriented perpendicular to the rolling direction to simulate a gullet crack in an actual blade. The starting crack length was about 20-35% of the width of the specimen.

Equipment and devices

To achieve a pure bending condition, a four point bending fixture (Fig.6.41) attached to the Sonntag fatigue testing machine was employed. The fixture allowed a degree of freedom in the axial direction so that there was little or no axial force in the specimen while a desired bending load was imposed on the specimen. Its working mechanism is shown in Fig.6.41. The loading mechanism is the same as that discussed in **Chapter 4**. Because different crack lengths on the upper and lower surfaces were expected, one Krak-gage was mounted to each side of the specimens. The Krak-gages were then wired

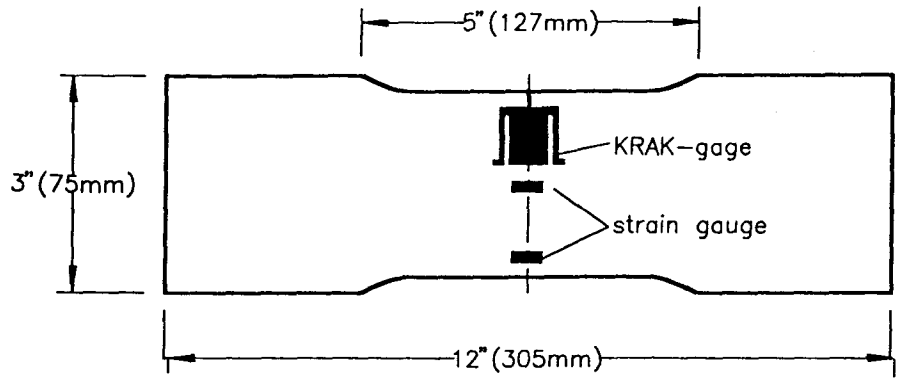

Figure 6.40: Geometry of the specimen for out-of-plan bending load

to the Fractomat crack monitoring device (see Fig.3.21). Two strain gages mounted on the each side of the specimen were used to monitor the current nominal applied stress level. The extension of the crack for each step was about 0.8mm. The data collection (crack length and cycles) was performed manually stepwise. The machine had to be shut off for each step for data collecting and load adjusting.

6.2.3 Test results and analysis

The recorded data included the crack lengths on each side of the specimen, the applied stress and the number of cycles. The relationship between crack length (on tension side) and cycles under different stress ratios are presented in Fig.6.43-6.48. Fig.6.49 shows all six curves (least-square fitted) superimposed on the same $da/dN - a/W$ graph for comparison. Observing Fig.6.49, the following observations can be made:

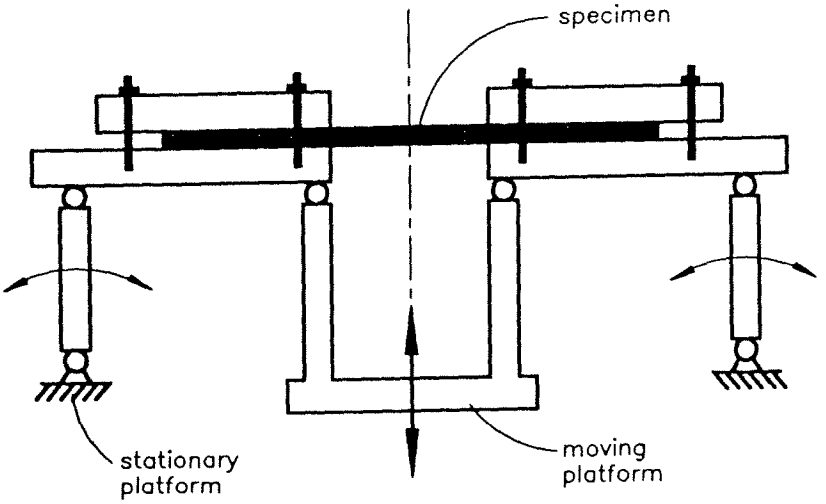

Figure 6.41: A four-point bending fixture

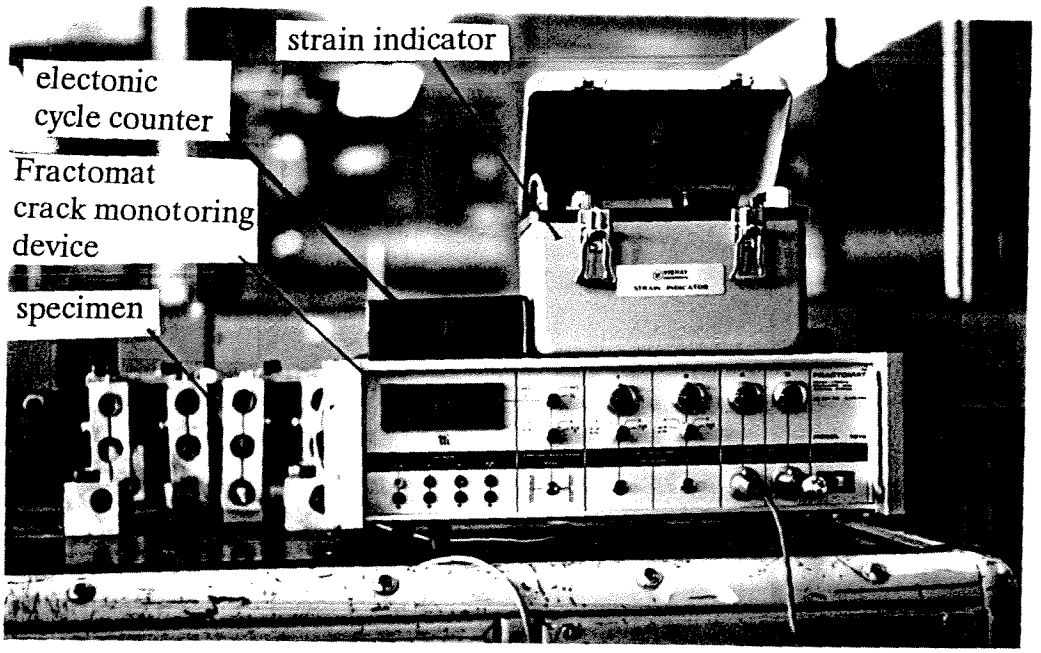

Figure 6.42: A test set-up for out-of-plane bending test

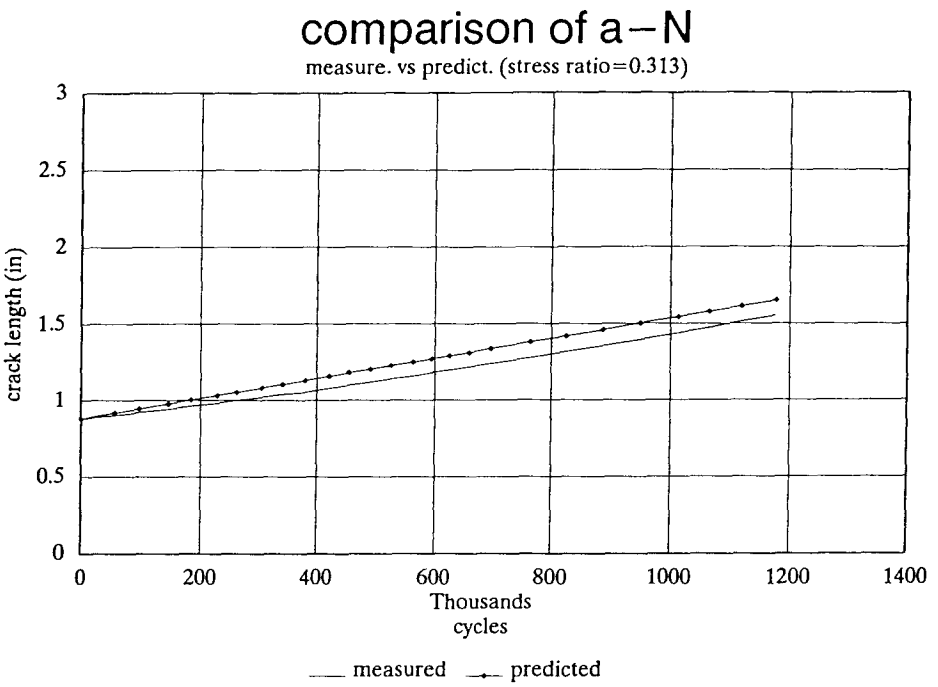

Figure 6.43: Crack growth: R=0.313

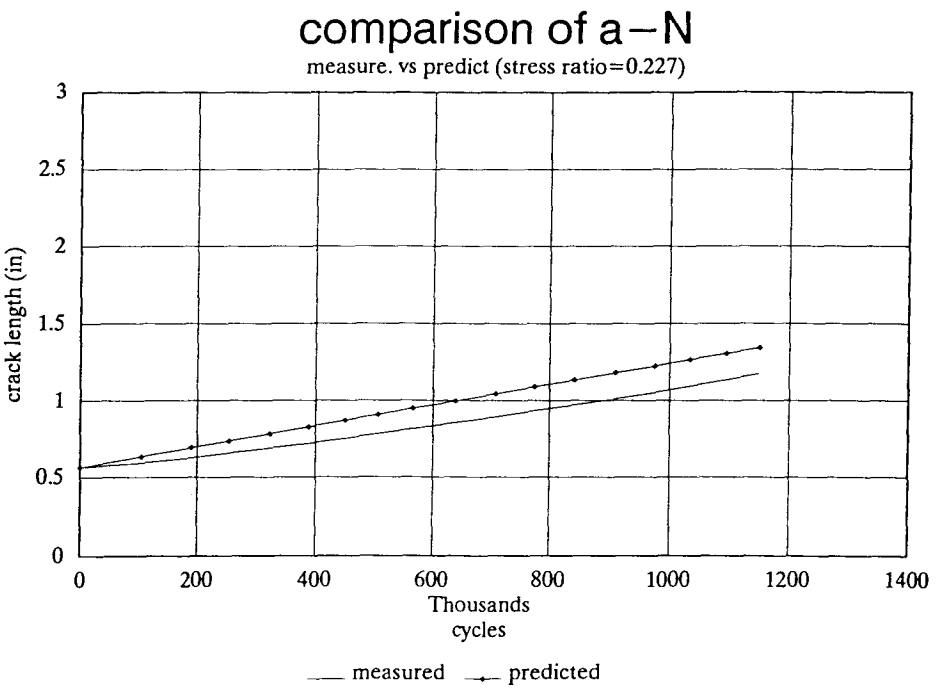

Figure 6.44: Crack growth: R=0.227

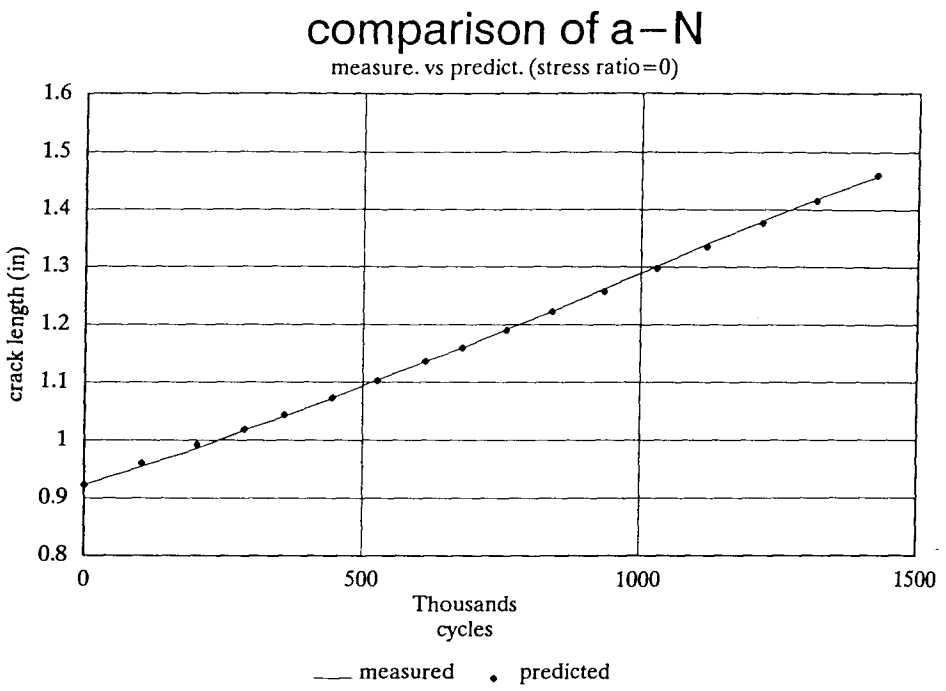

Figure 6.45: Crack growth: R=0

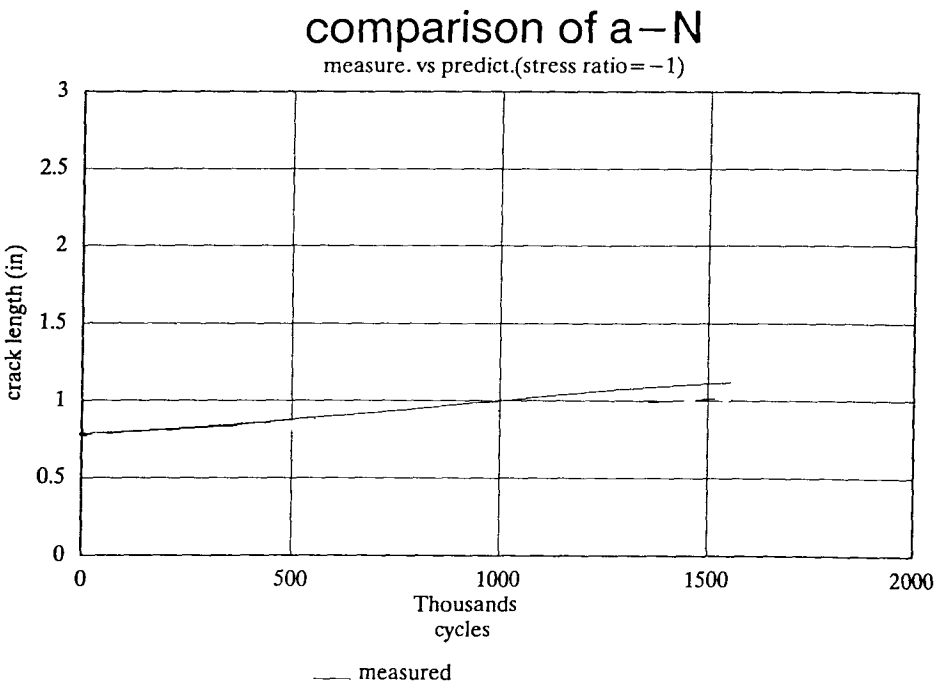

Figure 6.46: Crack growth: R=-1

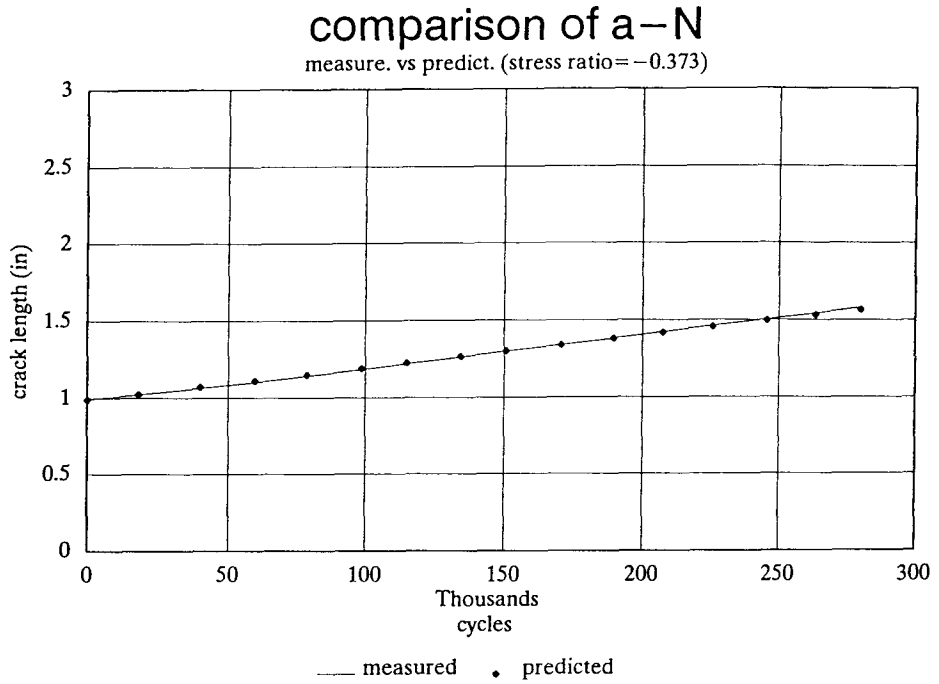

Figure 6.47: Crack growth: R=-0.373

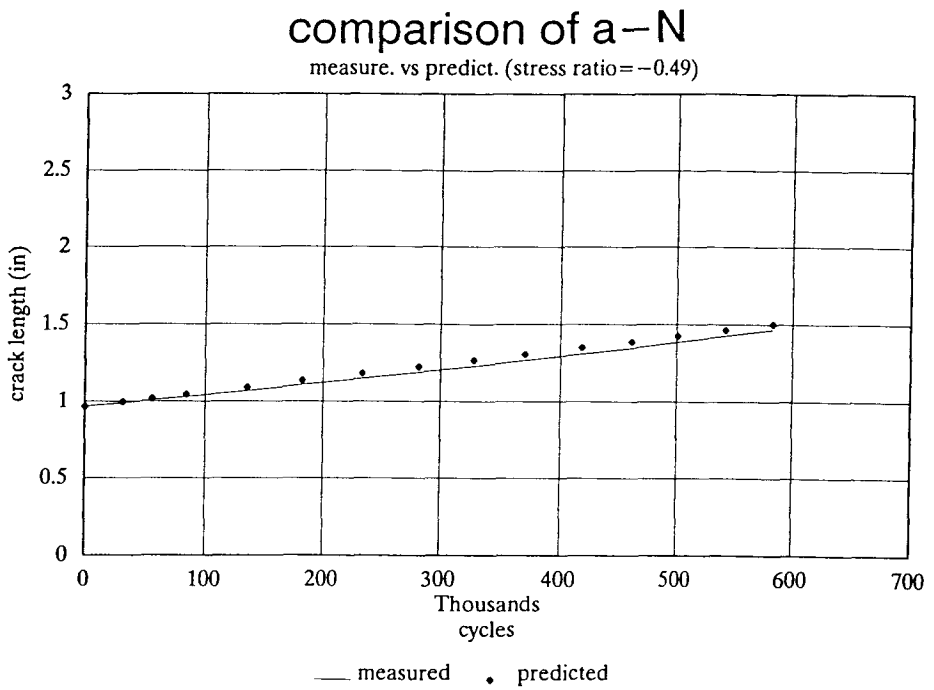

Figure 6.48: Crack growth: R=-0.49

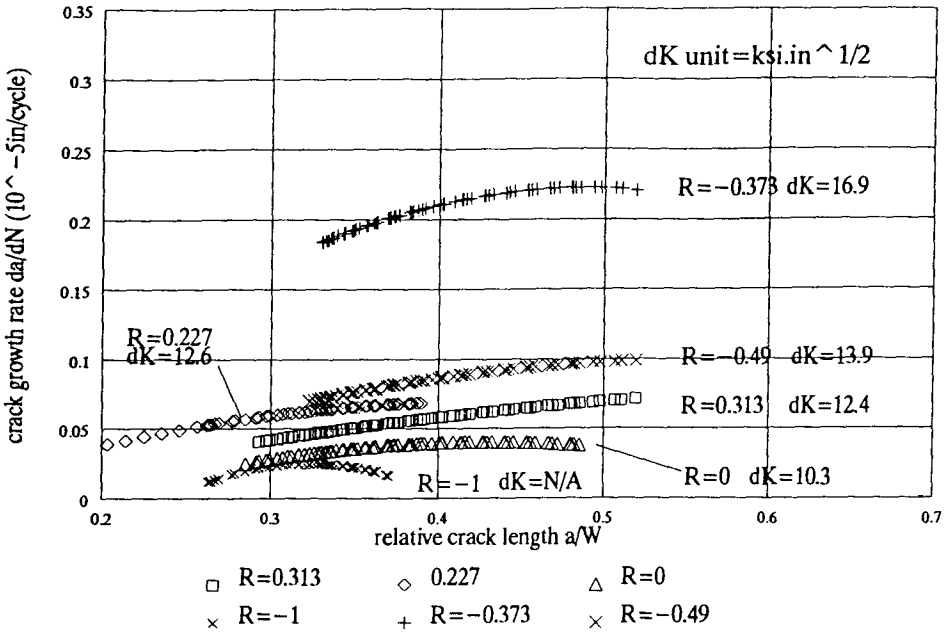

Figure 6.49: Comparison of different crack growth rate

1. The crack growth rate is only slightly dependent on crack length. In Fig.6.43—6.48 one common tendency is shared by all specimens—crack extension is almost proportional to numbers of cycles, in other words, the crack growth rates were almost constant. This implies that the stress intensity factor range ΔK does not change very much in pure out-plane-bending load condition.

2. Stress ratio effect is distinguishable (Fig.6.49).

Fractographical analysis

In order to have a better understanding of the above phenomena, all of the tested specimens were cut open and the crack surfaces examined using the Scanning Electronic Microscope (SEM). The final crack profile of each specimen was measured using an optical microscope and the data were used for the calculations of crack growth.

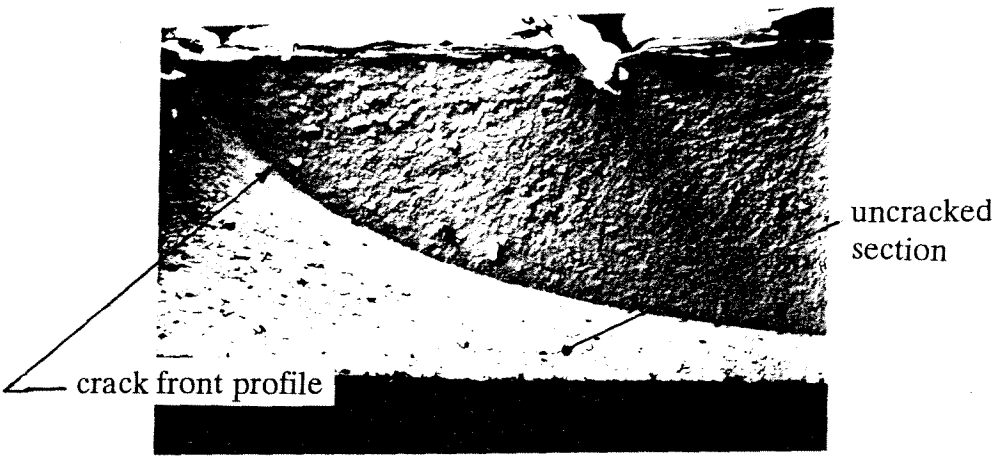

Figure 6.50: A typical crack front profile

Fig.6.50 shows a typical final crack front profile—a smooth, elliptical curve front, which was shared by all six specimens.

In order to obtain a record of the crack propagation process using discrete points a *tinting technique*, a method to mark the crack front by heating the specimen to form an oxide film on the newly created crack surfaces, was used. The specimen was tinted four times by using four different temperatures to mark the four different crack fronts with four different tints of colour. Fig.6.51 shows a photo of the crack front traces.

In Fig.6.51 the process of crack advance can be seen, i.e. the crack growth starts from the corner on the tensile side, grows radially to some distance, then starts to accelerate at a point on the tensile surface—the circular crack front grows into an elliptically curved front, finally the lower part of the front reaches the compressive surface. After this point the crack front advances while maintaining its shape relatively unchanged. This evidence is very similar to that found by Ingema on a sample from a failed blade [1].

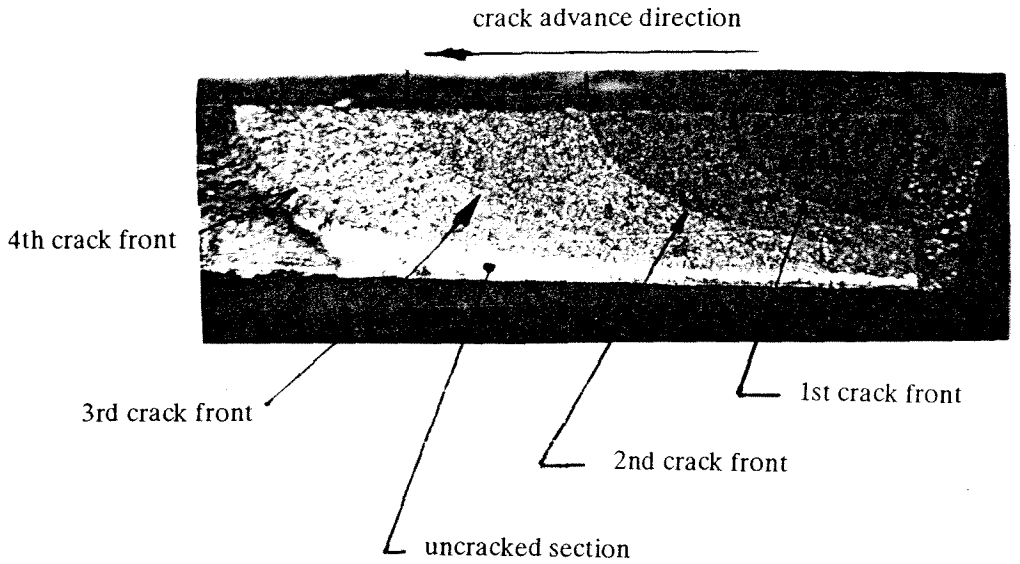

Figure 6.51: The trace of crack advance

As noted in Fig.6.49, the rate of crack growth (da/dN) as a function of crack size is nearly constant. Given the above propagation pattern, the following can be one of the explanations for this behaviour:

According to Paris' assumption [15], crack growth rate is controlled by stress intensity factor range. Therefore, the small change in da/dN means little change in the effective stress intensity factor range. From Fig.6.51 it can be seen that as the lower part of the crack front reaches the compressive surface of the specimen, the crack advances with almost the same crack front shape. On the other hand, the bending load also remains constant, therefore it is reasonable to expect little difference in the stress field around the crack-tip, thus little change in the stress intensity factor range.

Stress intensity factor for out-of-plane bending

In the above analysis, the crack front advances with a curved profile under the out-of-plane bending load. To determine its stress intensity factor, the crack front can be

approximated as a quarter elliptical crack.

In 1981, J.C. Newman and his co-worker [23] published their work on stress intensity factor for a surface crack. They correlated their previous three dimensional finite-element analysis results which covered a wide range of configuration parameters for a semi-elliptical surface crack under tension and out-of-plane bending. Being multiplied by free edge correction factor [9], the formula were used to calculate the stress intensity factor for the crack in the out-of-plane bending tests. The details of the formula are quoted in **Appendix A**.

The stress intensity factors for the final profiles of crack front of all specimens were calculated. The results proved that the higher SIF range is, the faster the crack grows (see Fig.6.49).

Calculation of the crack growth rate

To show the validity of the crack growth rate experimentally obtained (see **Chapter 5**), the crack front profile data and the crack growth rate described by equation (5.17) (in **Chapter 5**) were used to calculate the crack growth in the out-of-plane bending tests. These results were presented in Fig.6.43-6.48. The maximum difference for all six specimens is 4.56% (for details see **Appendix A**). The predictions are encouraging, which proves that the stress intensity factor formula obtained by C.J. Newman and the crack propagation rate experimentally obtained for the bandsaw material are useful. Therefore, they were both used in the failure analysis of a bandsaw blade. It is worth mentioning that without the crack front profile data the calculations would be based on some assumptions of the crack initiation shape which needs further investigation in future study.

Chapter 7

Fatigue-Life Prediction of a Bandsaw Blade

7.1 Introduction

Life predictions of bandsaw blades have been made by previous investigators [10, 5]. The predictions are based on two approaches: (1) the traditional smooth body design approach [10, 5] and (2) the fracture mechanics based fatigue theory approach [5].

Smooth body design approach

Smooth body design assumes that there are no cracks present in the structure. It does, however, include surface roughness and stress concentration effects. The smooth body design approach also qualitatively ignores the distinction between the initiation, propagation and failure phases and only estimates the time to failure. Allen [10] made use of the modified Goodman Diagram to calculate blade life and the allowable stresses in the blade. Allen's approach, however, is based upon the assumption of achieving an infinite life of one million cycles, which is not achieved in practice. In addition, like other previous investigators, Allen did not distinguish the SCF under tension loading from those under out-of-plane bending. The stress concentration factor he used was far larger than expected in service. Lehmann [5] performed finite life calculations based on an S-N diagram employing the material fatigue limit and yield strength. However these results could not explain the existence of the cracks in the blades at low lives as seen in service. Unfortunately, Lehmann's assessment lacked first-hand experiments to provide data on the material studied, therefore, the results could not satisfactorily explain the

blade life-span of typically less than four hours.

Fracture mechanics approach

The fracture mechanics approach allows for a quantitative differentiation between initiation, propagation and failure stages of crack growth. Specifically,

- *crack initiation*—quantified by the numbers of cycles consumed for a crack to be nurtured and grow to some arbitrarily defined length a_i.
- *crack propagation*—(1) propagation rate: quantified by experimentally obtained relations [15], e.g. the Paris' law: $da/dN = C(\Delta K)^b$ (C and b are material constants). (2) propagation time : quantified by integrating the above relation with an upper limit of a_C defined in the following item and a lower limit of a_i.
- *failure*—quantified by critical crack length a_C which is calculated from the fracture toughness K_{IC} or K_C.

As noted previously, Lehmann applied fracture mechanics concepts to explain cracking problems in saw blades [5]. However most of his results were based on assumed material properties, such as fracture toughness and crack propagation rates. In the following sections the assessment of fatigue life for a bandsaw blade in this research program are discussed. In comparison to the previous investigators, a much better assessment is possible as more first-hand information about the fracture aspects of bandsaw blades has been obtained. In this analysis, it is assumed that the pre-strain stresses and the bending stress fields as created by the wheel provide the dominant driving force for cracks forming in the blade (see **Chapter 2**).

load cases \ critical crack length			static load (in)	dynamic load (in)	difference (in)
without residual stress	pre-strain force level	20,000 lb	2.825	1.24	1.04
		18,000 lb	3.00	1.34	1.66
		15,000 lb	3.12	1.44	1.68
with 10 ksi residual stress	pre-strain force level	20,000 lb	2.48	0.94	1.54
		18,000 lb	2.52	0.99	1.54
		15,000 lb	2.62	1.09	1.53

Table 7.4: The assessment of critical crack length

7.2 Critical crack length of a bandsaw blade

The criteria for component fracture is typically assumed to be the critical crack size, beyond which the crack growth may become and catastrophically fast. The critical crack sizes for commonly used blade loading conditions have been estimated. For comparison, two cases were considered: the blade (1) without residual stress and (2) with an assumed residual stress of 10 ksi.(69 MPa) [5]. The model assumed the an edge crack in a plate of finite width subjected to tension and bending. Table 7.4 lists the results of this analysis (See **Appendix A** for the details of the calculations).

According to the results listed in Table 7.4 it is clear that both pre-strain force levels and residual stresses have a significant influence on the critical crack length. As far as the pre-strain force is concerned, the difference in critical crack length can be up to 16%. If a residual stress of 10 ksi (69 MPa) is involved, the difference jumps to as high as 50%.

The difference in crack length between the dynamic and static load condition can be as much as 1.68 in.(42.7mm). The range covered by the dynamic critical crack length under the condition considered is 0.94-1.24 in.(25.1mm—31.5mm).

In practice [5], when a cracked blade is removed from the machine and examined, the length of the crack(s) are typically on the order of 1/16 in.(1.6mm), i.e. just visible, to a maximum of about 1.5 in. (38mm). The Worker's Compensation Board of British Columbia defines (see [12] article 66.36 (1)) the maximum safe length of a crack to be 1/10 of the blade width (i.e. about 0.95 in.(23mm) for the blade studied in this program). This limit is believed to be on the conservative side of practical experience. Generally speaking, a crack in a blade can grow in a stable manner up to about 0.95 in.(23mm) in length. At this point, it is below or very close to the estimated non-residual stress critical length range from 1.24-1.44 in.(31.5-36.6mm). The above predictions of critical crack length suggests that depending on the initial assumptions, a crack may grow as long as 0.94-1.44 in (23.9-36.6mm) prior to reaching the critical length.

7.3 Propagation life of a bandsaw blade

7.3.1 Fatigue loads experienced by a blade

According to the experimental evidence obtained from the crack growth tests (see **Chapter 6**), a crack starts at the corner of the outer surface (Fig.6.50), then propagates radially as a corner crack until the crack front reaches the inner surface. The crack then propagates as a through-thickness crack. In this process, both bending and tensile stresses are involved in driving the crack. As discussed in **Chapter 6**, in half of a revolution, the blade experiences two different load periods: 1) pure tension; and 2) tension plus bending. Thus, the outer surface of the blade experiences 1) tension produced by pre-strain force, 2) pre-strain tension plus the tension induced by bending, while the inner surface

experiences 1) pre-strain tension, 2) pre-strain tension plus the compression induced by bending (Fig.1.2). Therefore, both the inner and the outer surfaces experience two different alternating stress fields. The changes in crack configuration and stress field require different methods to evaluate the SIF along the crack front.

Before the corner crack becomes a through thickness crack the stress field changes along the whole crack front can be calculated using the formulation developed by Newman [23] (see **Appendix A** for details), while after the crack penetrates the thickness, the through thickness feature must be considered in the calculation of the SIF along the curved front. During this stage, the SIF under tension as expressed by eqn. (3.11) (**Chapter 3**), and the SIF under out-of-bending loads correlated by Wilson and Thompson [24] (see **Appendix A** for details) were used to evaluate the stress intensity factors at both the outer and the inner tips of the crack front.

An assumption for the initial crack shape

The actual initial flaw shape in the blade is typically unknown, therefor, an assumption was made that the initial crack front has a specific symmetric geometric profile, e.g. a quarter circle. Certainly, this assumption effects the final prediction of life-time of the component studied. In the case of a bandsaw blade, as discussed in **Chapter 6**, because of the out-of-plane bending load, a crack initiates as a corner crack, and extends in two dimensions. If the dimension of the initial crack is sufficiently small, the assumed profile of a quarter circle should be a close approximation. *In the following prediction, a quarter circle profile with a 1mm radius was assumed for the profile of initial crack front in the blade.*

An assumption for the transition from a corner crack to through-thickness crack

In a blade, crack growth from a corner crack to the critical crack length is not a single-phase process in terms of crack configuration, i.e. the crack grows, firstly, as

a corner crack, then in a transition phase, and finally as a through-thickness crack. Theoretically, there is a critical point through which the crack transforms itself from a part-through or corner crack into a through-thickness crack. Crack growth behavior before and after this point are different because of the different crack configurations, therefore, the corresponding SIF's must be evaluated in different ways. How a crack behaves during this transition phase is still unknown. An assumption must be made about this transition (see Fig.7.52)

In the following assessment, it is assumed that as soon as the side tip of the crack front reaches the inner surface of the blade (point **A**), the crack growth at point **A** starts to propagate towards the center of the blade. At the two tips of the crack front, crack growth occurs at different rates as they precede into the blade until the final critical crack length is reached.

Notch field dimension

As discussed in **Chapter 2**, each individual tooth of the blade acts as a notch which sharply raises the stress level when the blade is loaded. The contributions to the stress increase are different for the pre-strain loading component and for the out-of-plane bending component. In the crack propagation calculations the stress concentration effects are accounted for in the form of the so-called *'notch field'* [25]. The notch field defines the distance to which the stress concentration effect extends. In 1981, Smith [25] developed a simple equation to quantify the dimension of the notch field which is dependent on both the notch depth and its radius of curvature (see Fig.7.53). For a notch with a depth of α_n and radius of curvature of ρ_n, the dimension of the notch field can be expressed as $0.13\sqrt{\alpha_n \rho_n}$. For the bandsaw tooth studied having $\alpha_n = 0.55in$, $\rho_n = 1.08in$, the notch field is evaluated as $0.13\sqrt{\alpha_n \rho_n} = 0.13\sqrt{0.54 \times 1.08} = 0.1in = 2.54mm$, which is close to the thickness of the blade (0.073 in), i.e. the stress concentration factors for the tension and the bending have effect only within this distance. It can be seen that a crack

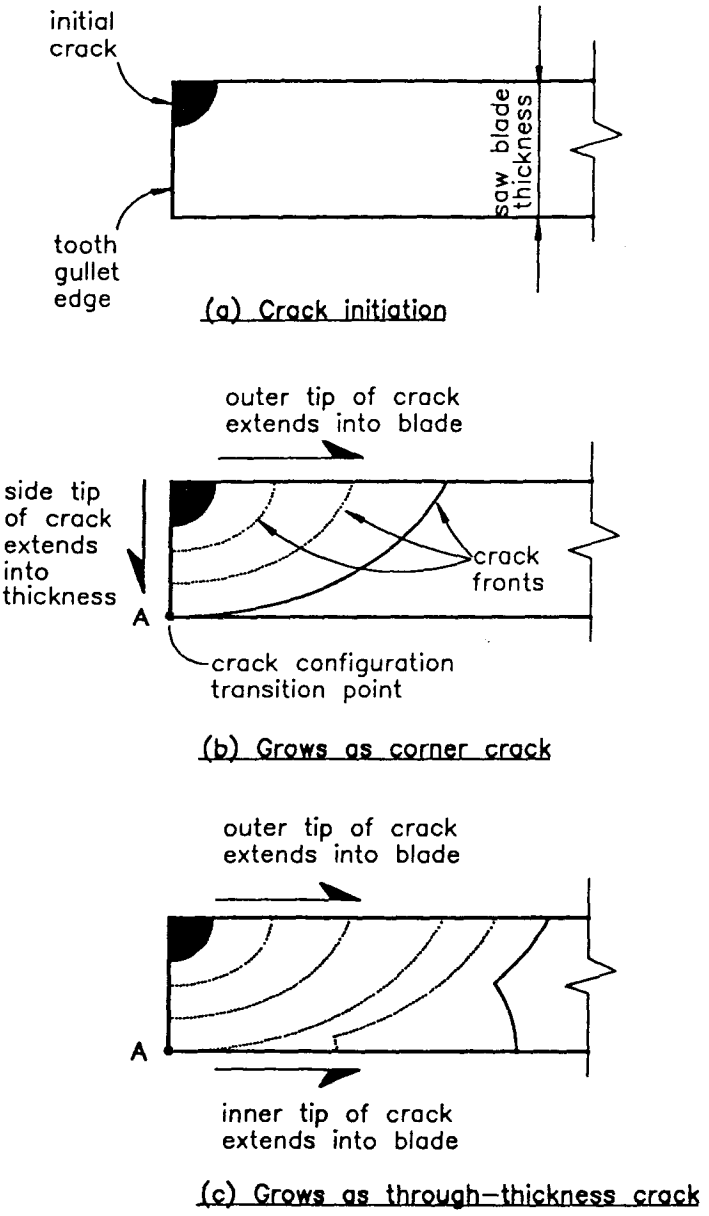

Figure 7.52: Transition of crack growth

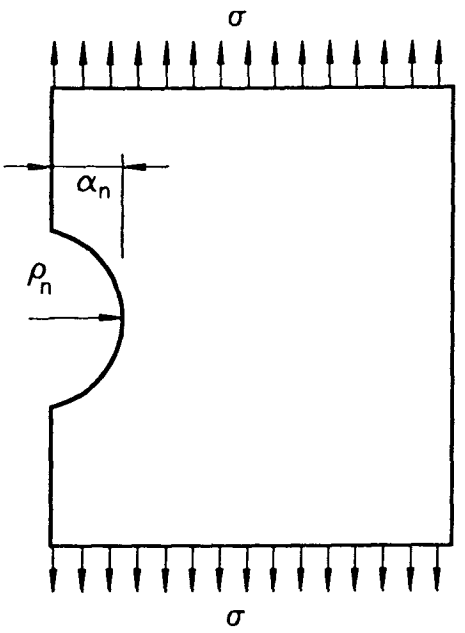

Figure 7.53: Definition of a notch field

experiences different stages, i.e. initiation, growth through the notch field, and growth up to the critical crack length. During the whole propagation period, the crack driving force, and the SIF along the curved crack front varies from stage to stage, thus the crack growth rate varies in these different stages. Therefore, any prediction must evaluate the varying growth rates in these individual stages.

7.3.2 Analysis of growth life for a blade

Based on the critical crack length, assumed initial crack shape and notch field dimension described, and using the assumptions discussed previously, assessments of the cyclic life of a blade were made using the experimentally obtained da/dN—ΔK relationship (eqn.(5.18) in **Chapter 5**). Table 7.5., 7.6 and Fig.7.55-7.63 show the results (see **Appendix A** for the details of calculations). The crack initiation life as experimentally

obtained from the small specimen tests were used (see **Chapter 4**). The specific geometry and load parameters used in the prediction are listed in **Appendix A**.

How a crack grows in the blade—qualitative analysis

Fig.7.54 shows a schematic illustration of the crack growth process in a blade of a bandsaw machine having a driving wheel of 5 ft.(1.5m) diameter working with a pre-strain force of 20,000 lb.(89,000 N). To assist in the description of the crack growth process, the entire growth period is divided into five 'snap-shots'. Each of these 'snap-shots' represents the crack front profile at one or more typical points during its growth period.

Snap-shot (a)—Crack initiation. The crack initiates one way or another as a quarter crack with a radius of 1mm.

Snap-shot (b)—The crack grows as a corner crack. In this period, the SIF along the entire crack front can be evaluated from Newman's equation (eqn.(A.21) in **Appendix A**). However, in this period there are two stages. In the early stage, it is clear from Newman's equation that the SIF range along the crack front are determined only by the bending load ($\Delta K = (\sigma_B + H\sigma_T)F - H\sigma_T F = \sigma_B F$, where H, F are geometry factors accounting for the shape of the crack front). Therefore, the crack growth in this stage is controlled by the bending load. Since the stress field produced by the bending is a linear distribution across the thickness, the SIF range of the side tip of the crack front becomes zero at some point **A**. From point **A** down, the second stage starts, at the side tip, the SIF produced by the bending is either equal or less than zero, while the SIF generated by the tension stays constant, thus the SIF range at the side tip of the crack front is evaluated by the pre-strain force. Therefore, crack growth in this second stage is controlled by the pre-strain force. In the entire period, the outer tip (point **C** of the crack front grows faster because of its higher SIF range, while the side tip of the crack front grows slower and slower because its stress intensity becomes lower and lower as the tip approaches point A. Therefore, the crack front is stretched into a quarter of an

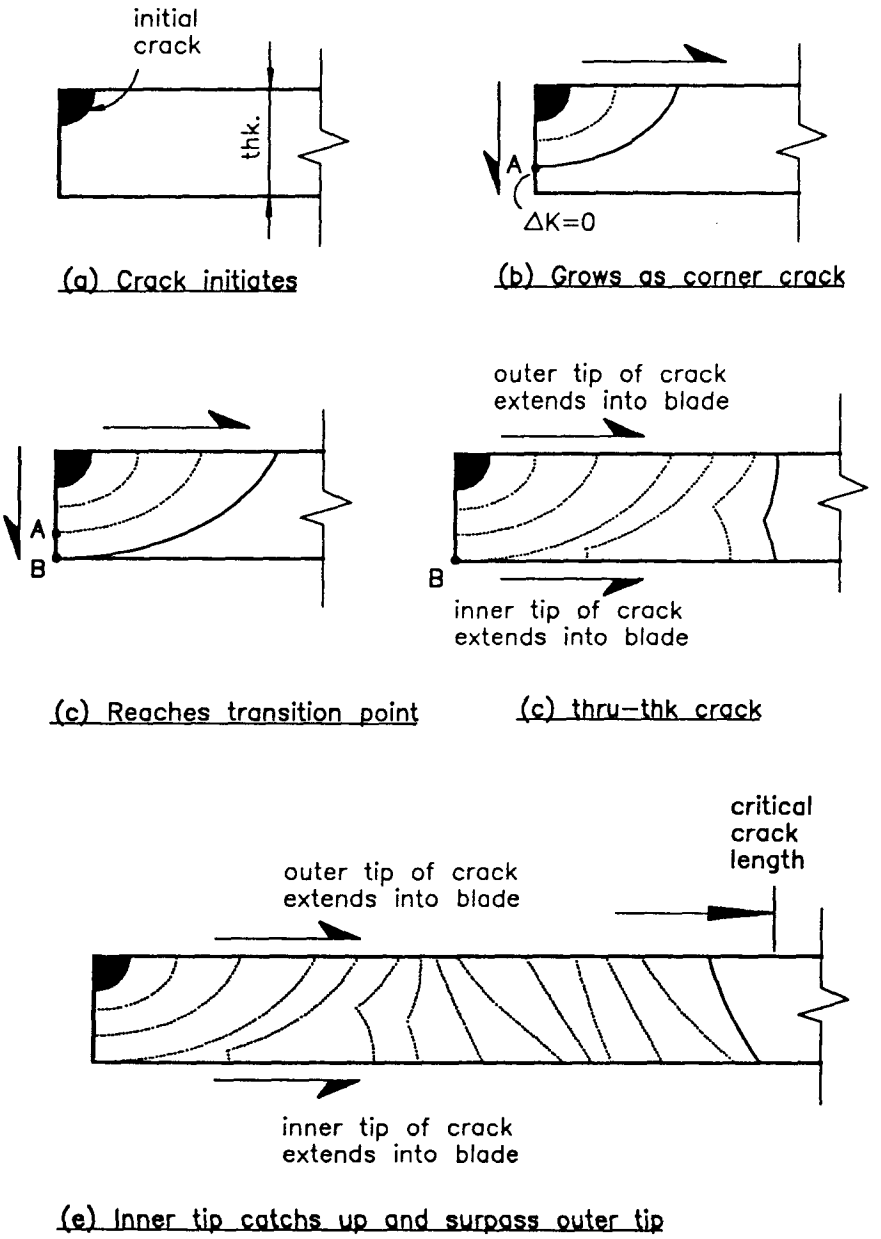

Figure 7.54: Schematics of crack growth in a blade

elliptic profile.

Snap-shot (c)—Transition into a through-thickness crack. As soon as the side tip of the crack front reaches the inner surface, the tip starts to precede into the center of the blade. The extension in each of the first several thousand cycles are relatively large because the SIF at point **B** is driven up by both its sharp corner and the stress concentration of the tooth 'notch field'. After the crack becomes through-thickness, the SIF generated by the bending can be evaluated using Wilson's equation (eqn.(A.36) in **Appendix A**), while the SIF produced by the pre-strain force was calculated using eqn.(A.37).

Snap-shot (d)—The inner side of the crack front catches up. After the transition into a through-thickness crack, the SIF range at the inner crack tip of the crack front is higher than that at the outer crack tip, therefore the inner crack tip advances faster and catches up to the outer crack tip.

Snap-shot (e)—The inner-side tip surpasses the outer-side tip. After the inner-side tip catches up the outer-side tip, for a period of time, it leaves the outer-side tip behind further and further. At a point, the difference between the two tips is large enough so that the outer tip develops a sharp corner which raises its SIF range, thus advancing faster than before for a period of time. Then the distance between the two tips becomes smaller and smaller until SIF range of the outer tip becomes lower than that of the inner tip, then the distance starts to wider again. This process repeats itself again and again until the critical crack length is reached. In this period, the inner-side crack tip is always ahead of the outer tip after it catches up the outer crack tip in the case of 20,000lb. pre-strain force. It should be stressed that although the inner tip is always ahead of the outer one, the final failure is still controlled by the outer crack tip because no matter what the pre-strain force is, the maximum SIF (not SIF range) at the outer tip is always far higher than that of the inner-side tip.

How a crack grows in the blade—quantitative analysis

Table 7.5 and 7.6 present the prediction of the crack propagation life for a bandsaw blade. The tables also include the crack initiation lives of the specimens with different surface roughness (see **Chapter 4**). A tensile residual stress of 10 ksi. was also considered as different cases in the calculations. The residual stress was estimated in reference [5] accounting for the stress induced by the roll tensioning process. In this calculation, the residual stress was treated as if an extra pre-strain stress field was imposed on the blade. To visualize the prediction, the information contained in tables is also presented in graphical form in Fig.7.55-7.63. The crack growth lives are all presented in units of time (i.e. minutes) which is converted from number of cycles based on the assumed speed of the saw blade. The loads and geometry parameters used in the calculations are all listed in **Appendix A**.

Crack growth life

According to Table.7.5-7.6, without the assumed residual stress, the crack growth life for each of the three pre-strain levels exceeds 240 minutes (4 hours). The crack growth life for a 20,000lb pre-strain force level is just over 240 minutes (4 hours). However, with the assumed residual stress, the growth life for all cases are reduced dramatically, even the longest does not reach 120 minutes (2 hours). The residual stress reduces the crack growth life by at least 70%, at the worst by 90%. This observation has great practical significance as in actual sawmills, it is typical that a new blade is rolled [5] so that the center strip is slightly longer than the tooth edge (called 'back crown') to maintain a straight cutting edge. This rolling introduces a compressive stress in the middle strip and tensile stresses at the tooth and back edges. Therefore it is expected that the crack propagation life may be much shorter than 240 minutes (4 hours). For instance, in the case of a 10 ksi. residual stress, the crack growth life can be as short as 76-113 minutes (1.2-1.6 hrs). Even if a crack initiation life of 44-47 minutes (for a rough gullet surface)

A. without residual stress (unit: minutes)

Pre−strain	crack initiation		crack growth life		total fatigue life	
Force Level (1000 lb)	fine surface	rough surface	as corner crack	as thru−thk. crack	for fine surface	for rough surface
20	427	44	49	194	670.2	287.4
18	455	44	55	268	778.4	367.4
15	600	47	70	461	1131	577.8

B. with residual tensile stress of 10 ksi. (unit: minutes)

Pre−strain	crack initiation (assumed)		crack growth life		total fatigue life	
Force Level (1000 lb)	fine surface	rough surface	as corner crack	as thru−thk. crack	for fine surface	for rough surface
20	427	44	36	40	503.2	120.4
18	455	44	37	48	540.4	129.4
15	600	47	39	74	713	159.8

Table 7.5: Crack-growth life prediction in a bandsaw blade (A)

A. without residual stress

Pre−strain Force Level (1000 lb)	crack initiation % of total fatigue life		as corner crack % of total growth life	as thru−thk. crack % of total growth life
	fine surface	rough surface		
20	64	15	20	80
18	59	12	17	83
15	53	8	13	87

B. with residual tensile stress of 10 ksi.

Pre−strain Force Level (1000 lb)	crack initiation % of total fatigue life		as corner crack % of total growth life	as thru−thk. crack % of total growth life
	fine surface	rough surface		
20	85	9	47	53
18	84	8	44	56
15	84	7	35	65

Table 7.6: Crack-growth life prediction in a bandsaw blade (B)

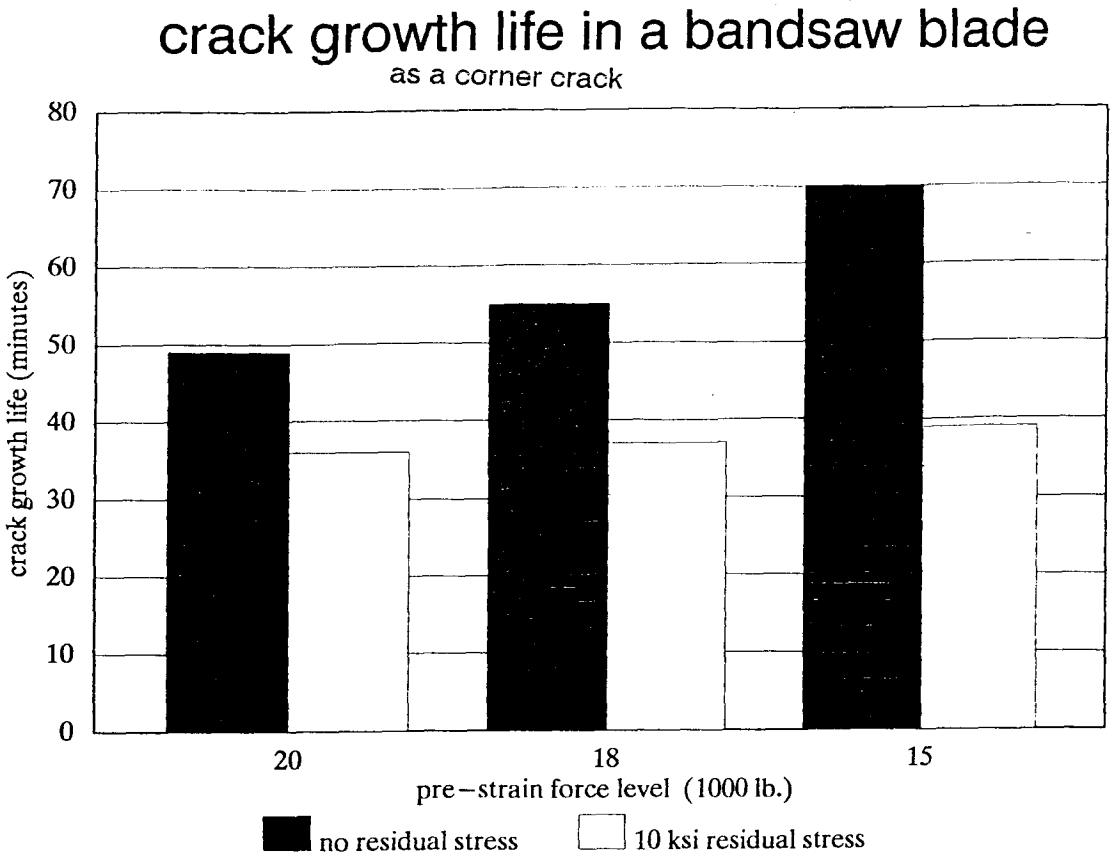

Figure 7.55: Crack-growth life: as a corner crack

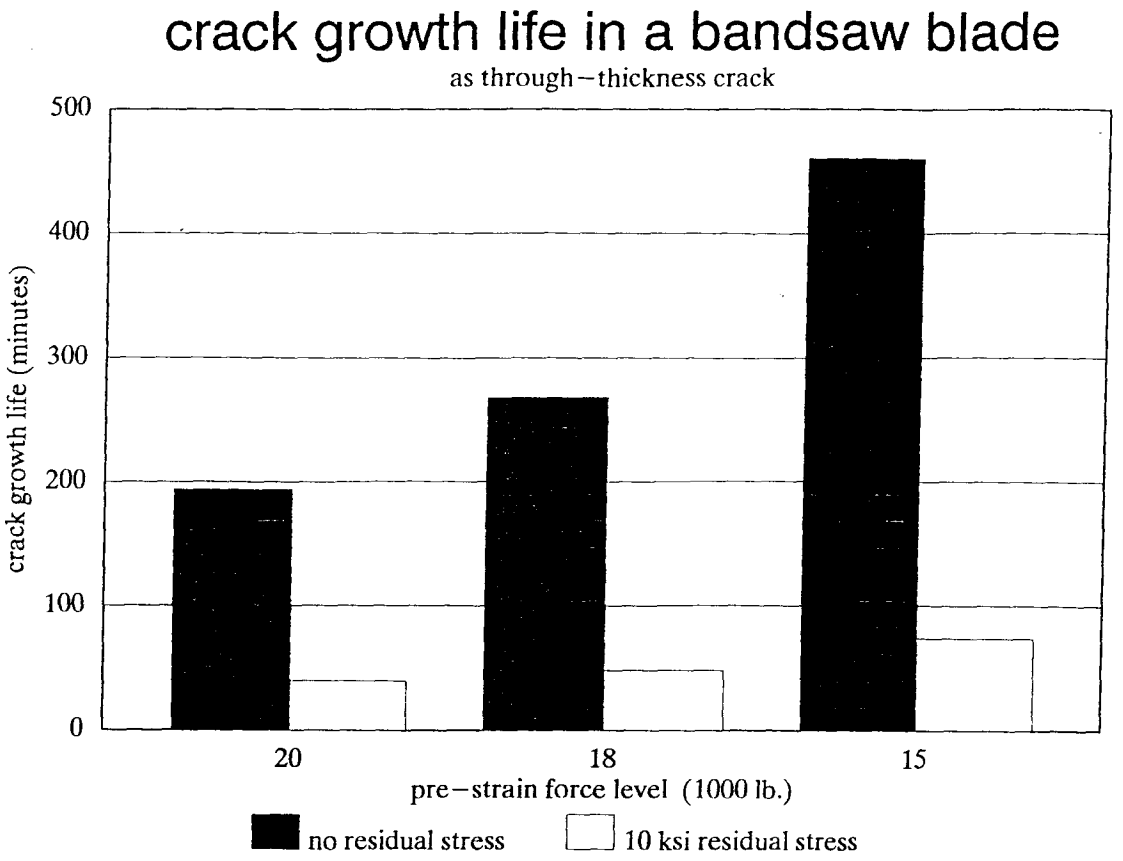

Figure 7.56: Crack-growth life: as a through-thickness crack

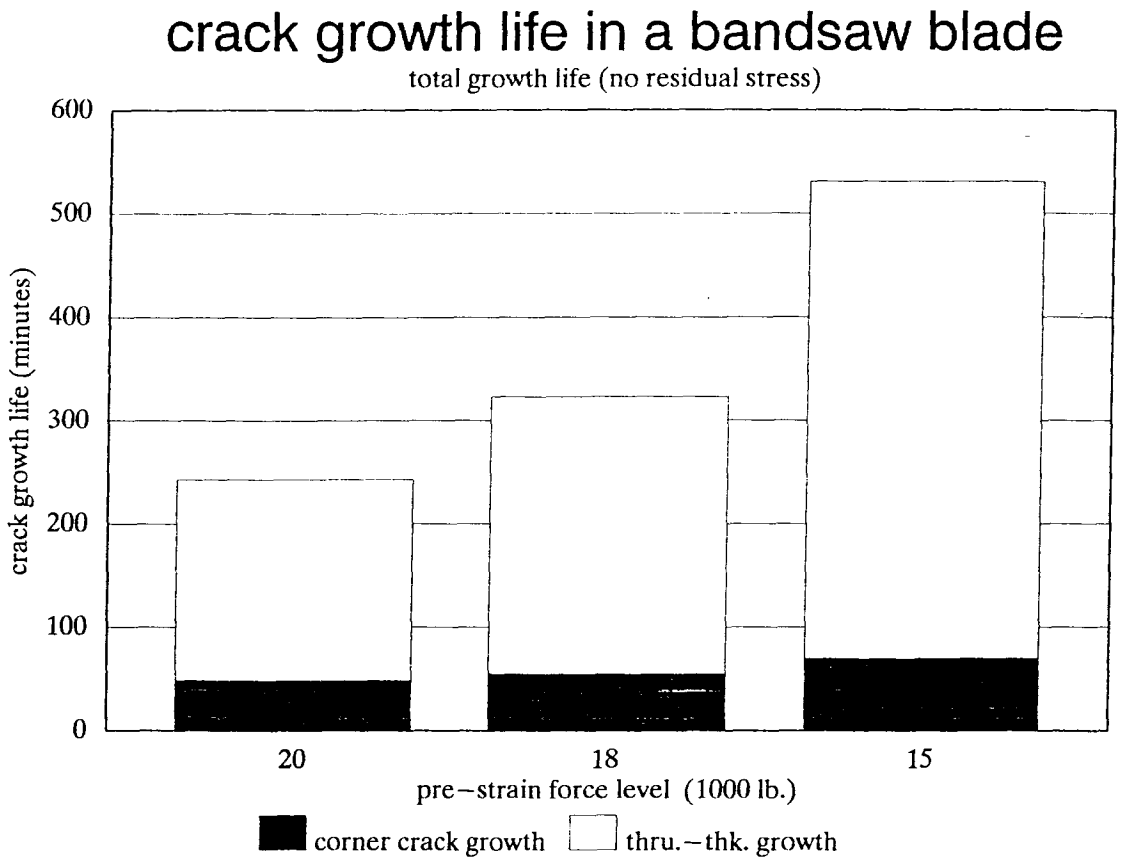

Figure 7.57: Total crack-growth life: no residual stress

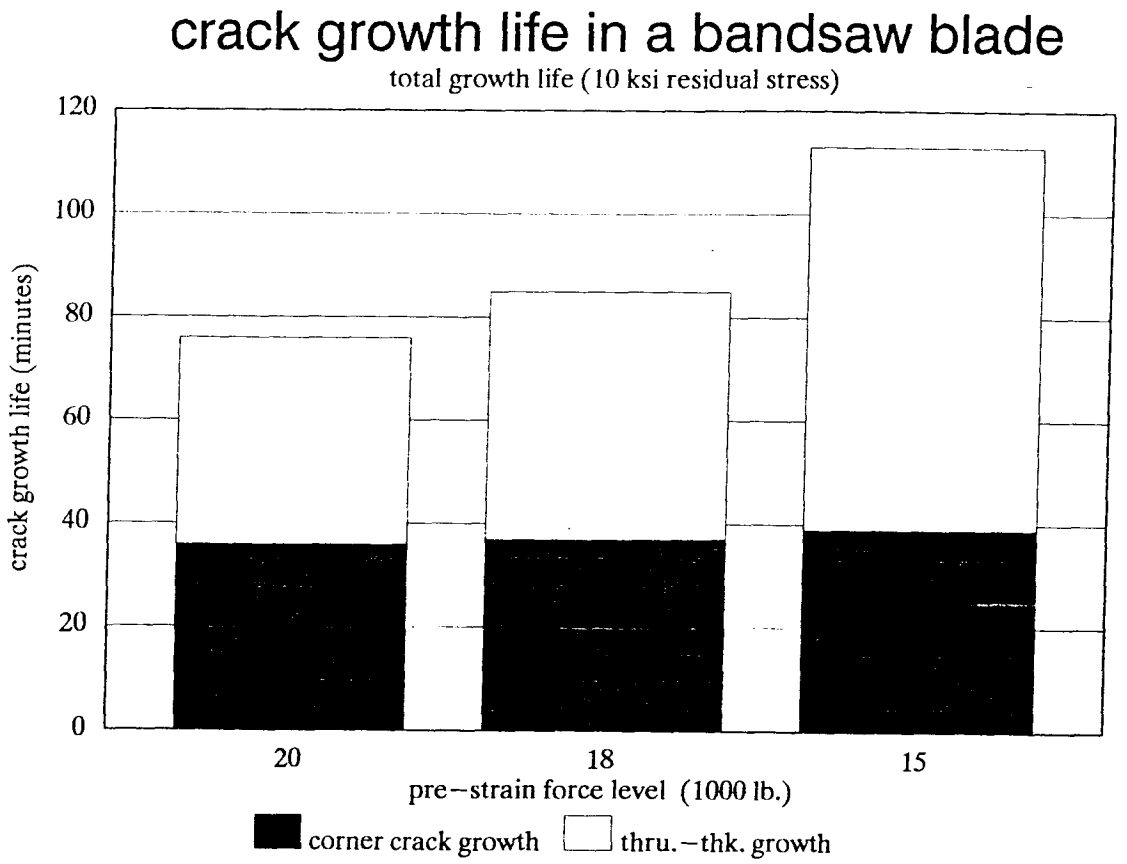

Figure 7.58: Total crack-growth life: 10 ksi. residual stress

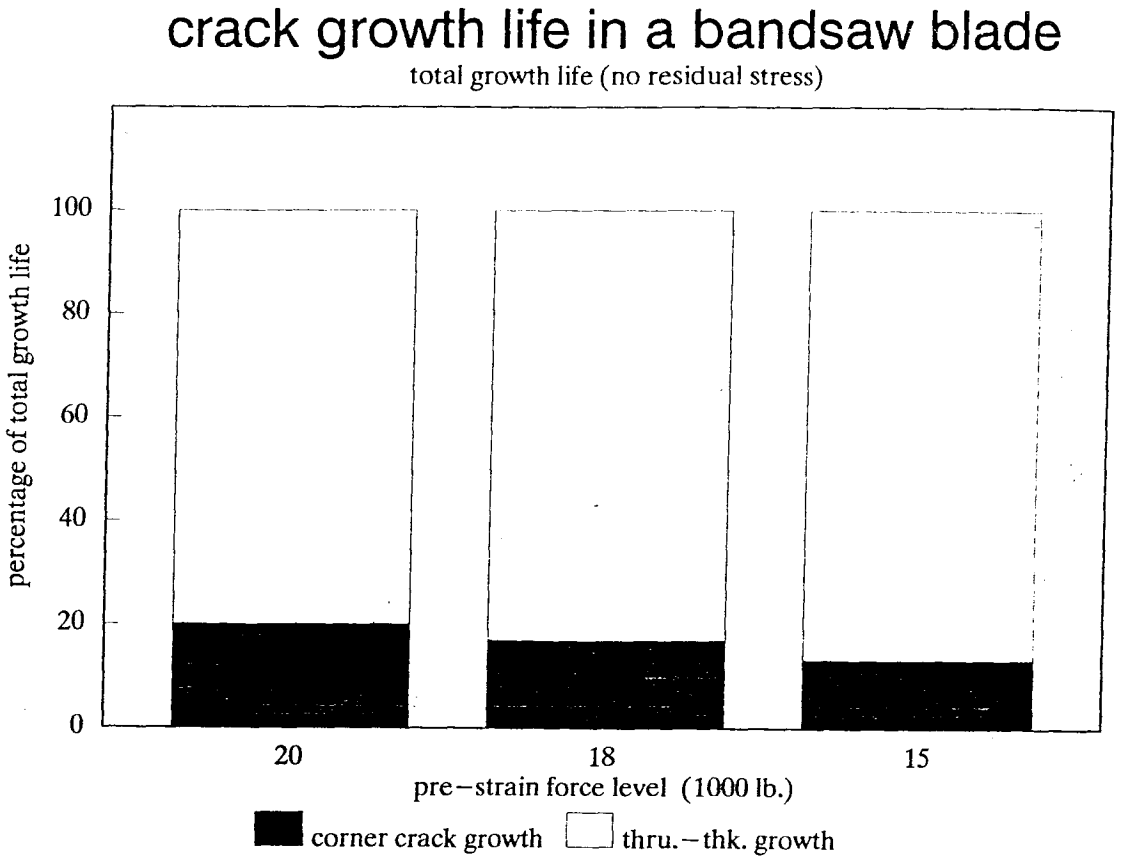

Figure 7.59: Crack-growth life distribution (%): no residual stress

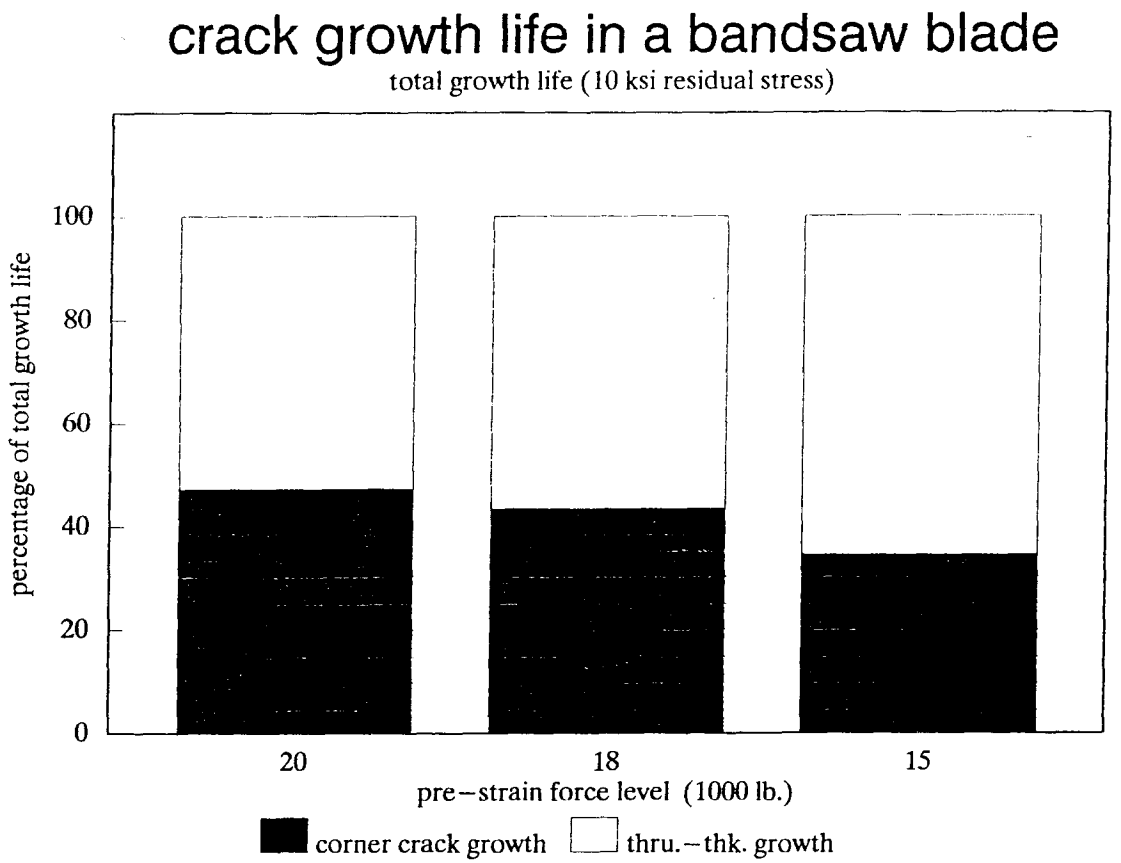

Figure 7.60: Crack-growth life distribution (%): 10 ksi. residual stress

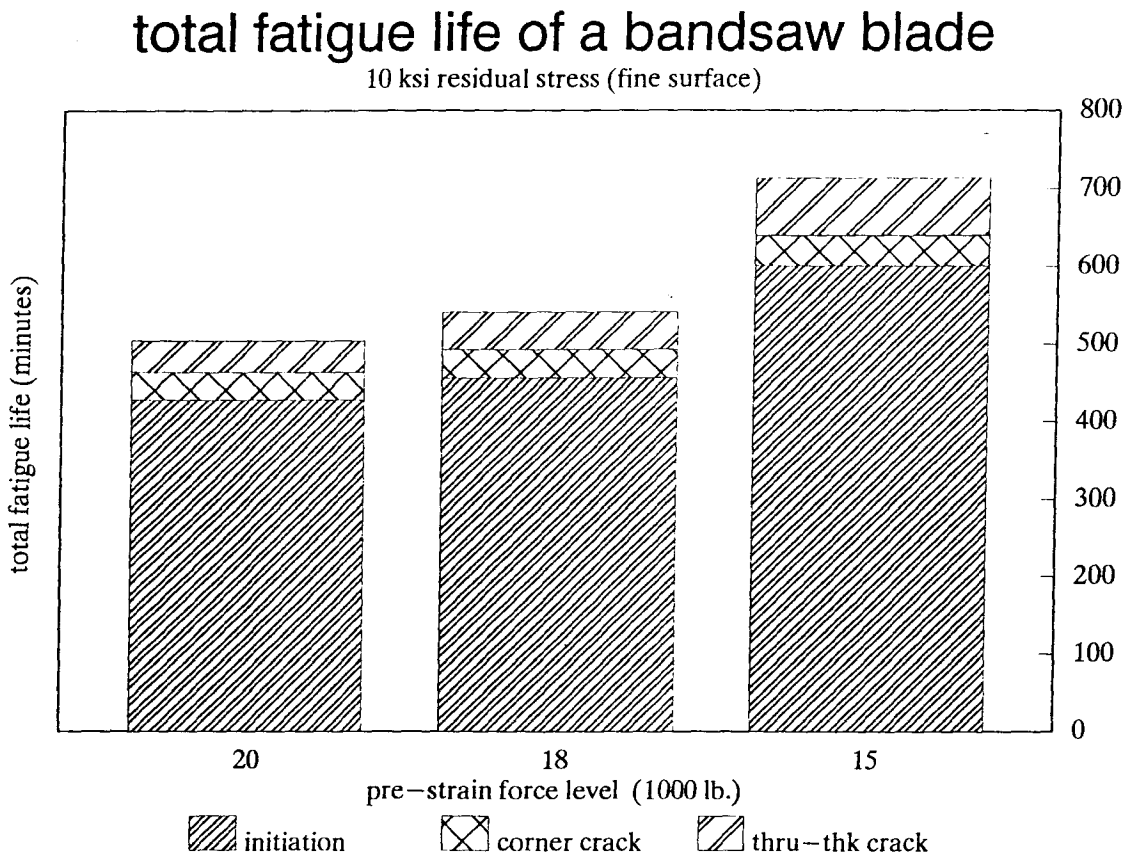

Figure 7.61: Total fatigue life of a blade: fine surface

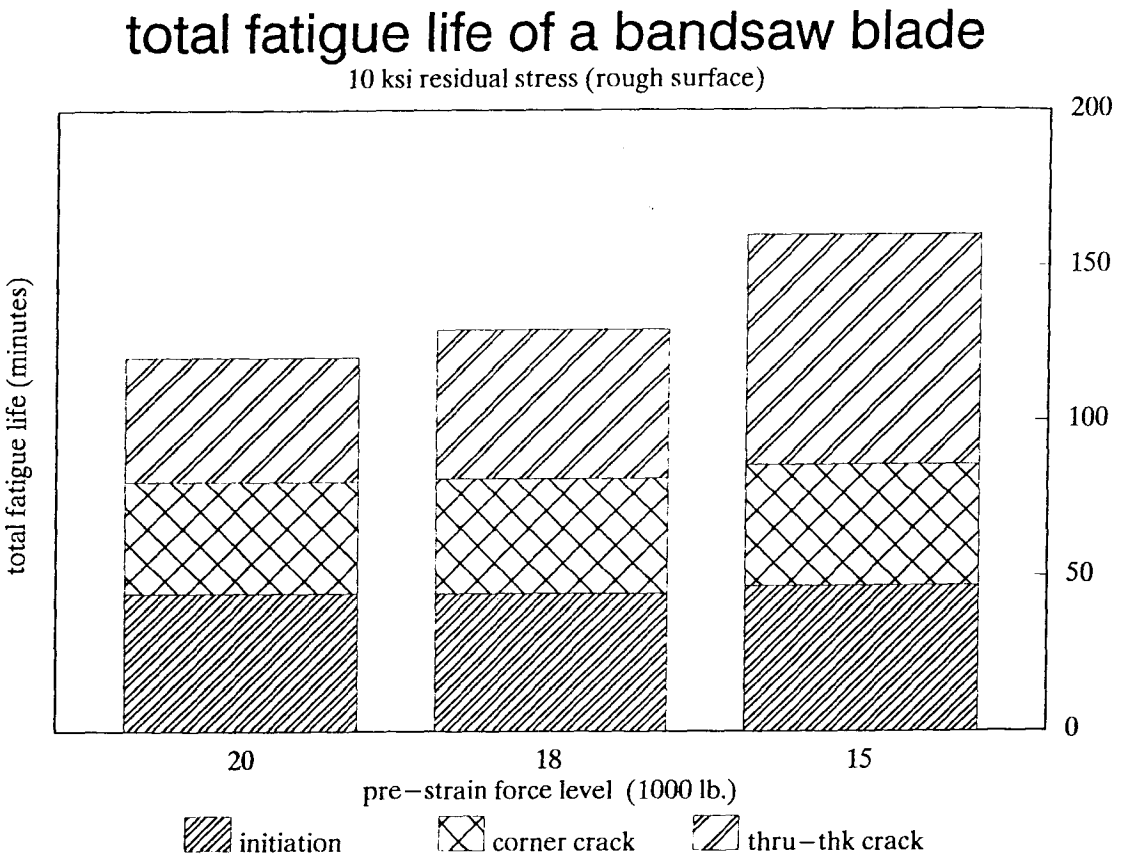

Figure 7.62: Total fatigue life of a blade: rough surface

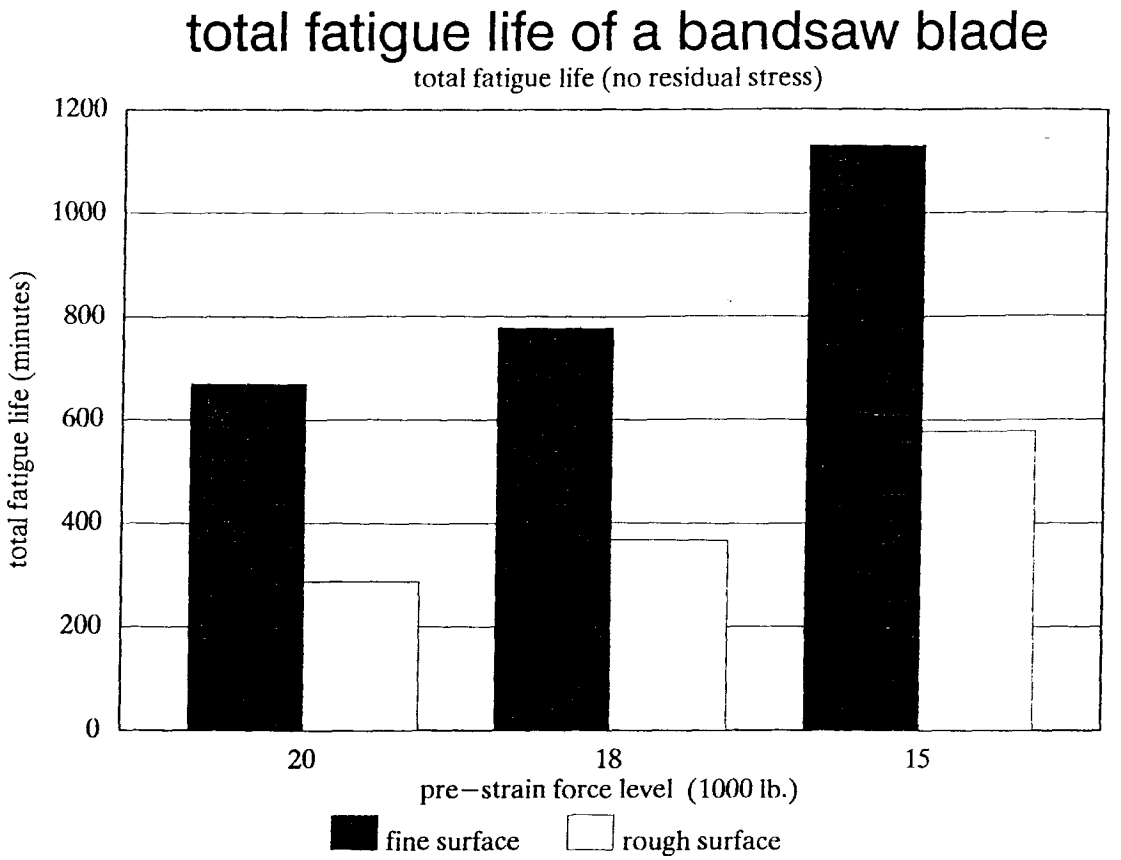

Figure 7.63: Total fatigue life of a blade: surface roughness effect

are added to the crack propagation life, the blade is still predicted to fail prior to one shift of 240 minutes (4 hours). This explains why it is possible that failure can happen to a freshly ground saw blade (although visible cracks are expected to be removed in the grinding process).

Residual stress effect can also be used in favor of a blade fatigue life. If a compressive residual stress field is introduced in the gullet region and its immediate neighbor area, crack growth can be slowed down dramatically and even stopped. The widely used 'hammering' technique is based on this idea.

Distribution of crack growth life and the role of pre-strain force

In Table 7.5-7.6 (or Fig.7.55-7.63) it can be seen that in the case of a 20,000 lb. pre-strain force, most of the crack growth life is consumed as a through-thickness crack, i.e. the propagation life is controlled mainly by pre-strain force since the pre-strain force controls the SIF during the through-thickness propagation (see the discussion in the snap-shots (b) and (e)). On the other hand, as the pre-strain level increases, including tensile residual stress, the percentage of the propagation life occupied by corner crack increases up to 47%. This means that the bending load has relatively more contribution in promoting crack advance.

Residual stress effect

From Fig.7.56 it can be seen that in the process of through-thickness growth a tensile residual stress of 10 ksi can reduce the growth life upto 80%. This is a very strong influence. If a compressive residual stress can be introduced into the blade, the crack growth life can be prolonged in the same scale.

Role of crack-initiation life—surface roughness effect

The crack initiation lives obtained empirically are used in calculating the total fatigue life for the assumed blade configuration. For the same pre-strain force, the crack initiation lives are different for varying surface roughness. Fig.7.61-7.63 show the influence of the

surface roughness on the total fatigue life of the blade (here 10 ksi. residual stress is considered).

A fine surface finish can prolong the fatigue life by at least 300 more minutes (5 hours), while the severe residual stress and high pre-strain force can reduce the propagation life to about 60 minutes (one hour), ideally, a fine surface finish on the tooth gullet still can eliminate the possibility of failure during a single 240-minute (4-hour) shift.

The efficient method to improve fatigue life of a blade

This detailed study of each phase of the cracking process of the blade leads one to recommend more realistic methods to improve the total fatigue life of a blade. Generally speaking, there are a number of ways to improve fatigue life of a bandsaw blade, they are:

1. To improve fracture properties such as increasing critical stress intensity factor, increasing the fatigue limit and decreasing the propagation rate.

2. To decrease pre-strain force level to as low as is practical.

3. To redesign the gullet region tooth shape.

4. To introduce compressive residual stress on the gullet region.

5. To improve the surface finish of the tooth gullet.

To improve the fracture properties of a material is usually a long term and expensive proposition. Almost every stage of the manufacturing process has to be involved. Furthermore, to increase the critical stress intensity factor and decrease the propagation rate are not a positive method because these properties show their influence only after a crack occurs. If a crack comes into being, the performance of the blade will be affected,

particularly when the crack grows longer. Therefore, in this sense, to improve these properties does not help to improve the performance of the blade significantly.

To decrease the pre-strain force level is always limited by production requirements. The room for decrease is always limited in actual service.

Improvement on the design of the tooth profile is very effective method to decrease the SCF at the tooth gullet region. Its effect can be seen in Fig.2.5. The 'flattening' and 'shaving' proposed by Lee and co-worker was also this kind of effort. However, modification of the gullet region profile is always balanced by the production rate (since the tooth profile effects the tooth capacity), tooth strength and its stability.

Introducing a compressive residual stress distribution in the gullet region can either increase crack initiation time and slow crack propagating, or may even prevent a crack from initiating if the residual stresses are sufficenttly high. This is effectively equivalent to a decrease in pre-strain force level *locally* and will improve the fatigue life, while still maintaining the globe pre-strain force level unchanged, therefore retaining the desired blade stiffness. An example of imposing a compressive residual stress field is the 'hammering' or 'pressing' method used currently on some bandsaw blades. It is recalled that tensile residual stresses are produced through blade 'rolling' employed to assist in maintaining blade position on the wheel and cutting edge stability. As this analysis indicates that the presence of tensile stresses can significantly reduce crack propagation time, blades free of rolling will ultimnatelly have a longer life. These alternative methods to 'rolling' which maintain blade position and stability should be considered.

As the previous discussion shows, surface roughness in the gullet region of a blade is the most sensitive factor affecting its initiation life, and therefore the total fatigue life of a blade. Accordingly, in addition to introduction of compressive residual stress field, improving the surface finish appear to be the most economical, efficient and practical way to prolong the fatigue life of a blade. In the above example, it can be seen that if the

tooth gullet of a blade is carefully ground, the blade life could be several times longer. What is more important is that the initiation life could be extended beyond one shift, so that cracks initiated could be ground away before the next shift starts.

Future work

Although this author believes that the prediction is more realistic than those done by the previous researchers since several very important fracture properties of blade material are now available, the following factors may still make it difficulty to provide accurate predictions of fatigue life for actual bandsaw blades:

1. The nature of crack initiation is random. A test of the specific blade steel with a large sample population is required to gain a high confidence level. Even so, a specific life-time, e.g. its mathematical expectation, is meaningful only in the sense of probability. Also the initial shape of the corner crack has a strong effect on how the crack will extend. To quantify the initial crack shape requires further theoretical and experimental study. However, up to date predictions for 2-dimension crack propagation have to be based on assumed initial crack shapes.

2. The actual residual stresses induced by the manufacturing process are different for each individual blade. The information about the residual stress distribution for each individual blade is usually not available. Also each individual residual stress distribution has a different effect on initiation and propagation.

3. Other loads such as those induced by cutting, guiding, tilting, crowning etc. may become more influential when a crack appears, and may become even more so as the crack grows.

4. The global behavior of a blade may change when a crack becomes long and blade vibration becomes involved. For example, cracking may substantially release the

strain on one part of the blade, the consequent unbalance of strain plus the blade vibration may, in the worst case, derail the blade. In practice it is highly possible that subsequently the stress field may change dramatically so that the current stress modelling becomes invalid.

The above factors should be the focus of future study.

Chapter 8

Conclusions

In this research program, fracture mechanics theory was employed as a guide to conduct a series of experimental tests to obtain the fracture properties of bandsaw material. Based on the data obtained, failure prediction of a bandsaw blade was performed to explain gullet cracking in bandsaw blades, and a method to improve fatigue-life of bandsaw blade was recommended. The following are the major conclusions of this research work:

Material properties—tensile strength

The bandsaw material tested has a very high strength, i.e its 2% offset yield strength is 184 ksi. (1270 MPa) and the ultimate strength is 207 ksi. (1421 MPa). These results are in very good agreement with those obtained by a previous researcher [2].

Material Properties—R-curve

The crack-line-wedge-loaded specimen technique was employed and the related loading devices were designed and constructed. A more reliable strain based double-calibration method was developed and used in correlating the experimental records into a cracking resistance curve of the bandsaw material.

The cracking resistance curve for the bandsaw material was obtained. The critical stress intensity factor assessed using the R-curve is $220 ksi.in^{1/2} (242 MPa.m^{1/2})$ which reflects the material ability to handle a crack of a specific length when it is subjected to a static load. When the load is cyclic, as in a bandsaw blade, the toughness of $70 ksi.in^{1/2} (77 MPa.m^{1/2})$, which is the turning point on the R-curve, should be used . Therefore, the toughness under dynamic loading is only about 30% of that under static

loading.

Crack initiation life

Both the stress level and surface roughness of a blade have effects on the crack initiation life. However, within the range of the pre-strain forces used in an actual sawmill, the stress level, or in other words, the pre-strain level has a far weaker influence on the crack initiation life than does the gullet surface roughness. A carefully ground gullet can prolong crack initiation life by as much as **nine times** longer than that produced with the same sharpening wheel but without the extra care. What is more important is that a fine surface finish on a gullet can help a blade survive one shift of four hours so that the cracks initiated can be removed in the upcoming resharpening process.

What is alarming is that for those specimens with a surface roughness which is considered to be very close to an actual blade, crack initiation take place only after 44 minutes under a 20,000 lb. per-strain force! Microscopic examination on a sample from a failed blade shows that the actual surface of a tooth gullet can be much rougher. It is easy to accept that if the blade is in high-strain system, crack initiation life can be expected to be even shorter.

Crack growth rate for mode I crack in the bandsaw material

The mode I crack growth rate tests of the bandsaw material shows that within $\Delta K > 10 ksi.in^{1/2} (11 MPa.m^{1/2})$ the stress ratio R has no noticeable effect on the crack propagation rate.

When $\Delta K > 46 ksi.in^{1/2} (50.6 MPa.m^{1/2}$, the crack starts to advance with stable, but much larger growth increments, which shows the dynamic feature of the R-curve.

Crack growth behavior under out-of-plane bending

When subjected to an out-of-plane bending load, crack growth starts from the corner on the tensile side, grows radially to some distance, then starts to accelerate at a point on the tensile surface—the circular crack front grows into an elliptically curved front,

and finally the lower part of the front reaches the compressive surface. After this point the crack front advances while maintaining its shape relatively unchanged.

The crack growth life predicted using the empirical crack-growth rates were in agreement with the actual testing data, which proved that both the crack-growth rate and Newman's stress intensity factor equation are close to reality and useful.

Failure analysis—critical crack length

With the critical stress intensity factor under both static and dynamic loads, the critical crack lengths under different pre-strain forces have been assessed. The maximum possible net critical crack lengths under dynamic loads range from 1.04 to 1.24 in (26.4-31.5mm) if residual stress is not considered. This explains why the existence of 1 in. (25.4mm) cracks in a blade is possible.

Failure analysis—crack growth model

A crack grows from the assumed initial corner crack of 1mm radius, then the crack front gradually becomes elliptical as the crack grows into the blade. When the side tip of the crack front reaches the inner surface of the blade, the crack becomes a through-thickness crack and extends as a through-thickness crack until the critical crack length is reached.

The predictions based on the above model indicate that there are some cases that a bandsaw blade can only last about two or even just over one hour. This explains why a mid-service failure is possible. These predictions also indicate a significant effect of the presence of residual stress on blade fatigue life. For the pre-strain force levels considered in this study, a reduction factor of 4 on propagation life of a crack in the blade was predicted as result of the presence of a 10 ksi tensile residual stress. Since tensile residual stress effects crack initiation life in the same manner as pre-strain force level does, total fatigue life of blade are expected being reduced even further. This indicates strongly that 'rolling' will have a detrimental effect on blade service life. In contrast, the introduction

of compressive residual stress should act to increase life. Thus methods which impose these compressive stress (e.g. hammering or pressing) should be considered as a means of extending blade service life.

Improvement of bandsaw blade fatigue life

In addition to introduction of compressive residual stress field in gullet region, the most efficient, economical and practical way to improve bandsaw fatigue life is to grind it with extra care. In this way, the crack initiation life can be prolonged many times as long as that without extra care.

Bibliography

[1] Ingema, E., 1977, "Reports on Gullet cracking in Bandsaw Blades", *Uddeholm Steel Research*

[2] Porter, A.W., 1971, "Some Engineering Considerations of High-Strain Band Saws", *Forest Products Journal, vol. 21, No. 4, pp. 24-32*

[3] Lee, C., Robinovitch, S., Romilly, D.P., 1988, "Stress Analysis of a Bandsaw Blade for Improved Fatigue Life", *Final Report for Mech 455/456*, Department of Mechanical Engineering, University of British Columbia, Vancouver, B.C., Canada.

[4] Jones, D.S. 1965 "Gullet Cracking Saws" *Australian Timber J, 31 (7): pp 22-25*

[5] Lehmann, B.F., 1988 "Factors in the Cracking of Bandsaw Blades", *Report for Mech 550*, Department of Mechanical Engineering, University of British Columbia, Vancouver, B.C., Canada.

[6] Eschler, A., 1982 "Stress And Vibrations In bandsaw Blade", *M.A.Sc. Thesis*, Department of Mechanical Engineering, University of British Columbia, Vancouver, B.C., Canada.

[7] Targard, C., 1989, "A Test Report: the Composition of Bandsaw Blade steel ", Stress Analysis Lab., Department of Mechanical Engineering, University of British Columbia, Vancouver, B.C., Canada.

[8] Osgood, C.C., 1970, "Fatigue Design", Wiley-Interscience pub.

[9] Broek, D., 1986, "Elementary Engineering Fracture Mechanics", 4th edition, Martinus Nijhoff Publishers

[10] Allen, F.E., 1973, "High-Strain/Thin Kerf", *proceedings of the Modern Sawmill Techniques*, Portland, Oregon, Feb.1973

[11] Timoshenko, S., 1955, "Strength of Materials" 3rd edition, McGRAW-Hill Book Company.

[12] 1980, "Industrial Health and Safety Regulations", *Workers' Compensation Board of British Columbia*

[13] Krafft, J.M., Sullivan, A.M., and Boyle, R.W, 1961, "Effect of Dimensions on Fast Fracture Instability of Nothch Sheets", *Proceedings of the Crack Propagation Symposium*, College of Aeronautics, Cranfied, England, Vol. 1, pp. 8-26.

[14] ASTM Designation: E561-81, "Recommended practice for R-curve Determination", Am. Soc. Testing Mats., 1981.

[15] Paris, P.C., 1964, "The Fracture Mechanics Approach to Fatigue", *Proceedings of the Tenth Sagamore Army Material Research Conference*, Syracuse University Press, 1964, pp 107-132.

[16] Elber,W.,1971, "The Significance of Fatigue Crack Closure", ASTM STP 486, 1971, pp 230-242.

[17] Irwin, G.R., 1957, "Analysis of Stresses and Strains Near the End of Crack Travelling a Plate", J. of Applied Mech., **24**, pp 361-364, 1957.

[18] Griffith, A.A., 1920, "The Phenomena of Rupture and Flow in Solids", Phil. Trans. Roy. Soc. of London. **A221**, pp 163-198,1920.

[19] ASTM Designation: E647-86a, "Standard Test Method for Measurement of Fatigue Crack Growth Rates", Am. Soc. Testing Mats., 1986

[20] Cook, R.D., 1988 "Concepts and Applications of Finite Element Analysis", 3rd edition, John Wiley & Sons.

[21] Savin, G.N., 1961, "Stress Concentration Around Holes", Pergamon Press.

[22] Heyer, R.H., and McCabe, D.E., 1972 "Plane-Stress Fracture Toughness Testing Using a Crack-Line-Loaded Specimen", *Engineering Fracture Mechanics*, EFMEA, Vol. 4, pp. 393-412

[23] Newman, Jr. J.C., and Raju, I.S. 1981 "An Empirical stress-Intensity Factor Equation for the Surface crack", *Engineering Fracture Mechanics*, Vol.15, No.1-2, pp. 185-192

[24] Wilson, W.K., and Thompson, D.G., 1971 *Engineering Fracture Mechenics*, Vol. 3, pp 97-

[25] Smith, R.A., and Miller, K.J., 1977 *International Journal of Mechanical Science*, Vol 19, pp 11-

[26] ANSYS FEM Software, Version 4.3, Swanson Analysis System Inc, 1992.

[27] Roberts, R., and Rich, T., 1967 "Stress-Intensity Factor for Plate Bending", *J. of Applied Mech.*, **34**, pp777-779, 1967.

[28] Alkins, A.G., and Mai, Y-M., 1988 "Elastic and Plastic Fracture Mechanics", Ellis Horwood Ltd.

Appendix A

Calculations in the Failure Analysis

A.1 Bandsaw parameters used in the calculations

The following assumptions are made in the following calculations:

Sawmill machine and blade parameters:

1. The diameter of the wheel: 5 ft.(1524mm).
2. The distance between the axis of the wheels: 5 ft.(1524mm).
3. The travelling speed of the bandsaw blade: 147.6 ft./sec. (45m/sec).
4. Effective width of the blade: 9.5 in. (241mm).
5. The thickness of the blade: 0.073 in.(1.85mm).

Simplification of the loads

1. Only the bending load caused by the wheel and the tensile load caused by the pre-stain force are counted because of their magnitude and cyclic nature.
2. Simple beam theory [11] is used for the bending stress and one dimension tensile theory [11] for stress caused by pre-strain force.
3. Three pre-strain force levels are used: 20,000 lb (90,000 N), 18,000 lb.(72,000 N) and 13,000 lb.(58,500 N).

See the Table A.7 for the results.

load cases \ stress level			static stress (ksi)	bending stress (ksi)
without residual stress	pre-strain force level	20,000 lb	14.6	35
		18,000 lb	11.68	35
		15,000 lb	9.49	35
with 10 ksi residual stress	pre-strain force level	20,000 lb	24.6	35
		18,000 lb	21.68	35
		15,000 lb	19.49	35

Table A.7: The calculated loads

A.2 K-formula used in the calculations

According to the load-crack configuration of the blade, the actual stress field at the crack tip is produced either by pure tensile load or by combination of bending and tensile loads. A crack goes through two different stages, i.e. a corner crack, and as through-thickness crack. The formula used to evaluate the stress intensity factor depends on the load type as well as the crack configuration. Therefore, in the case of a gullet crack in a bandsaw blade subjected to pre-load and out-of-plane bending, three formula were used in the calculations.

Newman's equation for a corner crack under tension and bending

Newman and co-worker [23] developed an empirical stress-intensity factor equation for a surface crack. The stress-intensity factors used to develop the equation were obtained from their previous three-dimensional, finite element analysis of a semi-elliptical surface crack in finite elastic plates subjected to tension or bending loads. A wide range of configuration parameters were included in the equation. The ratios of crack length to plate thickness and the ratio of crack depth to crack length ranged from 0 to 0.1. The effects of plate width on stress-intensity variations along the crack front were also included. In order to facilitate readers in refering to his original paper, the original symbols were preserved in the following citation.

Notations used in Newman's equation

For the following definitions of the notations, refer to Fig.A.64 and Fig.A.64.

a = depth of surface crack.

b = half-width of cracked plate.

c = half-length of surface crack.

F = stress-intensity boundary-correction factor.

h = half-length of cracked plate.

K_I = mode I stress-intensity factor.

K_{cr} = elastic fracture toughness.

M = applied bending moment.

Q = shape factor for elliptical crack

S_b = remote bending stress on outer fiber, $3M/bt^2$.

S_t = remote uniform-tension stress.

t = plate thickness.

Φ = parametric angle of the ellipse.

Stress-intensity factor equation for the surface crack

The empirical equation for the stress-intensity factor for a surface crack in a finite plate subjected to tension and bending loads were fitted as follows,

$$K_I = (S_t + HS_b)\sqrt{\pi \frac{a}{Q}} F(\frac{a}{t}, \frac{a}{c}, \frac{c}{b}, \Phi) \tag{A.21}$$

The equation is valid for $0 < a/c <= 1.0, 0 <= a/t < 1.0, c/b < 0.5$ and $<= \Phi <= \pi$.

A useful approximation for geometric factor Q is

$$Q = 1 + 1.464(\frac{a}{c})^{1.65} \qquad (\frac{a}{c} \leq 1) \tag{A.22}$$

The function F and H are defined so that the boundary-correction factor for tension is equal to F and boundary-correction factor for bending is equal to the product of H and F. The function F was taken to be

$$F = [M_1 + M_2(\frac{a}{t})^2 + M_3(\frac{a}{t})^4] f_\Phi g f_w \tag{A.23}$$

where

$$M_1 = 1.13 - 0.09(\frac{a}{c}) \tag{A.24}$$

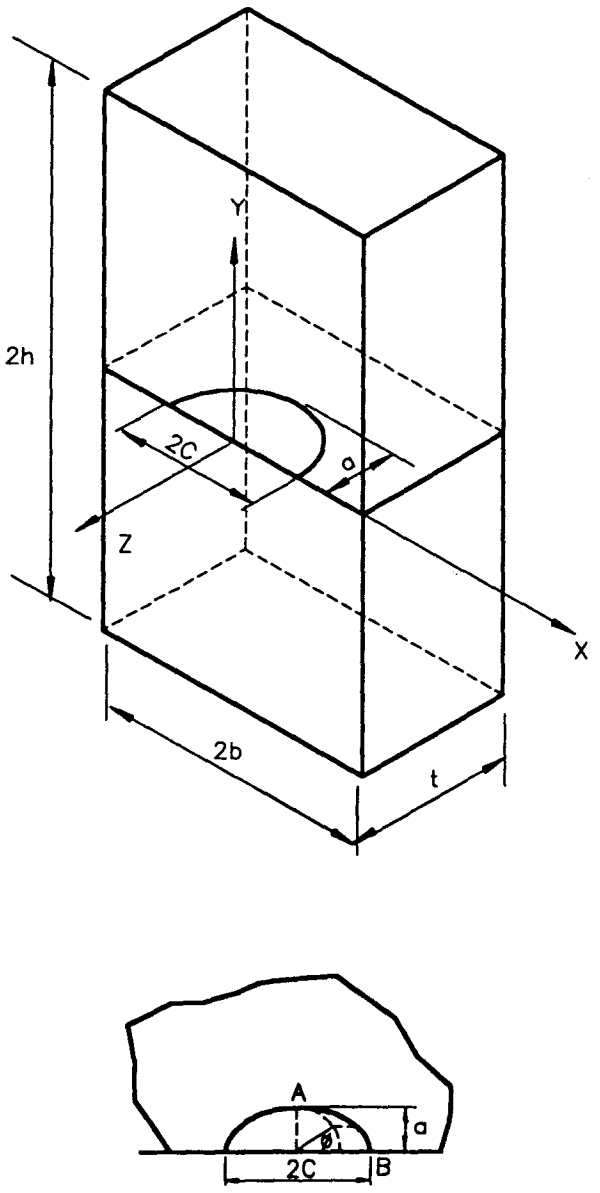

Figure A.64: Surface crack in a finite plate

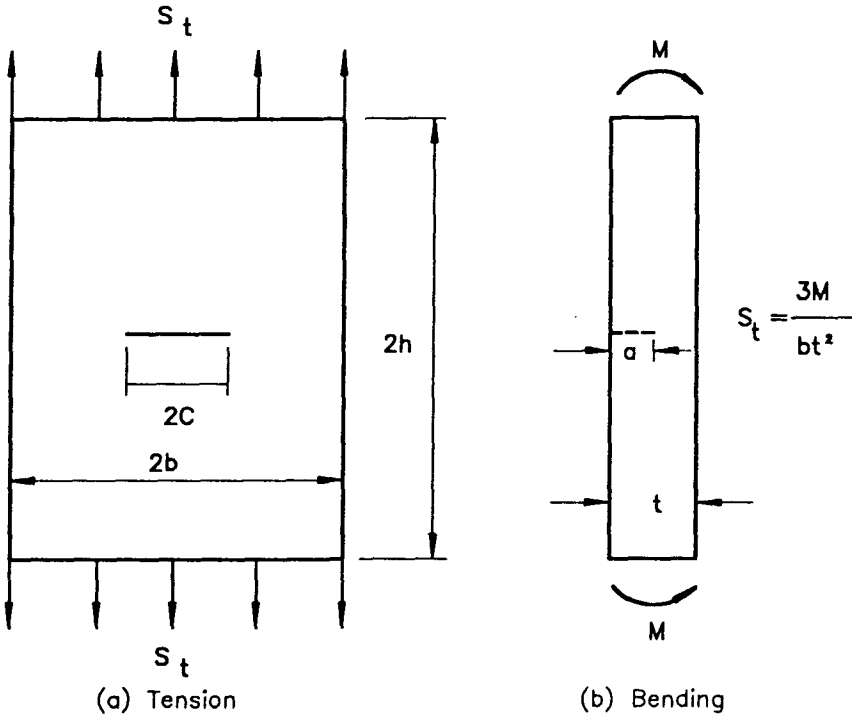

Figure A.65: Surface-cracked plate subjected to tension or bending loads

$$M_2 = -0.54 + \frac{0.89}{0.2 + (a/c)} \tag{A.25}$$

$$M_3 = 0.5 - \frac{1.0}{0.65 + (a/c)} + 14(1.0 - \frac{a}{c})^2 4 \tag{A.26}$$

$$g = 1 + [0.1 + 0.35(\frac{a}{t})^2](1 - sin\Phi)^2 \tag{A.27}$$

The angular function f_Φ is

$$f_\Phi = [(\frac{a}{c})^2)cos^2\Phi + sin^2\Phi]^{1/4} \tag{A.28}$$

The finite-width correction function f_w is

$$f_w = [sec(\frac{\pi c}{2b}\sqrt{\frac{a}{t}})]^{1/2} \tag{A.29}$$

The function H is

$$H = H_1 + (H_2 - H_1)sin^p\Phi \tag{A.30}$$

where

$$p = 0.2 + (\frac{a}{c}) + 0.6(\frac{a}{t}) \tag{A.31}$$

$$H_1 = 1 - 0.34(\frac{a}{t}) - 0.11(\frac{a}{c})(\frac{a}{t}) \tag{A.32}$$

$$H_2 = 1 + G_1(\frac{a}{t}) + G_2(\frac{a}{t}) \tag{A.33}$$

In the equation for H_2,

$$G_1 = -1.22 - 0.12(\frac{a}{t}) \tag{A.34}$$

$$G_2 = 0.55 - 1.05(\frac{a}{c})^{0.75} + 0.47(\frac{a}{c})^{1.5} \tag{A.35}$$

For a corner crack as in the case of bandsaw blade, eqn.(A.21) should be corrected by factor 1.12 [9] to account for the free-edge effect.

In the prediction calculation, eqn.(A.21) was used in snap-shot (a), and (b) (see **Chapter 7**).

Wilson's equation for a through-thickness crack under bending

Wilson and co-worker's work [24] concerns a long plate of width $2b$ and thickness t which contains a crack of length $2a$ located symmetrically between the edges of the sheet and perpendicular to them (Fig.A.66). The plate is subjected, remote from the crack, to a uniform moment M about an axis parallel to the crack line. Using a finite element method, they studied this configuration. The opening mode stress intensity factor K_I at Point A was calculated and fitted to a curve K_I/K_o vs a/b (see ref.[24]. K_o is the opening mode stress intensity factor at point A for an isolated ($b = \infty$) crack and is given by

$$K_o = \frac{(1+\upsilon)}{(3+\upsilon)} \frac{6M}{t^2} \sqrt{\pi a} \tag{A.36}$$

For a edge crack as in the case of bandsaw blade, eqn.(A.36) should be corrected by factor 1.12 [9] to account for the free-edge effect.

It should be noted that in this equation, $6M/t^2$ is the maximum tensile stress in the outer fiber of the plate.

It is worth mentioning that within $a/b = 0.19$ the maximum ratio K_I/K_o is less than 1.02. In the case of bandsaw blade, the critical crack length is less than 19% of its width,

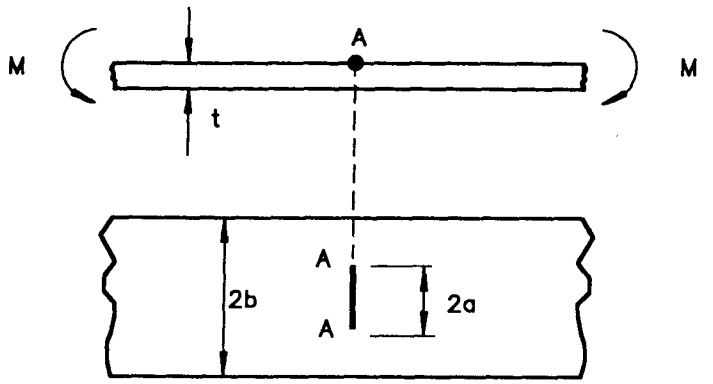

Figure A.66: A long plate with a crack subjected to bending

therefore eqn.(A.36) times a free edge factor (1.12 for tension, 1 for bending) can be used directly.

In the prediction calculation, eqn.(A.36) was used in snap-shot (c), (d),(e) and the critical crack length calculation (see **Chapter 7**).

K-formula for edge crack in a plate

A gullet crack in a blade under a pre-strain load can be classified as a typical *opening mode* (mode I) edge crack in a plate subjected to pure tensile stress. Its stress intensity factor formula is documented in reference [9] and re-presented as follows,

$$\begin{aligned} K &= \sigma\sqrt{a}\{1.99 - 0.41(\frac{a}{W}) + 18.7(\frac{a}{W})^2 - \\ &\quad -38.48(\frac{a}{W})^3 + 53.85(\frac{a}{W})^4\} \end{aligned} \tag{A.37}$$

A.3 Calculations of critical crack length

The critical condition

$$K = K_C \tag{A.38}$$

Where

K—the stress intensity factor at the tip of the crack in the blade produced both by the pre-strain force and the bending.

K_C—critical stress intensity factor for the blade material (obtained in **Chapter 3**).

To obtain the critical crack length a_C, substitute the equation (A.36) and equation (A.37) into equation (A.38), use *static stress* in the Table.A.7 for σ in equation (A.37) and *bending stress* in equation (A.36) and solve equation (A.38) for a numerically.

Critical crack length under static loading condition

As discussed in **Chapter 3**, in the case of 'absolutely' static load, the critical stress intensity factor is as high as 220 $ksi.in^{1/2}$, with an upper limit of 246 $ksi.in^{1/2}$ and a lower limit of 210 $ksi.in^{1/2}$ (see **Chapter 3**). Therefore, in the calculations of critical crack length under static load, the above toughness were used.

In the prediction calculation, equation (A.37) was also used in snap-shot (c), (d) and (e) (see **Chapter 7**).

Critical crack length under a dynamic load

From engineering design point of view, even a static load should be control below such a level that there is no more crack extension. Therefore, for a alternating load, its amplitude should be always restricted to a level so that there is no more crack extension. To this end, a alternative 'dynamic critical stress intensity factor' is defined as the point on R-curve where the R-curve starts to bend [28]. for the bandsaw blade this is 71 $ksi.in^{1/2}$. The 95% confidence upper limit and lower limit are 120 $ksi.in^{1/2}$ and 42

$ksi.in^{1/2}$ respectively. The effect on the critical crack lengths can be seen in Table 7.5.

A.4 Residual stress consideration

The estimated 10 ksi (68.89 MPa) tensile residual stress induced by the manufacturing process is assumed [5] and superimposed upon the static stress.

A.5 Calculations of crack growth life

Crack propagation rate

In the calculation of fatigue crack propagation, the following empirical formula was used (see **Chapter 5**).

$$\frac{da}{dN} = 0.66(\Delta K)^{2.86} \qquad (in/cycle) \tag{A.39}$$

The unit for ΔK is $ksi.in^{1/2}$.

Crack growth model for the out-of-plane bending

In Fig.6.51 (**Chapter 6**) the process of crack advance can be seen, i.e. the crack growth starts from the corner on the tensile side, grows radially to some distance, then starts to accelerate at a point on the tensile surface—the circular crack front grows into an elliptically curved front, finally the lower part of the front reaches the compressive surface. After this point the crack front advances while maintaining its shape relatively unchanged. Based on the above analysis and the crack profile data measured using a optical microscope, prediction of the crack growth for the six specimens tested were made. The following are the parameters and data used in the prediction.

Different crack growth rate in the two directions

According to the research done by J.C. Newman and co-worker [23], a surface crack has a different crack growth rate in the thickness and surface directions (see Fig.A.64)

even if the stress intensity factor ranges are the same. The crack-growth rates at point A and point B along the crack front can be described independently as follows,

At point A,

$$\frac{da}{dN} = C_A(\Delta K_A)^n \tag{A.40}$$

At point B,

$$\frac{da}{dN} = C_B(\Delta K_B)^n \tag{A.41}$$

For the same material, Newman and co-worker found that for their test data, a relationship $C_B = 0.9^n C_A$ exists to corelate the empirical data.

In the prediction for the out-of-plane bending testing, the result produced by using $C_B = 0.91^n C_A$ was found to be closer to the actual crack-growth data.

The crack closure/crack surface contact co-efficients

Since the specimens were subjected to out-of-plane bending, it is possible that crack closure or crack surface contact occurs during crack growth, especially in the case of negative stress ratios. The deviations in the predictions from the actual data were attributed to this closure or surface contact. If a coefficient U is introduced to account for these effects to match the actual data, the effective stress intensity factor can be correlated to the calculated stress intensity factor using the geometry of the crack, i.e. $\Delta K_e = U\Delta K$. In the prediction, the data (the crack extension and number of cycles) recorded for the last step of the crack growth was employed to develop the coefficient U and the ΔK_e was used to calculate the da/dN. Table A.8 shows the results. The values of ΔK explain the difference in growth rate shown in Fig.6.49 (**Chapter 6**).

The calculation procedure for the fatigue-life prediction

With the initial crack length assumed and the crack growth rate rule available, the

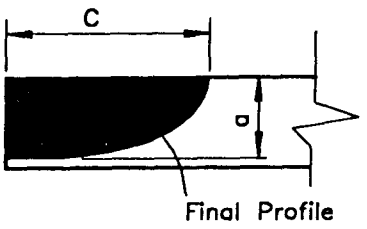

stress ratio at outer surface	hand meassured final profile a (in)	c (in)	final step dc	final step dN	estimated from dN=final step dN C_c=0.91^n*C_a dc	a/c	alternating stress(ksi)	mean stress(ksi)	dK at C ksi.in^1/2	U	max diff % in da/dN
R= 0.313	0.073	0.224	0.039	57906	0.039	0.32	16	30.6	12.38	0.93	2.95
R= 0.227	0.071	0.266	0.039	55344	0.039	0.27	16	25.4	12.55	0.89	4.65
R= 0.000	0.056	0.189	0.039	109891	0.043	0.30	16	16	10.28	0.98	0.49
R= -1.000	N/A	N/A	0.015	97536	N/A	N/A	32	0	N/A	N/A	N/A
R= -0.373	0.068	0.177	0.039	16462	0.027	0.38	32	14.6	16.88	1.10	0.95
R= -0.490	0.057	0.162	0.039	40461	0.038	0.35	32	10.95	13.94	0.96	1.2

Table A.8: The crack growth calculation for the out-of-plane bending testing

crack growth life was calculated using a accumulation or cycle-by-cycle procedure, that is,

- input the initial crack geometry and stress intensity factor range, obtain *da* and *dc* after one cycle.
- add the crack increment *da* and *dc* obtained in the previous step to the initial crack lengths to obtain new crack lengths.
- input the new crack lengths and current stress intensity factor, obtain *da* and *dc* after one cycle.
- repeat ... until the desired crack length is reached.